Chemical Engineering Journal 522 (2025) 167554

Contents lists available at ScienceDirect

Chemical Engineering Journal

journal homepage: www.elsevier.com/locate/cej

Review

Engineering high-performance IR photodetectors: From material design to multifunctional applications

Phuong V. Pham [a,*], S. Cathrin Lims [a], Anuj Kumar [b], Rajesh K. Ulaganathan [c], Rayko I. Stantchev [a,d], Raman Sankar [e,*]

[a] Department of Physics, National Sun Yat-sen University, Kaohsiung 80424, Taiwan
[b] Department of Chemistry, Institute of Humanities and Applied Science, GLA University, Mathura 281406, India
[c] Centre for Nanotechnology, Indian Institute of Technology Roorkee,247667, India
[d] Department of Physics, University of Warwick, Coventry CV4 7AL, United Kingdom
[e] Institute of Physics, Academia Sinica, Taipei 11529, Taiwan

ARTICLE INFO

Keywords:
IR photodetector
Optoelectronic
2D material
Plasmon resonance
Scattering effect
Interfaces

ABSTRACT

Infrared photodetectors (IR PDs) are vital components in optoelectronics, facilitating a wide range of applications, including security systems, search and rescue missions, biomedical diagnostics, meteorological observations, and astronomical studies. Despite their versatility, the performance of IR PDs is hindered by several challenges, such as scattering effects, high surface and interface contact resistance, dark current, limited photo responsivity, low sensitivity, and suboptimal noise equivalent power. These limitations are primarily attributed to the inherent properties of the semiconductor materials used in their construction, including abundant defect states, thermal instability, large bandgap widths, and the zero-bandgap nature of graphene. This review provides a comprehensive overview of recent advancements in IR PD technology, focusing on strategies to overcome these performance bottlenecks. Innovative approaches include the use of novel low-dimensional materials, the development of advanced device architectures, and the application of direct-growth techniques for 2D heterostructures. These methods aim to mitigate the physical and material constraints that currently restrict device efficiency. In addition to detailing these advancements, the review examines the diverse applications of IR PDs to highlight their importance in various fields. The discussion extends to future prospects, emphasizing the potential of IR PDs to achieve higher performance and broader applicability. However, it also addresses the existing challenges that must be resolved to realize these goals. This analysis underscores the critical role of IR PDs in modern technology and the continuous need for research to push their boundaries further.

1. Introduction

Modern optoelectronics, which involves the transformation of light into electrical signals, is a rapidly advancing field that continues to captivate widespread interest across the scientific community due to its considerable applications in communication [1–3], medical and health care [4–6], environmental detection [7,8], and even astronomy [9]. Over the last decades, while researchers have observed the creation of excellent PDs in the ultraviolet (UV) and visible (Vis) regions, the wavelength range from 700 nm to ~2500 nm, which is within the IR region [10] and occupying more than 55 % of the energy in sunlight, has experienced much bigger difficulties in achieving great detection capabilities thereby preventing the full utilization of the IR region. In optical communication, 1550 nm is the wavelength for which optical fibers have the lowest losses making it the most preferred wavelength [11]. For health care, the human skin under healthy conditions stays within a narrow range hence detecting thermal abnormalities is indicative of underlying health problems [12]. In environmental monitoring, hazardous gases that are otherwise undetectable to the human eye can be effectively identified through their characteristic absorption signatures in the IR spectrum [12,13], and thermal imaging is also a necessity in the rigorous thermal management of any system be it large or small. Finally, for astronomy the longer wavelengths of IR radiation are able to penetrate interstellar gas clouds which is why the James Webb Space Telescope uses IR detectors. All of these applications will greatly benefit from the improvement of IR detection technology. For example, faster

* Corresponding authors.
E-mail addresses: phuongpham@mail.nsysu.edu.tw (P.V. Pham), sankarraman@gate.sinica.edu.tw (R. Sankar).

https://doi.org/10.1016/j.cej.2025.167554
Received 19 April 2025; Received in revised form 11 August 2025; Accepted 20 August 2025
Available online 27 August 2025

detector response can lead to higher data transfer rates, whereas cheaper costs will result in a much more widespread use for medical studies and environmental observation, and any improvement in the sensitivity of IR telescopes will help astronomers answer the big questions of life. These are some of the motivations that have fueled the development IR PDs over the past two decades, and have thus made it an attractive research field with the growth of this research field as evidenced by the yearly number of publications from 2010 to 2024 **(**Fig. 1**).**

For all types of PDs, the device performance is usually evaluated through five key parameters which are the photo-to-dark current ratio, selectivity, response speed, sensitivity, and stability [14]. However, in the IR range PDs capabilities are degraded by high dark current, low photo responsivity, high scattering effects and contact resistance at interfaces which places limitations on their usage, thus necessitating further research to improve and overcome the current limitations [15,16]. Herein, it identifies critical gaps and highlights emerging trends and breakthroughs, distinguishing itself through a focused analysis. It points out several limitations in current IR PDs technologies, such as material issues like abundant defect states, thermal instability, and unsuitable bandgap properties, particularly in graphene and traditional semiconductors. Trade-offs between achieving narrow bandgaps and managing recombination and noise, challenges with high contact resistance and scattering effects, dark current issues, and the complexities of manufacturing novel 2D materials are also emphasized. Moreover, the review identifies difficulties in balancing performance parameters like high quantum efficiency and fast response, along with the need for better integration with silicon technologies for affordable, mass-producible IR systems. Instability of promising 2D materials like black phosphorus (BP) further complicates progress. To address these gaps, the review showcases emerging strategies such as leveraging low-dimensional materials and heterostructures, advancing fabrication techniques, employing surface and interface engineering, and integrating plasmonic materials to enhance light absorption. It discusses methods to reduce contact resistance and suppress scattering, thereby improving electron mobility. Specific application-driven innovations, particularly in healthcare, imaging, and optical communication, are explored, reflecting a shift from traditional military uses to broader technological landscapes. Finally, the review outlines future prospects in areas like ultrafast optical sensing and neuromorphic computing, while acknowledging persisting challenges. Overall, by explicitly linking current challenges to cutting-edge solutions and new research directions, the review provides a critical, insightful contribution that goes well beyond a simple aggregation of existing literature. we present a comprehensive guide addressing the critical challenges associated with IR PDs and offer strategies to overcome them.

This review is structured to provide a clear and systematic discussion, beginning with Section 1, which introduces the fundamental context and significance of IR PDs in modern technology. Beyond the introduction, the content is divided into three detailed sections to streamline the exploration of current challenges, advancements, and prospects in IR PD research.

In Section 2, we delve into the existing limitations identified in current research on IR PDs. We emphasize innovative solutions aimed at enhancing device performance, such as doping techniques to optimize material properties, architecture design to refine device designs, and direct growth techniques tailored for two-dimensional (2D) nanostructures. These approaches represent cutting-edge strategies to address issues like dark current, responsivity, sensitivity, and noise equivalent power.

Section 3 focuses on the remarkable applications of IR PDs across various fields. To provide clarity, these applications are categorized into five key domains: healthcare, imaging technologies, optical devices, environmental and gas sensing, and thermal/optical communication systems. This section highlights the indispensable role of IR PDs in diverse technological ecosystems.

Finally, in Section 4, we present a forward-looking perspective on the future of IR PDs. This section discusses the potential directions for innovation while addressing the technical and material challenges that must be overcome to achieve the next generation of high-performance IR PDs. Unlike previous reviews that focus solely on either material choices or device level performance, this review presents a dual-perspective classification based on both 'material strategies' and 'mechanism design.' This combined approach allows us to systematically map how material innovations (e.g., doping, 2D heterostructures) integrate with functional mechanisms (e.g., Plasmon Resonance, Dark Current Reduction) to drive performance in IR photodetectors. Through this framework, the review offers not only a synthesis of recent advances but also a roadmap for future research.

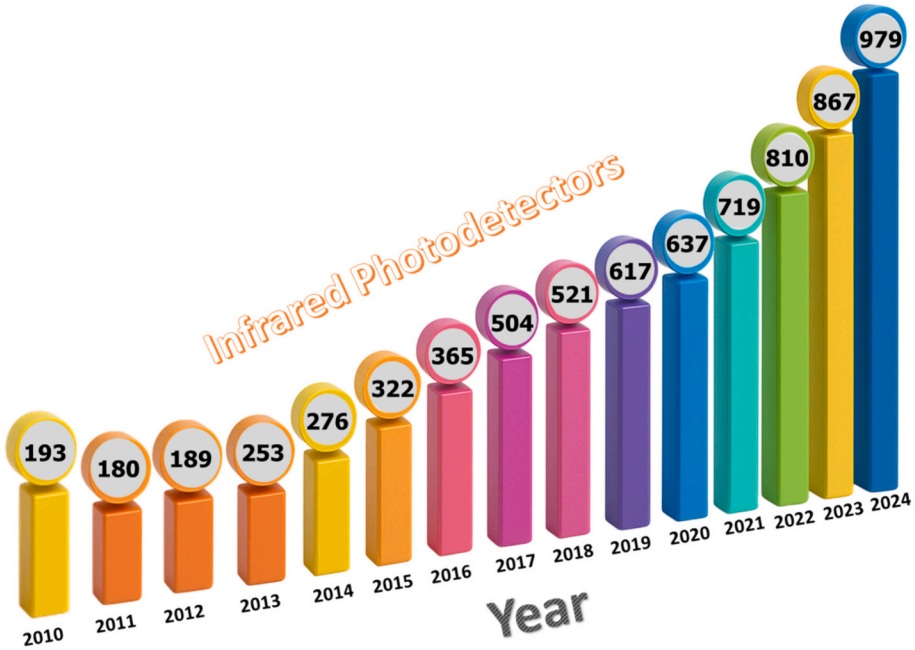

Fig. 1. The Growth of IR PDs development through annual publications from 2010 to 2024. (Source: Web of Science).

2. Breaking down the limits of IR photodetectors

As IR PDs continue to evolve, improving their performance beyond conventional limits requires a comprehensive understanding of the physical, material, and architectural factors that constrain their functionality. This section presents a structured overview of the critical challenges in current IR PDs technologies and outlines the key strategies developed to address them. These strategies are classified into material-level approaches (such as doping and 2D heterostructures), device-level architectural enhancements, and system-level innovations including computational readout.

2.1. Existing challenges on current IR photodetectors

A broad spectrum of materials has been employed in the fabrication of photodetectors, encompassing compound semiconductors from groups II-V [17–21], III-V [22–25], III-VI [26–29], II-VI [30–32], IV-VI [30,33–36], V-VI [37–40], as well as perovskite [41–45], organic [46–50] and other semiconductor systems. For IR PDs, the choice of material is primarily governed by its bandgap, as detection requires that the incident photon energy be equal to or greater than the bandgap to enable excitation of electrons from the valence band to the conduction band, generating photo-induced electron–hole pairs [51]. Importantly the IR region corresponds to photon energies lower than approximately 1.55 eV (wavelengths longer than 800 nm), in contrast to the visible region, where energies like 2.675 eV (~464 nm) are much higher. While narrow band gap materials are suitable for IR detection, they often suffer from increased recombination and noise, which can reduce photocurrent. However, the overall photocurrent depends on a combination of factors including material quality, defect density, surface states, and device architecture. There is also the issue of the dark current which is defined as the current when there is no light falling onto the IR PDs **(**Fig. 2**).** It can be attributed to the extrinsic leakage phenomena (surface leakage current, Ohmic leakage current), thermal carrier generation, lack of high charge barriers, defect concentration, difference in Fermi level [52–54]. A higher dark current increases the power consumption and sets the highest operating temperature of the device [51,55] leading to a decrease in the sensitivity of PDs performance **(**Fig. 2**).**

As a result, current research teams have made certain strategies to develop many structures encompassing different materials to improve IR PDs [55,56]. However, an issue that cannot be avoided when fabricating PDs is the contact resistance at the interface of the combined materials and between the metal electrodes and the semiconductors as well **(**Fig. 2**).** The common sources of contact resistance can be listed including defect concentrations, thermal treatment and work function [57–59]. High resistance at the contacts prevents photo-generated electrons from being efficiently collected in the electrodes and leads to their recombination with holes to the valence band in the active materials meaning less current was generated, which is undesirable. Beyond material and structural challenges, the performance of IR PDs is fundamentally constrained by intrinsic noise mechanisms that define the theoretical limits of detection. Chief among these are photon shot noise, Johnson (thermal) noise, and the background-limited infrared photodetection (BLIP) condition. Photon shot noise originates from the statistical nature of photon arrival even under constant illumination, photons arrive randomly in time, generating fluctuations in the photocurrent [60,61]. This noise scales with the square root of the photon flux and becomes the dominant noise source under high-illumination conditions. Its presence sets a floor to the signal-to-noise ratio (SNR), particularly in low-light or fast-detection regimes. Johnson noise, also known as thermal noise, is generated by the random motion of charge carriers in resistive elements within the detector, even in the absence of light. It is directly proportional to the temperature and inversely proportional to the resistance, and becomes particularly significant in narrow-bandgap semiconductors and uncooled detectors. Johnson noise is often characterized by the expression $\sqrt{4kT/R}$, where k is Boltzmann's constant, T is the absolute temperature, and R is the resistance. In optimized systems, BLIP (background-limited IR PDs) operation represents the gold standard for detector sensitivity [62]. Under BLIP conditions, the dominant noise originates not from the detector itself, but from the background IR radiation (e.g., ambient thermal emission from optics or the scene). Achieving BLIP requires extreme suppression of dark current and internal noise to the point that further reductions offer no performance benefit. Detectors in this regime operate at the fundamental physical noise floor and are ideally suited for applications like passive thermal imaging, where minimal photon flux must be accurately resolved. The interplay between these noise mechanisms determines the noise equivalent power (NEP) and specific detectivity (D*), key metrics for IR detector performance. For instance, under shot-noise-limited conditions, the NEP is given by NEP = $\sqrt{2qId}$, where q is the electron charge and IdI_dId is the dark current. Similarly, Johnson-noise-limited NEP can be described as NEP = $\sqrt{4kT/R}$. These

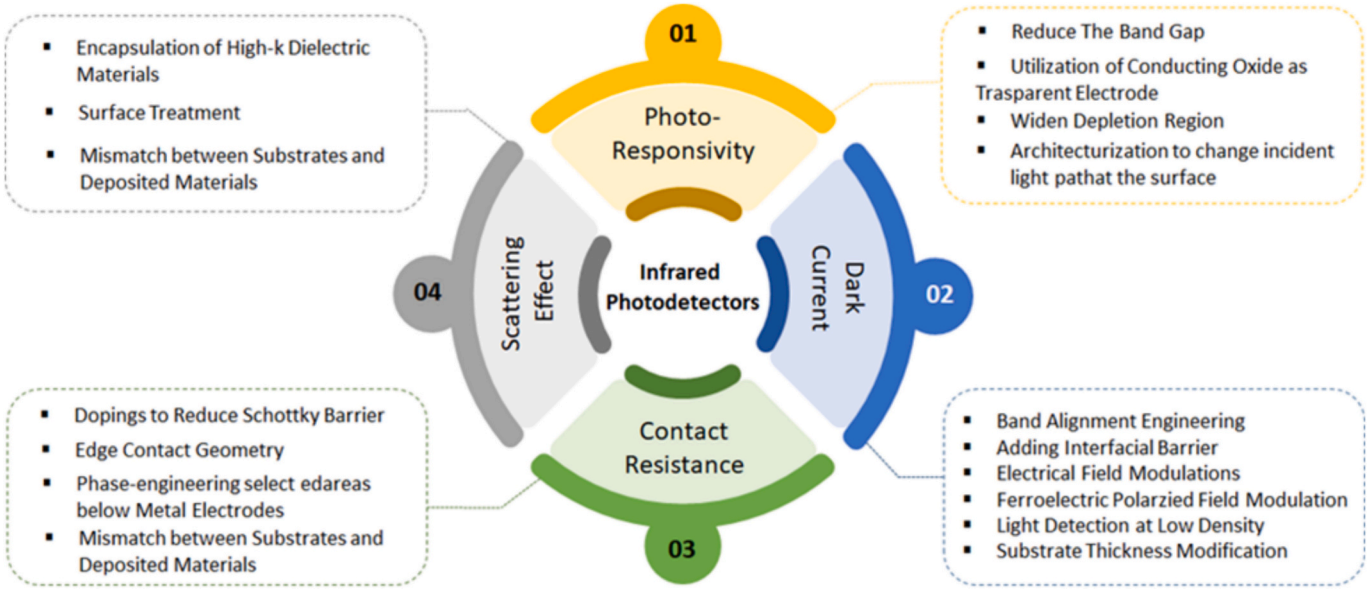

Fig. 2. Currently remarkable challenges of optical sensing devices operating in the IR region.

relationships highlight the need for engineering efforts that not only enhance responsivity and reduce dark current, but also approach the theoretical limits dictated by the physics of noise. The scattering effects that occur within the nanostructures when interacting with incident light mainly influence the electronic mobility of materials (Fig. 2) [63–65]. There are several sources of them including optical and acoustic scattering, phonon scattering, electron-electron scattering, electron-phonon scattering, interface scattering, and Coulomb scattering at the lattice defects and charged impurities [66,67]. These scattering effects result in reducing the responsivity of devices because the light-induced charge carriers may scatter, for example by colliding with an ion of the crystal lattice, on their way to the electrodes and recombine to the valence band before arriving to the electrode, especially at a low bias voltage [68]. In fact, using a higher voltage can reduce Schottky barrier height (SBH) and minimize scattering phenomena, leading to an enhanced photocurrent but it also breaks down the device structures and reduces their durability. Scattering phenomena arising from phonons, defects, or interfaces are a major source of performance degradation in IR PDs. While applying higher bias can mitigate some of these effects, it also raises power consumption and risks device breakdown. Strategies such as surface passivation, interface smoothing, and low-defect synthesis have shown measurable benefits. However, quantitative correlations between specific scattering mechanisms and device performance are still underdeveloped. More systematic studies, including temperature-dependent transport analysis and noise modeling, are needed to fully understand and mitigate scattering in complex device architectures. Furthermore, the observed low photocurrent is due to the combination of Coulomb scattering and phonon scattering preventing the charge carrier's transportation to the electrode channel at high temperatures [68,69].

2.2. Strategies to overcome performance limitations

To systematically address the performance limitations of IR PDs, recent research has pursued a multilayered strategy that can be broadly categorized into three levels: (i) material-level modifications (e.g., doping, 2D materials), (ii) device-level architectural innovations (e.g., heterostructures, plasmonic coupling, dark current suppression), and (iii) system-level engineering approaches (e.g., advanced fabrication methods, metasurfaces, and integration techniques). This categorization is not necessarily indicative of historical development or maturity, but rather reflects a progression from foundational material tuning to complex device enhancements and integration frameworks. This framework reflects a progression from foundational material development to advanced functional and scalable systems. IR PDs spans multiple spectral regimes including near-infrared (NIR), mid-wave infrared (MWIR), and long-wave infrared (LWIR) each requiring semiconductors with appropriately narrow bandgaps to absorb photons efficiently in those ranges. Traditionally, this role has been fulfilled by narrow-bandgap materials such as mercury cadmium telluride (HgCdTe), indium antimonide (InSb), and lead chalcogenides like PbSe and PbS. These materials have established themselves as performance benchmarks for high-sensitivity applications due to their high absorption coefficients, tunable bandgaps, and excellent detectivity, particularly under cryogenic cooling conditions that suppress thermal noise and achieve background-limited IR detection.

However, despite their exceptional performance, these traditional materials suffer from several limitations that restrict their broader commercial use. HgCdTe, for example, is highly sensitive to stoichiometric variation and requires complex, high-cost epitaxial growth processes. InSb and PbSe offer strong mid-IR performance but often rely on cooling systems and are not readily compatible with complementary metal-oxide-semiconductor (CMOS) technologies [70,71]. Additionally, toxicity, environmental concerns, and difficulty in flexible or large-area integration remain persistent challenges. As a result, the field has seen a growing push toward alternative material systems that support room-temperature operation, mechanical flexibility, and cost-effective fabrication. One such class of emerging materials is solution-processed quantum dots (QDs) notably HgTe, PbS, and PbSe QD which offer bandgap tunability through quantum confinement effects and can be fabricated via low-cost, scalable deposition techniques. These QDs have demonstrated broadband IR absorption (from NIR to MWIR) and are being explored for applications in flexible, wearable, or printed IR sensors. Similarly, 2D materials such as MoS_2, Ta_2NiSe_5, and $ReSe_2$, as well as quasi-one-dimensional systems like $(TaSe_4)_2I$, exhibit thickness-dependent bandgaps, high responsivity, and enhanced light–matter interaction. Their van der Waals nature allows for the stacking of heterostructures without lattice-matching constraints, enabling custom-designed optoelectronic responses for IR detection [72].

In addition to individual materials, hybrid systems and photonic architectures have emerged as powerful tools to enhance IR performance. For instance, combining surface plasmon polaritons (SPPs) and surface phonon polaritons (SPhPs) in atomically thin heterostructures offers low-loss, dynamically tunable optical responses in the mid-IR to terahertz range, surpassing the capabilities of bulk materials. Colloidal indium tin oxide (ITO) nanocrystals have been shown to support tunable plasmonic resonances, providing strong near-field enhancement for IR absorption [73]. Meanwhile, nanostructured hybrid networks like Aerographite decorated with ZnO nanocrystals enable broadband photoresponse from the ultraviolet to IR, representing a class of materials with potential utility in multispectral imaging and broadband IR sensing [74]. To fully leverage these advanced materials, precise interface engineering and nanoscale characterization are essential. Emerging techniques such as AFM-IR, IR nanospectroscopy, and optical-photothermal IR-Raman microscopy now allow for chemical and structural mapping at the nanometer scale, offering crucial insights into phase distribution, defect density, and interfacial quality. These methods facilitate the optimization of charge transport pathways, minimize trap states, and ensure stable energy band alignment—all of which are vital for high-efficiency, low-noise IR detection.

2.2.1. Doping

Doping is one of the effective and quite easy ways to enhance the device's performance. The important requirement of this method is the compatibility between dopant and host material. Specifically, the constituent elements should exhibit an atomic radius difference of less than 15 %, and their electronegativities must be relatively similar to avoid significant mismatch. These are necessary conditions to substitute dopants for atoms in the host lattice and avoid morphology deformation. Dopants act as a role of donor or acceptor center that provides or receives excess charge carriers [75,76]. Due to the intermediate energy level formation within the band gap of the host materials and the effect of an enhanced electron-exchange potential, both the CB and VB energies are increased. Doping affects the band gap of materials leading to improved optical absorption and enhanced properties of PDs such as conductivity, defect states on structure, work function. To confirm experimental results, the calculation and simulation reports have been published. Jalaei et al. have designed and simulated a model of Se-doped monolayer BP and showed the obtained properties for application to fabricate near-Infrared (NIR) PDs [53]. Their calculations are based on DFT and the nonequilibrium Green's function (NEGF) to obtain the band gap values and evaluate the device performance of both pristine BP and monolayer BP doped with Se. The Se-doped BP photodetector, as presented through simulation in this work, exhibits a responsivity of approximately 0.75 μA/W at 4 μm under 0.0001 W cm^{-2} excitation intensity and moderate biasing conditions (Vg = 1 V, Vd = 0.5 V). While this suggests improved mid-IR absorption relative to pristine BP due to the reduction of the bandgap to ~0.4 eV, the absolute responsivity remains substantially lower than that of numerous experimentally realized van der Waals (vdW) heterostructure based PDs. For instance, BP/MoS_2 heterojunctions and $PdSe_2$-based hybrid devices have demonstrated responsivities above 500 mA/W with broadband sensitivity spanning

0.2–4.6 μm, further emphasizing the gap between theoretical predictions and practical device performance in the case of Se-doped BP. These disparities suggest that while Se-doping improves BP's absorption characteristics and IR responsivity in principle, the simulated device's performance must be validated experimentally and contextualized with respect to prevailing device architectures and integration strategies.

Equally important is the evaluation of key performance trade-offs that determine the applicability of these photodetectors in real-world scenarios. A recurring limitation in high-responsivity photodetectors is their inherently slow response time, a consequence of prolonged carrier lifetimes or interfacial trapping in layered or quantum dot-based structures. For example, MoS_2/graphene/WSe_2 p–g–n heterostructures exhibit increased responsivity with added graphene layers, but this also extends the carrier transit path and introduces mobility degradation, ultimately slowing the device's temporal response. A similar responsivity-speed trade-off is observed in TMD/0D hybrid systems, where ligands on quantum dots introduce resistive interfaces that hinder fast carrier transport.

Nevertheless, some recent developments aim to decouple this trade-off; for instance, MoS_2 hybridized with $CuInSe_2$ quantum dots has shown both ultrahigh responsivity (74.8 A W^{-1}) and drastically improved response times (0.8/1.5 s rise/decay), attributed to engineered depletion regions that suppress persistent photoconductance. Parallel to this, the detectivity (D*) of IR PDs is strongly impacted by noise performance, particularly dark current, which is elevated in narrow bandgap materials like BP [77]. Strategies such as type-II band alignment and band-offset engineering in $PdSe_2$-MoS_2 and BP/MoS_2/graphene pBp heterostructures have proven effective in reducing noise and increasing D* by minimizing carrier recombination and suppressing unwanted leakage currents. Moreover, the introduction of interfacial blocking layers (e.g., GeO_2 or Al_2O_3) has successfully lowered dark current in Ge- or TMD-based systems, although often at the expense of carrier injection efficiency and overall responsivity [78]. The optimization of these design parameters band alignment, interfacial quality, and contact engineering remains pivotal in balancing responsivity, speed, and detectivity. In this context, the current simulation-based performance of Se-doped BP PDs, while encouraging, requires further experimental validation and architectural innovation to achieve parity with state-of-the-art 2D heterostructure-based IR photodetectors. Thus, a comprehensive and quantitatively driven evaluation framework is essential to advance the rational design of high-performance IR PDs. Although Se doping in BP can influence its electronic structure, the observed photoresponse under 4 μm illumination is only 0.75 μA/W, which is insufficient for practical mid-IR applications. Furthermore, 4 μm lies in the mid-IR region, not near-IR, as sometimes misclassified. As a result, the band-to-band energy of Se-doped BP is 0.4 eV which is half that of a pristine BP sample. Under the illumination of a range of NIR wavelengths (from 3 μm to 5 μm), BP doped with Se exhibits a significant increase in absorption as a function of wavelength, and the simulated responsivity reaches 0.75 μA W − 1 at 4 μm light [79]. Therefore, PDs based on Se-doped BP has emerged as a potential candidate for NIR region. BP, a layered 2D material with remarkable optoelectronic versatility, has emerged as a highly promising candidate for photodetection in the mid-infrared (mid-IR) region, owing to its intrinsic anisotropy, high carrier mobility, and tunable direct bandgap. The bandgap of BP varies with layer thickness from approximately 2.0 eV in monolayer form to ~0.3 eV in the bulk enabling broadband optical absorption spanning from the visible to infrared spectrum. This tunability, coupled with its strong in-plane anisotropic behavior, makes BP not only suitable for broadband IR detection but also advantageous for polarization-sensitive optical systems. To evaluate its potential further, a comprehensive investigation combining density functional theory (DFT), finite-difference time-domain (FDTD) simulations, and electrical modeling was conducted to examine the influence of selenium (Se) doping on BP's electronic and optical properties, as well as its device-level performance in FET configurations.

Se-doping was found to substantially modify the electronic structure of BP, narrowing the bandgap from 0.88 eV (direct) in pristine monolayer BP to 0.4 eV (indirect) in the doped material. This shift effectively extends the material's absorption edge deeper into the mid-IR regime, enhancing its capability to detect photons in the 3–5 μm range. The simulations revealed a marked increase in optical absorption within this range, attributed to the reduced bandgap and increased refractive index, which together promote stronger light–matter interaction and prolonged photon residence time within the active layer. These characteristics are especially valuable for mid-wave infrared photodetection, where strong and selective absorption is essential for achieving high responsivity. On the electrical front, Se-doped BP retains the favorable charge transport characteristics of pristine BP, including high carrier mobility and pronounced gate tunability, both critical for phototransistor operation. A 12 nm-thick Se-doped BP-based FET was modeled and evaluated under varying illumination and gate bias conditions. The electrical measurements, including output (IDS–VDS) and transfer (IDS–VGS) characteristics, confirmed the formation of low-resistance ohmic contacts and the generation of photocurrent under IR illumination. The device exhibited a linear increase in photocurrent with increasing light intensity, demonstrating efficient generation and separation of electron-hole pairs. Most notably, the Se-doped BP FET achieved a responsivity of approximately 0.75 μA/W at a 4 μm wavelength under specified biasing conditions. This value, although moderate compared to traditional photodetector materials, reflects a significant enhancement over undoped BP devices operating in the same spectral window, underscoring the impact of doping in tuning optical response.

Otherwise, researchers have to control dopant composition because some previous publications have reported that excess doping can widen the band gap width [45,52]. This can be explained by the Burstein-Moss effect which the Fermi level lifts into CB due to spare carriers filling the lowest states of CB of host materials [80]. The inhibition of dark current in photodetectors through doping is primarily attributed to the Burstein-Moss effect. This phenomenon occurs when doping increases the carrier concentration, causing a shift of the Fermi level into the conduction band. The doping in IR PDs requires greater technical precision and clarity. Rather than an oversimplified overview, it is important to recognize that doping impacts device performance through distinct mechanisms, such as modulating carrier concentration, reducing contact resistance, and controlling recombination processes. For example, doping near metal contacts creates heavily doped regions that reduce the Schottky barrier width, significantly lowering contact resistance and enabling more efficient carrier injection and extraction, which directly improves photocurrent and reduces noise. Reducing contact resistance has emerged as a key strategy to enhance carrier injection and improve responsivity in IR photodetectors, particularly those based on 2D materials. Techniques such as work function engineering, interface passivation, and use of doped contact layers have led to significant improvements. Nevertheless, achieving ohmic or low-barrier contacts with high reproducibility remains difficult, especially for narrow-bandgap or ambipolar materials. In addition, trade-offs between contact resistance and interface stability need to be carefully balanced. Future research should prioritize scalable, low-temperature processes for contact optimization and explore novel interfacial layers that minimize Fermi level pinning. Additionally, carefully engineered doping profiles can generate built-in electric fields that enhance carrier separation and response speed. However, excessive doping can increase free carrier absorption and dark current, degrading detector sensitivity. Furthermore, the commonly mentioned Burstein-Moss effect, where heavy doping shifts the Fermi level and widens the apparent bandgap, is of limited practical relevance for IR PDs because it reduces infrared photon absorption and thus responsivity. Therefore, a balanced doping strategy aimed at optimizing conductivity and minimizing noise without compromising infrared absorption is crucial. A detailed and well-supported explanation of these effects is necessary to fully capture the challenges and strategies involved in doping engineering for IR PDs.

Fig.3 provides important insights into how doping can be used to

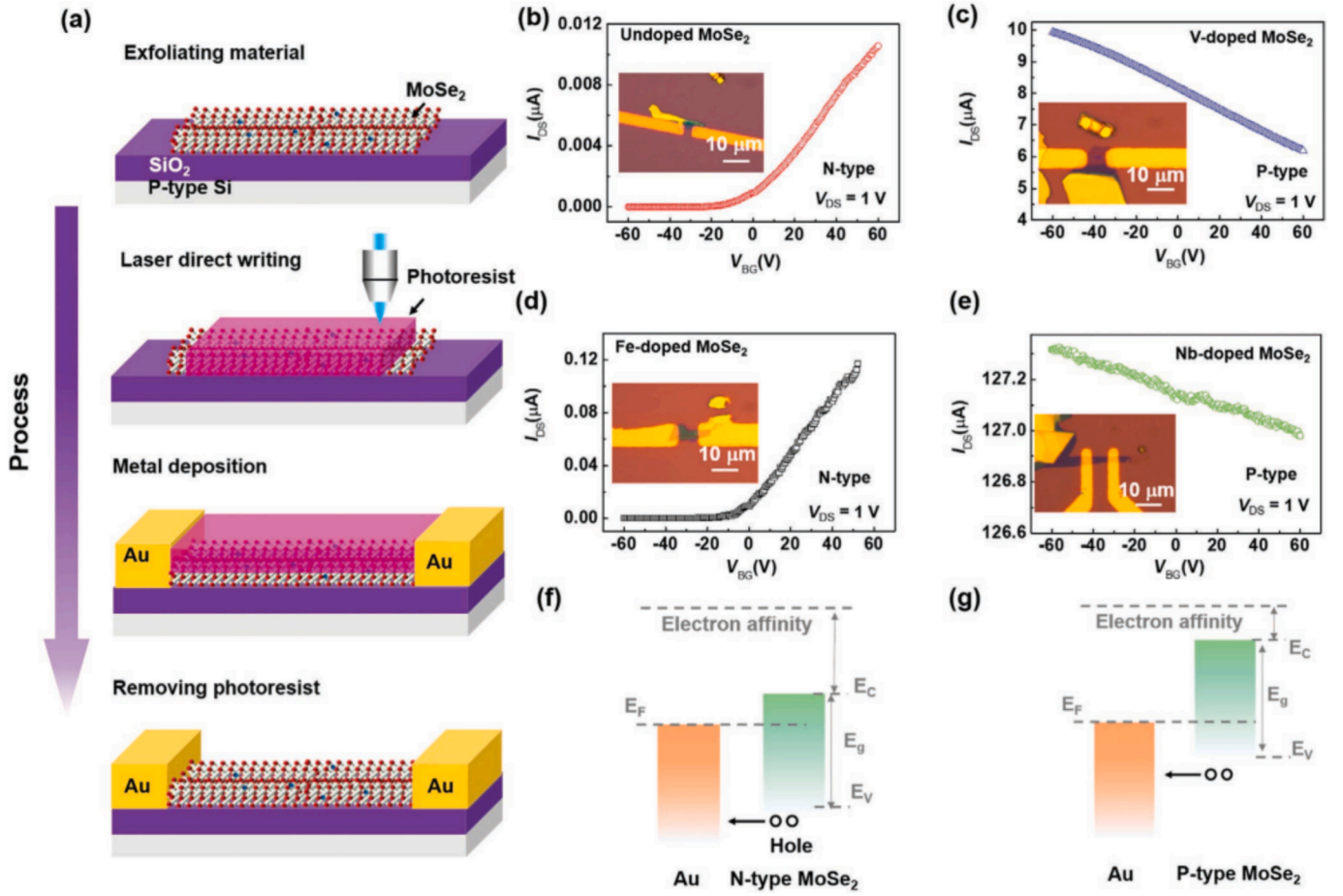

Fig. 3. (a) Schematic of $MoSe_2$ FET fabrication. **(b–e)** IDS–VGS curves of FETs based on undoped, V-, Fe-, and Nb-doped $MoSe_2$ (insets: optical images). **(f, g)** Schematics of Au contacts with n-type and p-type $MoSe_2$. Taken from [81] Copyrights© 2020 Wiley.

engineer the electrical properties of $MoSe_2$, a layered TMD, which is highly relevant for its application in IR PDs. Understanding and controlling the carrier type (n-type or p-type), mobility, and contact characteristics in $MoSe_2$ FETs emphasizing how different dopants (V, Fe, Nb) modulate carrier type, transport properties, and metal–semiconductor contact characteristic and directly impacts the design and performance of IR PDs, especially those relying on photogating, photoconductive, or photovoltaic mechanisms. In Fig.3a, the fabrication process of back-gated $MoSe_2$ FETs is schematically presented, typically involving exfoliated $MoSe_2$ flakes placed on a SiO_2/Si substrate, with patterned source and drain electrodes forming the device structure. Fig.3b shows the transfer characteristics (IDS–VBG) of an undoped $MoSe_2$ transistor, which exhibits typical n-type behavior, where electrons are the dominant charge carriers. The device displays a relatively low mobility of 2.3 $\times$ 10^{-2} cm^2 V^{-1} s^{-1} significantly below literature values primarily due to surface defects in the $MoSe_2$ flakes that introduce short-range carrier scattering. The threshold voltage (Vth) of −32 V and limited drain current also reflect high contact resistance at the metal–semiconductor interface, indicative of a Schottky contact with Au electrodes. Figs.3c to3e compare the IDS–VBG characteristics of $MoSe_2$ doped with V, iron Fe, and Nb. For V- and Nb-doped devices (Fig. 3c and e), the drain current increases as the gate voltage becomes more negative, indicating hole-dominated conduction and confirming a conversion to p-type behavior. This arises because both V and Nb have fewer valence electrons than molybdenum (Mo), and thus act as acceptor impurities when substituting Mo atoms in the lattice. These dopants trap electrons and enhance hole concentration, causing a significant shift in carrier type. Consequently, the on/off current ratio in these p-type devices differs drastically from that of the intrinsic n-type $MoSe_2$, since holes originally minority carriers now dominate conduction. The near-linear IDS–VBG curves observed are likely due to high doping efficiency, which increases hole density and minimizes gate modulation. V-doped $MoSe_2$ achieves the highest mobility among all samples at 6.2 cm^2 V^{-1} s^{-1}, while Nb-doped $MoSe_2$ reaches 2.3 cm^2 V^{-1} s^{-1}. Notably, no clear threshold voltage could be extracted for these p-type devices due to their inability to fully switch off within the tested gate voltage range. In contrast, Fe-doped $MoSe_2$ (Fig. 3d) retains n-type characteristics. The IDS increases with more positive gate voltage, consistent with electron-dominated conduction. This is because Fe, having more valence electrons than Mo, donates additional electrons, shifting the Fermi level closer to the conduction band and raising electron concentration [81]. The threshold voltage of −42 V, more negative than the undoped case, reflects this Fermi level shift. However, the on/off ratio remains relatively unchanged compared to the intrinsic device, as the small increase in electron concentration does not significantly alter the carrier profile in an already n-type system. The mobility for Fe-doped $MoSe_2$ is moderate at 0.62 cm^2 V^{-1} s^{-1}. Finally, Fig.3f and g schematically depict the contact interfaces between Au and both n-type and p-type $MoSe_2$. Fig. 2f illustrates the Schottky barrier formed at the Au/n-type $MoSe_2$ interface, which arises due to a work function mismatch—specifically, the higher work function of n-type $MoSe_2$ relative to Au—creating a potential barrier that impedes efficient electron injection. This explains the limited current and contact resistance observed in undoped and Fe-doped devices. Conversely, Fig.3g shows an Ohmic contact between Au and p-type $MoSe_2$. In this case, the lower Fermi level of p-type $MoSe_2$ (due to hole dominance) aligns better with Au, reducing the barrier and

enabling more efficient hole injection. This contact behavior contributes significantly to the improved electrical performance of the V- and Nb-doped p-type devices.

The synergistic combination of doping, ferroelectric modulation, and 2D materials represents a promising strategy for developing high-performance, low-noise photodetectors. Fig. 4. provides a clearer visualization of how various dopants impact device performance, aligning with the mechanisms discussed in the review (e.g., substitutional doping, Burstein-Moss effect, defect-state engineering, and others). There are several dopants classified into two main types: inorganic and organic, as listed in Table 1 [1,45,81–100]. It can be seen that dopants exhibit the enhanced performance of IR PDs when compared with pristine materials and have more space to research. Beyond doping-based material tuning, 2D materials and their heterostructures offer additional pathways to enhance photodetector performance through quantum confinement, interface engineering, and tailored band structures, as detailed in the following section. While the literature demonstrates a broad array of dopants and performance enhancements for IR photodetectors, certain trends can be distilled to guide future research. Transition metal dopants such as V, Nb, and Fe consistently improve carrier mobility and modulate the Fermi level to favor either p- or n-type conduction, thereby enhancing responsivity and reducing contact resistance. Halogen dopants (e.g., Cl, I) are effective in adjusting band alignment and defect states, often leading to improved response speed and reduced noise. Organic dopants such as benzyl viologen offer flexibility and are especially suited for hybrid or wearable systems, though often at the cost of stability and scalability. Across studies, responsivity gains range from modest improvements (~0.5 μA/W) to several orders of magnitude (>10^4 A/W), depending on the material system, device architecture, and dopant incorporation method. However, common trade-offs include increased dark current at high dopant concentrations (due to free carrier absorption), slower response times in highly resistive interfaces, and diminished absorption in cases where the Burstein-Moss effect widens the bandgap. Achieving optimal performance thus requires a careful balance selecting dopants and concentrations that enhance conductivity and absorption while minimizing recombination and leakage. A unified understanding of doping mechanisms such as carrier modulation, barrier tuning, and trap-state suppression is critical for rationally designing next-generation IR PDs with tailored spectral sensitivity and low noise. Beyond doping-based material tuning, 2D materials and their heterostructures offer additional pathways.

2.2.2. 2D Materials and heterostructures

2.2.2.1. Precision nanofabrication and optimization of low-dimensional materials. Low-dimensional materials bring researchers various options for the architecture design of a high-performance design due to exceptional inherent features of the spatial structure used (Table 2 and Fig. 5) [102–126]. Zero-dimensional (0D) nanostructures (e.g quantum dots, nanoparticles, nanocages, nanospheres, etc.) are found to have the ability to confine the electron in all three spatial dimensions and provide attractive fundamental physical properties such as the quantum confinement effect, and the Coulomb blockade effect [127]. Based on the size of quantum dots, confined electrons have higher energy than the electrons in the bulk counterpart. In the quantum dot structure, electrons are completely confined in all three spatial dimensions, so the scattering of electrons is enhanced at the boundaries of the dot [127]. One-dimensional (1D) nanomaterials, such as semiconductor nanorods, have widely attracted interest among the research community since they usually have special shapes, a simple synthesis process, a high surface-to-volume ratio, abundant chemicals in nature, cost-effective (small quantity of material), and a highlight point is that in the optoelectronic field they can provide a direct path for the excited charge carriers to move from the active components to the electrodes [128,129].

Starting from the first production of single-layer graphene through the Scotch Tape method by Andre Geim and Konstantin Novoselov in 2004 and the Nobel Prize in Physics 2010 for this achievement [130] more and more 2D nanomaterials have been discovered. 2D materials have become a new trend in optoelectronic devices due to their large surface area, and exceptional optical and electrical properties [131,132]. The low-density surface states of dangling bonds of 2D materials can minimize performance degradation caused by surface states and are easily combined with other photonic structures such as waveguides [133] to enhance the light absorption capability of the active materials. In addition, a prominent feature of 2D materials is the existence of weak Van der Waals bonds instead of conventional covalent bonds in the out-of-plane direction of the material [134,135]. Therefore, layers of 2D materials can be easily stacked on top of each other in the longitudinal direction to create heterostructures without lattice mismatch at the interface which occurs in bulk materials [136]. Another

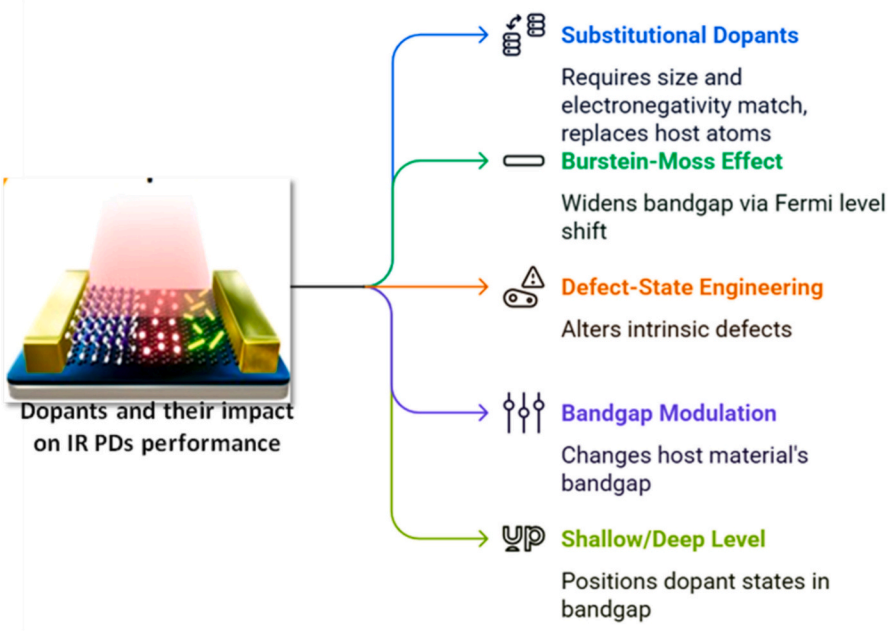

Fig. 4. Dopants and their impact on IR PDs performance.

Table 1
Species of dopant that used for IR PDs in previous publications.

Dopant	Structure	Performance	Ref.
Au	Au NPs-doped single-walled carbon nanotube–germanium (SWCNT/Ge)	λ = 1500 nm: R = 476 m μA/W; D* = 1.0 × 10^{12} Jones	[1]
Au	InSe/ Au-doped InSe	λ = 980 nm, 1 V: R = 7870 μA/W; D* = 1.5 × 10^{13} Jones	[97]
B	B-doped Si/Ge QDs	λ = 3.4 μm: R = 0.83 μA/W; D* = 8.1 × 10^{10} Jones	[96]
Be	Be-doped AlAsSb/GaSb	λ = 1.3 μm: R = 0.13 A W^{-1}	[101]
Cl	$ReSe_2$/ Cl-doped $ReSe_2$	λ = 980 nm: R = 4.96 × 10^3 μA/W; τ_r = 1.4 ms and τ_f = 3.1 ms	[91]
Co	Co-doped CdS/ZnO	λ = 820 nm: R = 0.22 μA/W; D* = 3.1 × 10^{11} Jones; EQE = 24.3 %; τ_r = 7 s and τ_f = 40 s	[94]
Inorganic type			
Fe	Fe-doped $MoSe_2$	λ = 1550 nm: I_{ph} = 0.8 nA	[90]
H	H-doped single-crystal VO_2 nanoparticles	λ = 780 nm: R = 35,280 μA/W; D* = 1.12 × 10^{13}; τ_r = 0.6 ns and τ_f = 2.5 ns	[92]
Mn	Mn-doped $CuInSe_2$	λ = 780 nm: R = 30 m μA/W; D* = 4.2 × 10^{12} Jones; τ_r = 1.9 μs and τ_f = 0.76 μs	[89]
N	N-doped multiwalled carbon nanotubes (MWCNT)	λ = 1550 nm: R = 0.388 μA/W; EQE = 31.1 %; τ_r = 11 s and τ_f = 9 s, λ = 1064 nm: R = 0.312 μA/W; EQE = 36.3 %; τ_r = 10.4 s and τ_f = 14 s	[87]
Te	p-type Si/ n-type Te-doped Si	λ = 1 μm: D* = 3.2 × 10^{12} Jones λ = 1.12 μm: R = 79 mA/W λ = 1.55 μm: R = 0.3 mA/W	[85]
Te	Te-doped GaAsSb NWs	λ = 1.2 μm: R = 580–620 μA/W; D* = 1.2–3.8 × 10^{12} Jones	[84]
Te	Te-doped GaAsSbN NWs	λ = 1100 nm: R = ~3800 μA/W; D* = 3.2 × 10^{10} Jones	[83]
V	V-doped MoS_2 with Mo vacancy	λ = 2240 nm: R = 2800 m μA/W; D* = 1.85 × 10^{10} Jones; τ_r = 27 s and τ_f = 31 s	[82]
V	V-doped $MoSe_2$	λ = 1550 nm: I_{ph} = 73.2 nA λ = 10 μm: R = 1.26 m μA/W	[81]
W	W-doped VO_2 NWs	λ = 980 nm: R = 21.4 m μA/W; τ_r = 228 ms and τ_f = 206 ms	[99]
Organic type			
Benzyl Viologen (BV)	p-type Al_2O_3-BP/ n-type BV- doped BP	λ = 1.47 μm: R = 180 m μA/W (V = 5 mV, P = 50 W cm^{-2}); τ_r = 15 ms and τ_f = 30 ms;	[98]
Benzyl Viologen (BV)	n-type BV-doped PMDPP3T:$PC_{61}BM$	λ = 850 nm: R = 0.56 μA/W; D* = 5.56 × 10^{12} Jones; EQE = 87 %	[45]
Polyacrylic acid (PAA)	PAA-doped Graphene/Ge	λ = 1550 nm: R = 1.27 μA/W; D* = 9.6 × 10^9 Jones	[100]
Tris(pentafluorophenyl) borane (BCF)	p-type BCF-doped PMDPP3T:$PC_{61}BM$	λ = 850 nm: R = 0.56 μA/W; D* = 5.11 × 10^{12} Jones; EQE = 86.1 %; τ_r = 126 μs and τ_f = 18 μs	[45]

interesting feature of 2D materials is their smaller volume compared to 3D materials, leading to strong light-matter interactions per unit volume and facilitating photoexcitation of electron-hole pairs [79,137]. Following the success of graphene, the family of 2D materials has widely been exploited for the next generation of IR PDs. Relying on the significant effort of researchers, more and more potential 2D nanostructures are expected to be applied to real-world applications. 2D materials possess outstanding properties consisting of high charge carrier dynamic, tunable optical band gap, large specific surface area, high mobility, and flexibility. [138–141] For example, Li et al. proposed a PD based on a 2D layered material Bi2O2Se which has weak electrostatic forces instead of van der Waals between the Bi2O2 and Se layers. This unique lattice allows the band gap of the material to reach a suitable value of 0.8 eV according to its absorption ability in the IR region [142]. These devices exhibited exceptional performance with responsivity of 6.5 A/W, detectivity of 8.3 × 10^{11} Jones, and response time of 3.2 ms under 808 nm light illumination at room temperature (300K). In a different study, Liu et al. used the unique properties of SnTe of large surface-to-volume ratio, high carrier mobility, and low carrier scattering to develop a NIR PDs structure on mica substrates with high-performance parameters under 980 nm laser exposure for flexible devices (R = 698 mA/W, D* = 3.89 × 10^8 Jones, τ_r = 1.45) [142,143]. In addition to common 2D nanostructures (such as graphene, hexagonal boron nitride (hBN) [144,145], BP [146,147], TMDs have become a major research focus due to their diverse chemical compositions and highly tunable properties [148,149] TMDs generally take the form MX_2, where M is a transition metal and X is a chalcogen (Se, S, or Te). Each layer consists of strong covalent bonds between the metal and chalcogen atoms, giving rise to excellent mechanical strength [150]. These layers are stacked together via weak van der Waals forces, forming a layered crystal structure [151]. This unique combination of bonding and stacking offers substantial potential for enhancing the performance of IR PDs.

Currently, researchers have used sophisticated and highly precise manufacturing methods to synthesize low-dimensional nanomaterials with high purity and good contact surfaces to create PDs with high performance. Methods based on the bottom-up approach have widely been used that allow the development of complex structures from small molecules of the initial components. The most common methods of the bottom-up approach are chemical vapor deposition (CVD), sol-gel, and self-assembly techniques [152–155]. In contrast to bottom-up, top-down nanofabrication is composed of advanced techniques such as lithography, CVD, physical vapor deposition (PVD), and so on which scale down from large materials to the nanoscale [156–160]. The top-down approach is efficient for large-scale production due to its highly precise and prompt control [161–168]. In addition, the template-based hybrid nanofabrication takes advantage of both bottom-up and top-down methods, and it often uses templates to control the assembly of nanomaterials to design the expected device structures [169,170].

Despite their exceptional optoelectronic properties, the integration of TMDs such as MoS_2 and layered metal chalcogenides like $PdSe_2$ into IR PDs architectures presents several unresolved challenges. MoS_2, for instance, offers a tunable bandgap and high on/off ratios, yet suffers from nonuniformity in large-area films synthesized via CVD. These films often exhibit grain boundaries, sulfur vacancies, and surface roughness, all of which introduce trap states that degrade charge transport and increase noise. Contact resistance remains another major bottleneck; forming low-barrier, stable ohmic contacts to MoS_2 is notoriously difficult due to Fermi level pinning and interface contamination, often requiring metal work function tuning or insertion layers. $PdSe_2$, a relatively newer layered semiconductor, has garnered attention due to its air-stable, narrow-bandgap characteristics suitable for LWIR photodetection. However, it faces other material-specific hurdles: it is not yet widely supported by scalable synthesis protocols, with most demonstrations relying on mechanical exfoliation or small-scale transfer methods. This limits its potential for wafer-scale fabrication and batch

Table 2
Representative 2D heterostructures-based IR PDs and their performances.

2D heterostructures	Fabrication Method	Performances of IR PDs	Ref.
2D/0D			
Graphene/HgTe	Wet transfer	λ = 2.5 μm; R = 6.5 mA/W; D* = 10^9 Jones	[104]
$SnSe_2/SnO_2$	Drop casting	IR; R = 6.51 mA/W; τr = 0.93 s.	[105]
2D/1D			
Graphene/InAs NWs	Wet transfer	λ = 1 μm; R = 0.5 A/W; Ion/Ioff = 5 × 10^2.	[106]
MoS_2/WS_2 NRs	Hydrothermal	λ = 1064 nm; D* = 17 × 10^6 Jones.	[107]
2D/2D			
MoS2/BP	Dry transfer	λ = 1550 nm; R = 153.4 mA/W; D* = 2.13 × 10^9 Jones; τr = 15 μs and τf = 70 μs	[102]
Graphene/BP	Dry transfer	λ = 1550 nm; Iph = 45 μA; R = 1.3 × 10^3	[108]
$InSe/PdSe_2$	Dry transfer	λ = 1250 nm; R = 161 A/W.λ = 1400 nm; R = 120 A/W.λ = 1550 nm; R = 90.5 A/W.	[177]
WS_2/Si	Wet transfer	λ = 980 nm; R = 224 mA/W; τr = 16 μs and τf = 29 μs.	[178]
$MoTe_2$/Graphene	Dry transfer	λ = 1064 nm; R = 970.82 A/W; D* = 1.55 × 10^{11} Jones; G = 4.69 × 10^8; τr = 78 ms and τf = 375 ms	[179]
BP/Bi_2O_2Se	Polystyrene transfer method	λ = 1.3 μm; Iph = 17 μA; R = 0.89 A/W; QE = 84 %; D* = 1.14 × 10^{10} Jones.	[110]
Graphene/$MoTe_2$/ Graphene	Dry transfer	λ = 1064 nm; R = 110 mA/W; EQE = 12.9 %; τr = 24 μs and τf = 46 μs	[111]
Graphene/$PdSe_2$/Ge	Wet transfer	λ = 980 nm; R = 691 mA/W; D* = 1.73 × 10^{13} Jones; τr = 6.4 μs and τf = 92.5 μs	[113]
γ-InSe/Ge	Dry transfer	λ = 1550 nm; R = 9.78 A/W; D* = 5.38 × 10^{11} Jones; τr = 46 μs and τf = 32 μs	[114]
Graphene/$MoTe_2$/ Graphene	Wet transfer	λ = 1064 nm; R = 635 A/W; D* = 2.26 × 10^9 Jones; τr = 19 μs and τf = 34 μs.	[115]
$SnTe/Bi_2Se_3$	Ex situ PVD	λ = 1064 nm; R = 635 A/W; D* = 2.26 × 10^9 Jones; τr = 19 μs and τf = 34 μs.	[116]
$Bi_2O_2Se/MoSe_2$	Wet transfer	λ = 780 nm; R = 0.413 A/W; D* = 3.7 × 10^{11} Jones.	[117]
WSe_2/α-In_2Se_3	Dry transfer	λ = 980 nm; R = 2.21 A/W; D* = 9.52 × 10^{10} Jones; τr = 4.3 ms and τf = 6.4 ms.	[118]
Te/MoS_2	Dry transfer	λ = 1550 nm; R = 4 A/W; D* = 3.4 × 10^9 Jones.	[119]
Bi_2O_2Se/InSe	Dry transfer	λ = 980 nm; R = 13.3 mA/W; D* = 2.06 × 1011 Jones.	[120]
Graphene/WS_2/n-Si	Thermal Evaporation Deposition	λ = 800 nm; R = 54.5 A/W; D* = 4.1 × 1012 Jones; τr = 45 μs and τf = 210 μs.	[121]
2D/3D			
$PdSe_2$/CdSe	Wet transfer	λ = 10.6 μm; R = 324.7 mA/W; D* = 3.3 × 10^{12} Jones; Ion/Ioff = 2.8 ×10^5; τ_r = 4.9 μs and τf = 8.3 μs	[122]
WS_2/AlOx/Ge	Dry transfer	λ = 1550 nm; R = 634.5 mA/W; EQE = 50.8%; D* = 4.3 × 10^{11} Jones; τ_r = 9.8 μs and τ_f = 12.7 μs.	[123]
WS_2/ Si	Wet etching	λ = 980 nm; R = 20 mA/W; D* = 4.3 × 10^{13} Jones; τ_r = 4.5 μs and τf = 21.7 μs (V = 0V).	[124]
WS_2/pyramid Si	Wet transfer	λ = 980 nm; R = 182 mA/W; Ion/Ioff = 2.6 × 10^6; D* = 3.7 × 10^{13} Jones; τ_r = 5.2 μs and τf = 22.3 μs (V = 0V).	[125]
BP/HgCdTe	Dry transfer	λ = 4.3 μm; R = 193 mA/W; Ion/Ioff = 104; D* = 7.93 × 10^{10} Jones.	[126]
MoS_2/PbSe	Wet transfer	λ = 808 nm; R = 19.7 A/W; Ion/Ioff = 102; D* = 2.65 × 10^{10} Jones.	[103]

processing. Moreover, its surface and interface chemistry under high-temperature or prolonged operational stress is not yet fully understood, raising concerns about long-term device stability and environmental tolerance. Integration with CMOS platforms presents additional complexity for both MoS_2 and $PdSe_2$. The high processing temperatures of back-end-of-line (BEOL) CMOS fabrication are often incompatible with these materials, which degrade or delaminate above ~400 °C. Additionally, cross-contamination between chalcogenide species and silicon-based dielectrics must be carefully mitigated, requiring the introduction of diffusion barriers or passivation layers. Without addressing these factors, the excellent lab-scale performance metrics (such as responsivity >1 A/W or D* >10^9 Jones) achieved using these materials may not translate into commercially viable IR sensor arrays.

2.3. Architecture design of 2D heterostructures

Simultaneously, the heterostructure formation in order to combine individual properties of 2D materials and different low-dimensional materials has attracted more attention to be studied deeper. It can open a new approach to improve the performance of previous IR PDs designs that are based on only one material [171]. Up until now, designing heterostructures between 2D and other low-dimensional materials has been introduced as the most effective to enhance the performance of IR PDs. By combining the unique properties of individual materials, PD operation can overcome the natural obstacles of the individual materials via device compositions and extend the PD application range. The difference between two combined materials can help improve the performance of devices significantly [172,173]. The architectural design of 2D heterostructures plays a vital role in enhancing the performance of infrared photodetectors by enabling efficient charge separation, tailored band alignment, and reduced recombination losses. Vertical van der Waals heterostructures, formed by stacking atomically thin layers such as MoS_2, WSe_2, and graphene, offer clean interfaces and strong interlayer interactions. Type-II band alignment facilitates spatial separation of photo-generated carriers, improving responsivity and carrier lifetime. Incorporating transparent electrodes like graphene enhances light absorption and charge

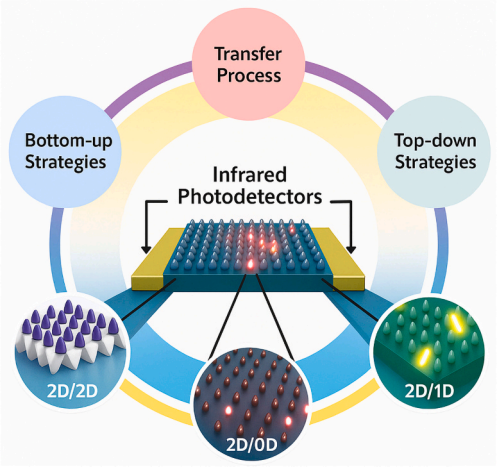

Fig. 5. Schematic of low-dimensional materials and nanofabrication procedure for IR PDs.

collection. Additionally, interface engineering, strain modulation, and integration of tunneling barriers or dielectric layers further improve signal-to-noise ratio, making 2D architectures highly promising for next-generation IR sensing applications (Fig. 6).

The high potential barrier and the formation of a built-in electric field at the interface play a critical role in separating photogenerated electron-hole pairs. This separation not only prevents early recombination but also extends the carrier lifetime, resulting in an enhanced photocurrent. Furthermore, IR PDs in 2D materials and their heterostructures operates through a combination of interdependent mechanisms, which are highly influenced by the selection of materials and the design of the device architecture. The process typically begins with the absorption of IR light by a 2D material that possesses a suitable bandgap such as BP or certain TMDs, including $MoTe_2$ and WSe that can efficiently absorb photons in the IR spectrum. Upon absorption, electron-hole pairs are generated, either as free carriers or excitons, depending on the intrinsic properties of the material. For efficient photodetection, these carriers must be swiftly separated and transported to avoid recombination losses. In 2D heterostructures, this separation is effectively facilitated by built-in electric fields at the interface, which originate from work function differences between materials or from p-n junction formation. These internal fields not only support carrier dissociation but also enhance directional carrier transport, contributing to improved detector sensitivity and performance. These internal fields drive the spatial separation of electrons and holes across the hetero-interface, enhancing carrier collection. Moreover, the integration of complementary 2D materials can lead to synergistic effects that further boost performance. For example, graphene can provide ultrafast carrier transport due to its high mobility, while TMDs offer strong light absorption, creating a hybrid system that leverages the strengths of each material. Additionally, band alignment engineering plays a critical role, where type-II heterojunctions are often favored for efficient carrier separation. Tailoring these alignments through material selection or external biasing enhances charge transfer and minimizes energy barriers [56,146,174–176]. The geometry of the heterostructure whether vertical or lateral also influences the detection mechanism, with vertical stacks benefiting from strong interlayer fields and lateral designs offering better planar integration. Together, these factors define the fundamental photodetection process in 2D materials, and optimizing them is key to advancing the performance of next-generation IR PDs. In addition, the disparity in the energy levels of the conduction and valence bands of the materials can exhibit different results depending on the characteristics of the used materials. Fig. 7 presents the overview of responsivity versus various wavelengths of 2D materials heterojunction PDs [15].

2.3.1. *Dark current reduction*

Dark current is defined as the current obtained by electrodes when there is no incident light falling on the PD. There are several possible sources of dark current in IR PDs listed such as the Shockley-Read-Hall effect in the depletion region of the heterostructure, surface leakage current at the surface of semiconductors due to defect density, thermionic emission, field-assisted emission, ground state sequential tunneling. In addition, Dark current poses a major limitation to the sensitivity, noise performance, and overall efficiency of IR PDs. Understanding the various mechanisms contributing to dark current is

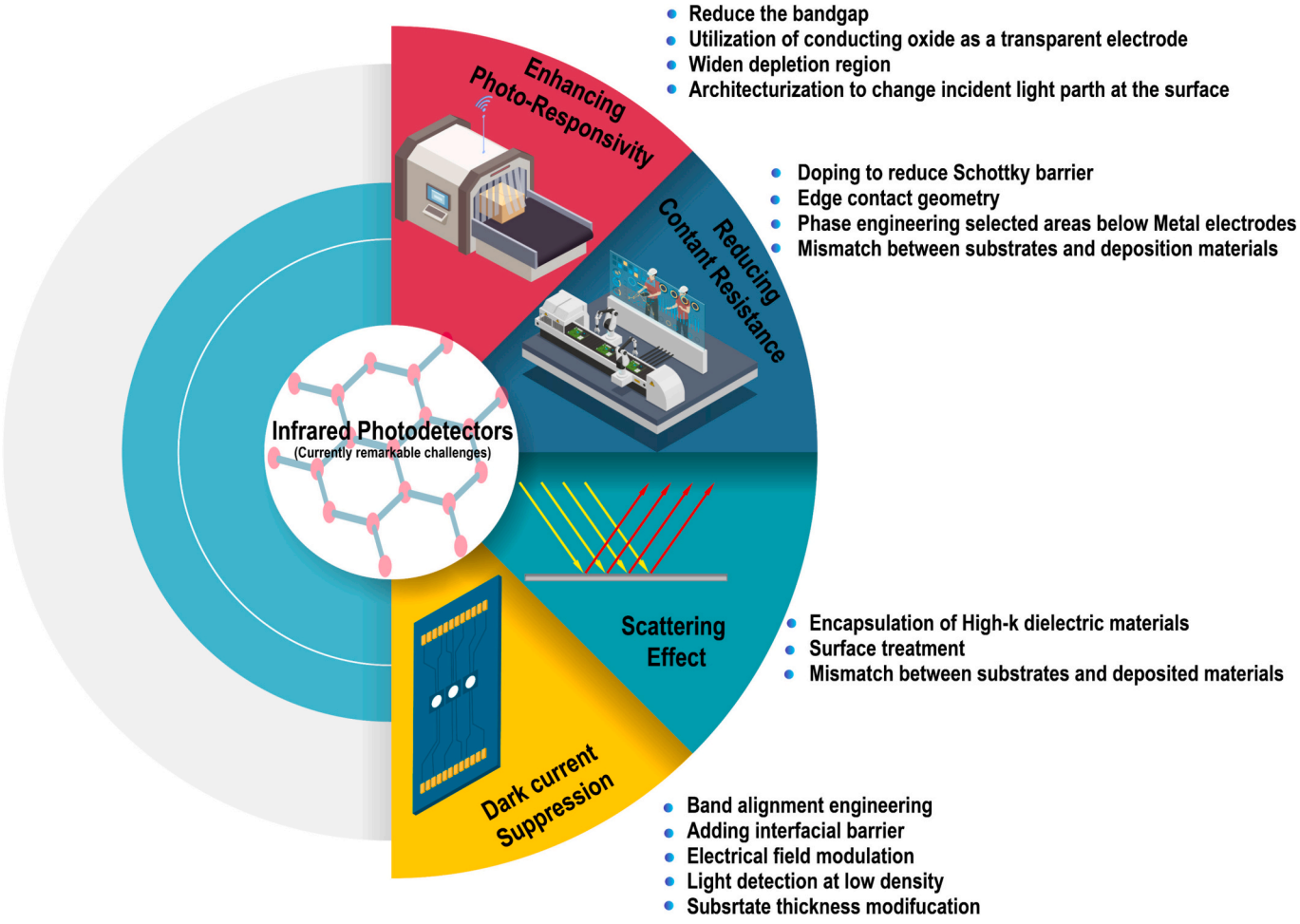

Fig. 6. 2D heterostructure design enhances charge separation and IR detection.

essential for devising strategies to suppress it and improve photodetector performance across diverse material platforms and device architectures. One of the most prevalent sources of dark current is defect-related conduction. In GeSn-based photodetectors, for instance, low-temperature epitaxial growth and lattice mismatches with substrates can introduce a high density of structural defects. These defects act as generation-recombination centers that facilitate unwanted charge carrier generation, particularly under low-Sn compositions. As the Sn content increases, the dominant dark current mechanism shifts toward generation current from the bulk material. Similarly, perovskite-based IR PDs suffer from substantial dark current due to uncontrolled charge carrier injection, defect traps, and morphological instability in the photoactive layers. These effects are closely linked to the film quality and the specific configuration of the device stack, such as interfaces between layers and electrode materials [180–182]. Trap-assisted dark current is another critical contributor, especially in organic and hybrid IR PDs. Imperfections in the active layer or at interfaces can form trap states that enable thermally activated carrier generation. These trap-assisted processes lead to elevated noise levels and reduced detectivity. Therefore, minimizing trap densities through material purification, interface passivation, or optimized fabrication techniques has been shown to systematically reduce dark current in these systems [183]. Tunneling and leakage currents also play a significant role, particularly in narrow-bandgap or type-II superlattice photodetectors such as InAs/GaSb systems. In these devices, carrier tunneling can occur across the junction even in the absence of illumination, especially under high bias or high doping conditions. The superlattice period and doping concentration critically influence the extent of tunneling, making the control of structural parameters an important design consideration for minimizing dark current [184]. Another often overlooked but increasingly important contributor is surface dark current, particularly in miniaturized III-V IR PDs [185]. As device dimensions shrink, surface effects become more dominant compared to bulk conduction mechanisms. Surface recombination, unsaturated dangling bonds, and unpassivated edges create leakage pathways that contribute to dark current [186–190]. Despite advances in bulk defect engineering, surface dark current mechanisms remain insufficiently understood and require further study to develop effective passivation techniques and device structures that can mitigate these effects. The dark current is one of the factors that limit IR device performance because it determines the highest possible operating temperature and power consumption of PDs [55] Therefore, reducing the dark current is one of the main missions for scientists when proposing to enhance the performance of IR PDs. In heterostructured systems, the interfacial potential barrier plays a crucial role in significantly suppressing dark current. This barrier height can be effectively modulated through better alignment of the constituent materials' Fermi levels. Photodetectors incorporating multilayer $PdSe_2$ and Pt/Au electrodes have demonstrated enhanced Schottky barrier heights, contributing to a substantial reduction in dark current [178,179,182,191].

However, this large resistance at the contact between an active material and electrodes decreases the photogenerated carrier collection so the device photoresponse decreases. However, the photo-to-dark current ratio of the $PdSe_2$ PDs is still relatively small since there is no considerable difference in device the device response with and without 10.6 μm light exposure. To this end, Long et al. approached a strategy to build a heterostructure based on weak Van der Waals forces between 2D nanomaterials. In detail, p-type $PdSe_2$ is combined with n-type MoS_2 to form a Van der Waals heterostructure junction, and the built-in electrical field at the interface will help reduce the dark current of PDs by deflecting electrons in a certain direction. The IR PDs based on graphene nanowalls (GNWs) on a silicon substrate with the existence of irregular Au nanoparticles (NPs) were proposed. The introduction of Au NPs ensures that the dark current is not too large and it also helps to adjust the work function of GNWs leading to a decrease in the potential barrier

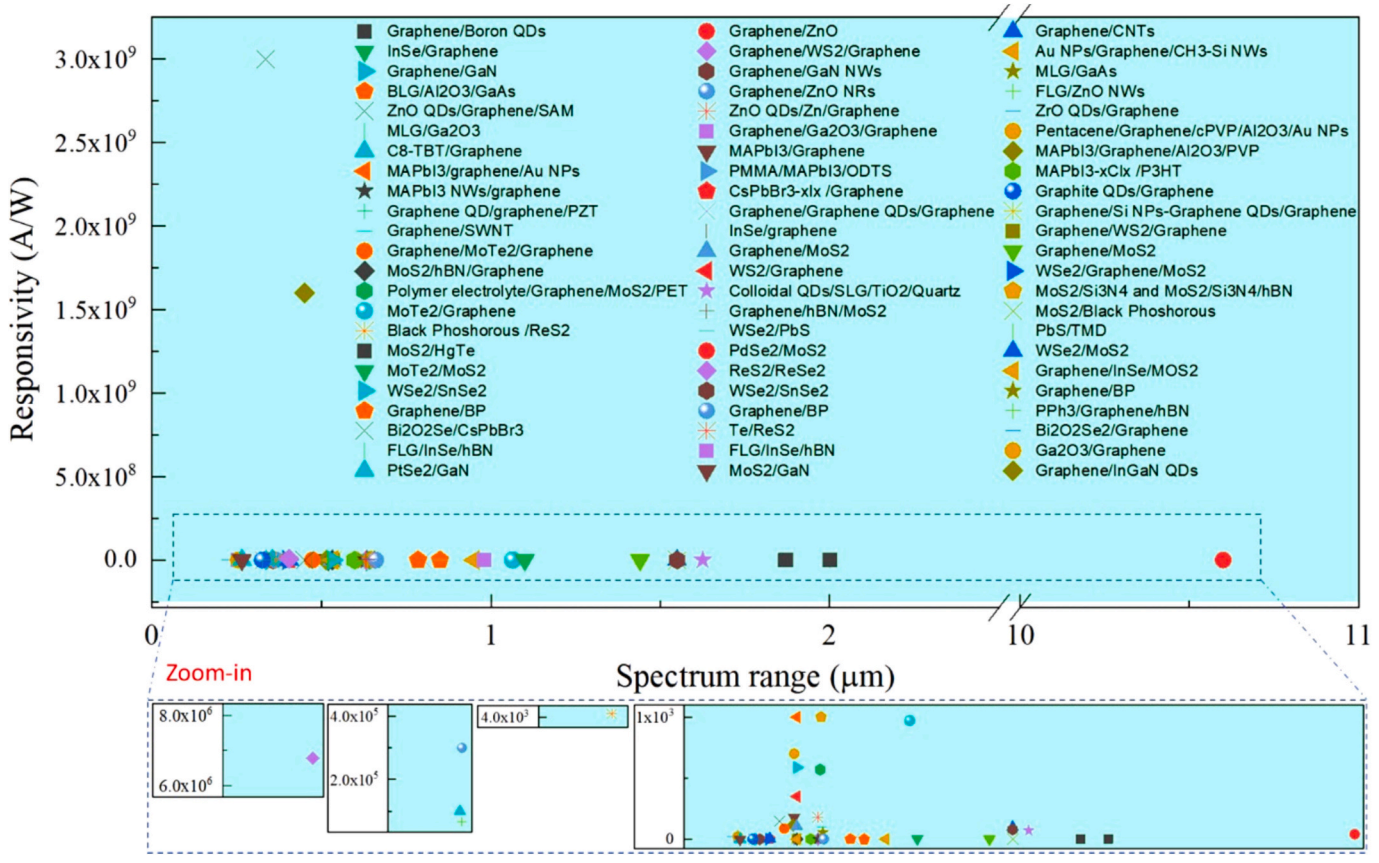

Fig. 7. Overview on responsivity of PDs using 2D heterostructures. Reproduced with permission from ref. [15] Copyright 2022 American Chemical Society.

height of this nanostructure. Liu et al. have compared the photoresponse of GNWs/Si, Au/GNWs/Si, and GNWs/Au/Si structures, respectively, and realized that PDs based on GNWs/Au/Si exhibit the lowest dark current at zero bias voltage and the largest photocurrent under 1550 nm illumination [192]. Up to now, many research teams have made a huge effort to study another method that can bring benefits in both dark current reduction and device performance improvements. Ferroelectric materials can eliminate dangling bonds and interface traps induced by charged impurities when they act as a passivation layer [193]. The integration of ferroelectric materials with 2D semiconductors such as MoS_2, WSe_2, and $MoTe_2$ has proven to be a highly effective strategy for improving photodetector performance [194–197]. This combination utilizes the spontaneous polarization inherent in ferroelectric materials to generate an internal electric field that significantly enhances charge carrier dynamics at the heterojunction interface. The built-in field facilitates the efficient separation and transport of photogenerated electron–hole pairs, minimizing recombination losses and resulting in increased photoresponsivity, enhanced external quantum efficiency (EQE), and faster response times [198–200]. Notable examples include photodetectors based on 2D ferroelectric perovskites like PMA_2PbCl_4, which exploit the combined effects of ferroelectricity, pyroelectricity, and photoconductivity known as the ferron pyro phototronic effect [201,202]. These devices exhibit high sensitivity and operate efficiently without external power sources. Similarly, α-In_2Se_3/Si heterojunctions leverage the room-temperature ferroelectric properties of α-In_2Se_3 to generate a strong depolarization field, enabling effective carrier separation and ultrafast photoresponse, making them ideal for high-speed applications [203]. Beyond enhancing charge separation, ferroelectric materials serve as effective passivation layers. They mitigate interface traps and eliminate dangling bonds typically caused by impurities or surface defects in 2D materials. This passivation reduces dark current and electronic noise, improving both the signal-to-noise ratio and overall device stability. Moreover, ferroelectric polarization allows for dynamic modulation of the band structure at the interface, enabling band bending, Fermi level tuning, and reconfigurable optoelectronic behaviors such as switchable photoresponse and spectral sensitivity [203]. This non-volatile band engineering further contributes to device reliability. Crucially, the internal electric field from ferroelectrics enables self-powered operation, an advantage for low-power, autonomous sensing platforms [202]. Altogether, the integration of ferroelectric materials with 2D semiconductors offers a versatile and robust pathway to developing high-performance photodetectors for emerging flexible, wearable, and intelligent optoelectronic systems [204–206]. Moreover, ferroelectric materials serve as effective passivation layers by removing interface traps and dangling bonds caused by charged impurities.

Zhang et al. have used poly(vinylidene fluoride-trifluoroethylene) (P(VDF-TrFE)) to cover and isolate the surface of InSb nanosheets (NSs) devices from the air [207]. Since P(VDF-TrFE) is a ferroelectric polymer film, it also acts as the role of the gate dielectric stack which leads to the suppression of the dark current significantly, and decreases the response time of the PDs. The existence of a passivation layer on the device surface can help avoid the absorption of oxygen molecules and moisture from the ambient environment [76,208–210]. This is of great benefits as the absorbed molecules will become carrier trap centers to capture electrons from the surface of the nanomaterials and lead to high currents within PDs under dark conditions [211]. In addition, P(VDF-TrFE) exhibits the ferroelectric local field that enables PDs based on InSb NSs to operate under IR light ($\lambda = 940$ nm) exposure in zero bias voltage which can cut down the power consumption. Due to these aforementioned functions, the dark current value of devices with P(VDF-TrFE) is reduced by four orders of magnitude when compared to that without this layer. Also, other important performance parameters such as responsivity and detectivity are enhanced considerably. This is because the surface defect density is decreased by the coverage of the P(VDF-TrFE) passivation layer helping to reduce the response time from seconds to milliseconds. For Ge PDs, the high dark current mainly depends on intrinsic defects of this material like threading dislocation [212]. In another example, Chen et al. inserted a GeO_2 layer between Ge and $MoTe_2$ in a sandwich structure [213]. The GeO_2 thin film acts as a blocking layer to prevent thermal emission at the interface by reducing the number of hot carriers that transport through the $MoTe_2$ and Ge layers. The current density obtained under the dark condition of devices with the existence of GeO_2 is depressed by four orders of magnitude and reaches a very small value of 0.03 nA/μm^2.

However, the insertion of the thick interfacial layers can degrade photocurrent while reducing the dark current so the thickness should be controlled appropriately [214]. Kim et al. have introduced the combination of an Al_2O_3 thin film layer between Ge and graphene to reduce the dark current by lowering the Fermi level pinning effect at the interface [55]. The performance effect of Al_2O_3 layer thickness is carefully investigated and can obtain a result that the dark current is depressed more and more effectively according to the increase in layer thickness. Notably, with 2 nm of thickness, the existence of Al_2O_3 thin film exhibits the largest performance both responsivity and detectivity are 1.6–2.3 higher than PDs based on regular Ge/graphene heterostructure [15,215,216]. In general, the photoresponse of Ge/graphene with Al_2O_3 interfacial layer shows the value of responsivity and detectivity is higher than that without this layer while the dark current also is depressed to an acceptable value.

The proposed mechanisms of this device in three cases clearly show an important role of Al_2O_3 layer thickness. In the case of PDs with a thin charge-blocking layer, photo-excited electrons are prevented while holes can transfer to the graphene by direct tunneling phenomenon and then recombine with the inherent electrons in the graphene. As a result, the dark current caused by transferred electrons is reduced and there is less of an impact on the photocurrent. With a too-thick layer, both electrons and holes cannot be overcome to transmit to the graphene, which leads to a considerable decrease in the photocurrent of the devices in addition to a dark current reduction [217]. The effective approaches for dark current suppression are exhibited in Fig. 8**.** Therefore, the thickness of the interfacial layer is a necessary factor to be considered when fabricating PDs in order to ensure that adding this layer because while it can decrease the dark current but also the photocurrent thus a trade-off is needed to not cause any significant degradation in device performance.

2.3.2. Plasmon resonance (PR) effects

To enhance the light absorption and electrical properties of IR PDs, 2D nanostructures have recently been combined with plasmonic materials (Fig. 9**).** Metallic nanoparticles are determined as plasmonic materials since they have a large number of free electrons which induce the collective oscillations on the surface due to electromagnetic field impacts [218].Besides, PR has emerged as a powerful strategy to boost the performance of IR PDs by enhancing optical absorption and improving the efficiency of light–matter interactions. However, realizing these benefits depends on the careful optimization of several interrelated factors, including material selection, structural design, and doping control, while also managing trade-offs related to fabrication complexity and quantum effects. Material choice is a foundational aspect in the design of plasmon-enhanced IR PDs. Incorporating noble metal nanoparticles particularly Au with semiconducting materials such as MoS_2 and silicon can substantially broaden the spectral response into the near-infrared region and significantly amplify the photocurrent [219]. Depending on the interaction between metallic NPs and incident light, these effects can be classified into three main types: plasmon resonance, surface plasmon resonance, and localized surface plasmon resonance. Similarly, 2D materials like graphene and BP show marked improvements in responsivity when integrated with well-designed plasmonic structures, owing to their strong coupling with localized surface plasmon fields [220]. Nanostructures such as bowtie antennas, nanocubes, or periodic nanodisk arrays can be precisely engineered to resonante at specific IR wavelengths, thereby concentrating electromagnetic fields in

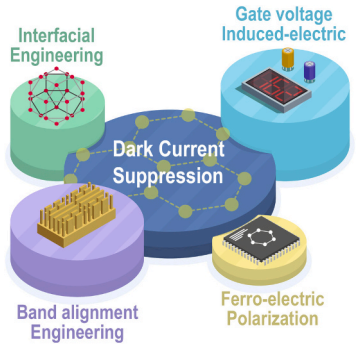

Fig. 8. Schematic representation of effective methods for dark current suppression.

the vicinity of the active layer. Furthermore, the incorporation of plasmonic nanocavities enhances field confinement and absorption [221]. However, as structural dimensions approach the nanoscale, quantum mechanical phenomena such as electron tunneling and non-radiative decay—may dominate, potentially suppressing plasmonic enhancement (a phenomenon known as quenching). Thus, a deep understanding of both classical and quantum effects is essential for optimal design [221]. Doping engineering provides another dimension for tuning plasmonic behavior. In materials like GaAs, controlled doping can tailor the free carrier concentration to enhance Plasmon carrier coupling, thereby boosting light absorption in quantum well IR PDs [222]. Despite their performance advantages, plasmonic integration poses notable challenges**.** The fabrication of uniform and reproducible nanostructures requires high-precision nanolithography and advanced deposition techniques, which can elevate manufacturing complexity and cost. Moreover, ensuring material compatibility between plasmonic metals and semiconductor substrates is essential for facilitating efficient energy transfer, minimizing optical losses, and preserving long-term device reliability [15,16]. While plasmonic resonance holds significant potential for improving both the sensitivity and spectral bandwidth of IR PDs, its practical realization demands a comprehensive design framework. This includes precise control over nanostructure geometry, careful consideration of quantum-scale effects, strategic doping to optimize charge carrier dynamics, and seamless integration of heterogeneous materials. A coordinated effort to address these interconnected factors is crucial for translating plasmon-enhanced photodetector concepts into scalable, high-performance technologies suitable for real-world applications. Tong et al. have proposed a unique structure a plasmonic 2D subwavelength hole array (2DSHA) with n-InAsSb/n-GaSb heterojunction [223]. Due to the suitable band gap of InAsSb and GaSb, the combination of two materials allows devices can operate in dual-band IR regions, including $\lambda = 1.7$ μm (NIR) and 3.4 μm (MIR). The gold 2DSHA was deposited onto the n-InAsSb/n-GaSb heterostructure by electron beam lithography (EBL) technique. The array dimensions were chosen to resonante at the two bands, thus this array allows for the largest optical field enhancement and increases the photocurrent at the two bands. This structure architecture has shown improved photoresponse parameters which are enhanced from 1.5 (1.5) times to 5.5 (3.8) times with the increase in bias voltage (from 300 mV to 800 mV) for the MIR and NIR bands, respectively when compared to preference bare n-InAsSb/n-GaSb. Chen et al. have used Au NPs to trap light with wavelength matching with plasmonic resonance and then absorbed by graphene [224]. The Au NPs array was fabricated by nanosphere lithography and used polystyrene (PS) to create a triangle-like hole between every three spheres. The electrical field distribution is observed near the triangle-like Au NPs. Therefore, the photoresponse of PDs based on graphene under 1550 nm exposure is improved by a factor 10 in the case having Au NPs. The distance between spots in an array should be controlled since its increase can lead to a prompt decrease in the average light intensity. Therefore, the plasmonic structure should be placed in proximity place to enhance the maximum plasmonic effect [225]. Enhancing light–matter interactions in IR PDs is critical to advancing their performance, especially considering the typically low absorption of IR radiation by conventional semiconductor materials. To address this limitation, researchers have increasingly turned to nanophotonic design approaches, including metasurfaces, Fabry–Pérot (F—P) cavities, and other sophisticated light-manipulating structures [76,187]. Metasurfaces engineered arrays of subwavelength elements dramatically improve light coupling into the active region of photodetectors by manipulating light propagation through diffraction and phase control.

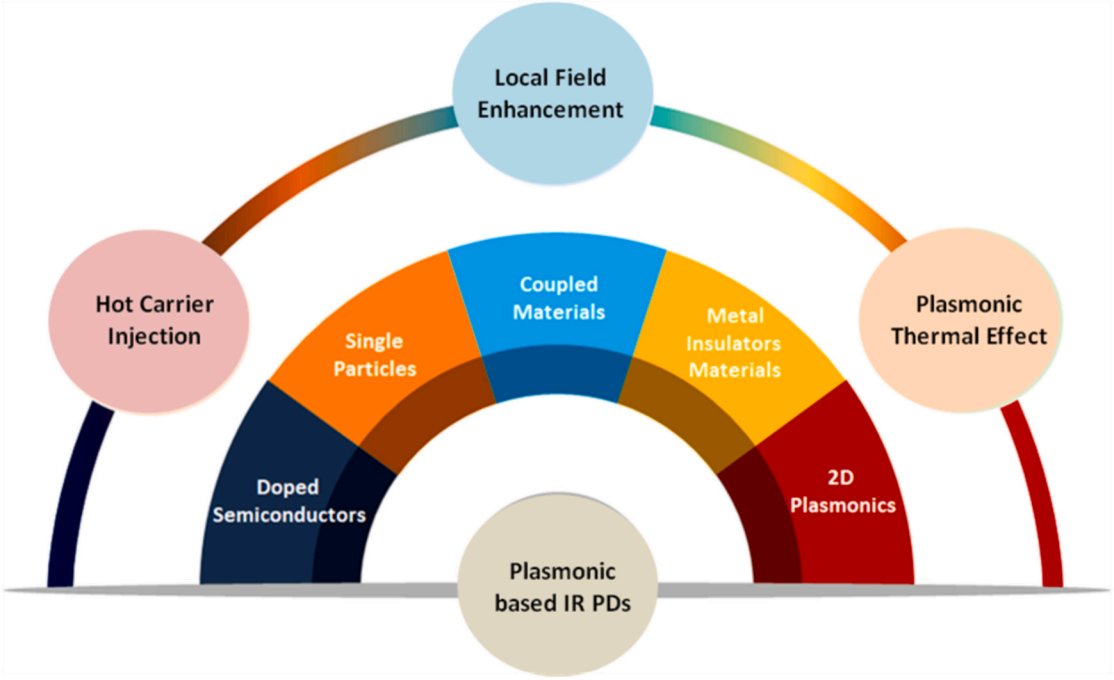

Fig. 9. Typical structures of IR PDs based on plasmonic effects.

These structures not only broaden the spectral response and enhance quantum efficiency but also allow for reconfigurable optical behavior when integrated with adaptive materials like phase-change compounds. Furthermore, metasurfaces can be tailored to deliver broadband, omnidirectional absorption, making photodetectors more effective under variable illumination conditions [226,227]. In parallel, Fabry–Pérot cavities serve as resonant structures that confine light within the active region, thereby amplifying light–matter interaction. By incorporating materials such as gallium-doped zinc oxide, these cavities can be spectrally tuned to target specific IR wavelengths, improving selectivity and signal strength. Advanced configurations, like metal–dielectric–metal layered cavities, support dual-band resonances in both the visible and mid-IR regimes, ideal for multifunctional photodetection systems [16,63,76]. Integrating metasurfaces into these cavities can further optimize optical throughput and facilitate high-fidelity color generation for precision imaging technologies. In addition to these approaches, the incorporation of 2D materials such as graphene, BP and various transition metal dichalcogenides into nanophotonic frameworks enhances IR light harvesting and carrier transport in ultra-thin device architectures. Moreover, coupling metasurfaces with quantum emitters or nanoemitters creates strong light–matter interactions that boost photoluminescence, enabling progress in quantum optics and sensing platforms [228,229]. Altogether, these advanced nanophotonic strategies are at the forefront of modern IR photodetector design, offering significant improvements in sensitivity, spectral range, and overall device functionality. Plasmonic enhancement techniques, in particular, have demonstrated strong potential by intensifying light–matter interactions at subwavelength scales, thereby improving IR absorption and responsivity. To achieve this, metallic nanostructures and doped semiconductor nanocrystals are commonly employed to tailor surface plasmon resonances to specific IR wavelengths especially in the mid- and long-wavelength IR regions. Despite their advantages, integrating plasmonic components without introducing optical losses or thermal degradation remains a significant challenge. Additionally, limitations in precise spectral tuning and scalable fabrication continue to hinder widespread adoption. Advancements in CMOS-compatible, low-loss plasmonic materials will be critical for transitioning these technologies into practical, real-world applications.

2.3.3. Diminishing of contact resistance

High resistance at the contact between metal electrodes and active materials is a common occurrence. It can be explained by the high work function of metal elements such as Al (Φ_m = 4.28 eV), Ag (Φ_m = 4.32 eV), Cr (Φ_m = 4.5 eV), Au (Φ_m = 5.1 eV), Pd (Φ_m = 5.12 eV), Ni (Φ_m = 5.15 eV), Pt (Φ_m = 5.65 eV), which leads to a high potential barrier due to the band alignment at the interface of metals and semiconductors. Electrons in the conduction band of materials that are excited by incident light and need larger energy to overcome this potential barrier to be collected at electrodes, then the photocurrent value is significantly affected so a high barrier height is the main reason for high contact resistance. Work function engineering of the contact is an effective method that has been proposed **(**Fig. 10**).** Graphene exhibiting free-barrier Ohmic contact for MoS_2 transistors is reported by Liu et al. Since the work function of a 2D material like graphene is tunable depending on voltage and temperature adjustment, it can easily match that of MoS_2, leading to considerable contact resistance decrease [230,231]. Relying on this platform, Chen et al. have selectively developed a rhombohedral lattice structure of antimonene (β-antimonene) on bilayer MoS_2 and this antimonene acts as the contact metal for devices based on MoS_2 [56,232]. The specific contact resistance of Au/antimonene is 0.785 Ω cm^{-2} while the value of Au/Ti electrodes is 3.09 Ω cm^{-2}, respectively [114]. The resistance value of devices using Au/antimonene electrodes is reduced by 1 order of magnitude when compared to that with common Au/Ti electrodes.

In addition, contact resistance is also effectively diminished by adding an insulating layer in order to separate the active materials from metal electrodes to generate the metal-insulator-semiconductor (MIS) structure **(**Fig. 10**).** This layer not only provides the tunneling channel but also removes the interface states, resulting in an improvement in contacts and a decrease in resistance. Moreover, reducing contact resistance is a pivotal strategy for enhancing the performance of various types of photodetectors. In graphene-integrated systems, the adoption of edge-contact architectures along with n-type doping has demonstrated substantial improvements in reducing contact resistance, leading to enhanced photoresponsivity and detectivity in graphene–perovskite hybrid devices [233]. Additionally, localized doping near the graphene–metal junction enables modulation of the built-in electric field, thereby affecting external quantum efficiency and the overall photodetection performance. Within organic electronics, the functionality of organic field-effect transistors (OFETs) can be significantly improved by engineering the polymer backbone such as adjusting the alkyl chain length in polymers like poly(3-hexylthiophene) which effectively lowers contact resistance and boosts photoreactivity. TMDs also benefit from meticulous interface engineering [234]. For instance, in MoS_2-based devices, semi-metallic electrodes reduce metal-induced gap states, resulting in exceptionally low contact resistance and heightened responsivity. Likewise, in WSe_2 p–n junctions, plasma-assisted doping transforms Schottky barriers into Ohmic contacts, facilitating superior charge carrier injection and extraction [235]. In the case of metal–semiconductor interfaces like those in GeSe photodetectors, using gold–indium alloy contacts diminishes the Schottky barrier height, thus increasing photocurrent efficiency. Similarly, in amorphous indium–gallium–zinc oxide (a-IGZO) phototransistors, customized metal contacts are critical for enhancing charge transport properties and broadening spectral response [236]. Altogether, these advancements underscore the indispensable role of interface and contact engineering in refining the operational capabilities of emerging photodetector technologies. Besides, A heterostructure based on $MoTe_2$ and the single-layer WS_2 tunneling contact has been proposed by Kim et al. with In/Au electrodes only contact with WS_2 tunneling layer [232,237]. Devices with WS_2 tunneling contact (WTC) exhibit a lower Schottky barrier height (SBH) at all temperature values when compared to that in direct contact with $MoTe_2$ (MDC). These results show that the WTC and MDC contact resistance at 300 K is 1 MΩ μm and 6.5 MΩ μm, respectively. It can be concluded that the existence of WS_2 as a tunneling channel helps to decrease the contact resistance of devices by 6-fold and this result is contributed by the reduction of barrier height between active materials and metal electrodes. Taking advantage of the heterointerface between two 2D materials, Khan et al. have fabricated a device structure possessing not only an efficient separation of photo-generated electron-hole pairs due to type II heterojunction formation but also Schottky barrier height decrease [176,238]. In this structure, bi-layer MoS_2 is stacked and acts as a tunneling layer for an underlying few-layered WSe_2. It is similar to the structure of $WS_2/MoTe_2$ as discussed above, there is no direct contact between the metal electrodes and the active material since abundant surface states of semiconductors can easily create a Fermi-level pinning effect, leading to high SBH. Therefore, MoS_2 has an important role in preventing this direct interaction and reducing the SBH. As a result, the calculated contact resistance by the Y-method of direct interaction of WSe2/metal electrodes and through an intermediate layer $MoTe_2$ is 1 MΩ μm and 80 kΩ μm, respectively which indicates that the contact resistance value is decreased by 85 times.

2.3.4. Resolving scattering effects on 2D materials and heterostructures

Defects in 2D materials especially have an important role since they act as the scattering centers and reduce electron mobility [239]. Mobility of materials strongly contributes to the photoresponse ability of the device so it is essential to suppress scattering effects inside 2D materials as well as at the interfaces of 2D heterostructures which has a severe impact on mobility. However, mobility can be severely limited by scattering effects arising from defects within the 2D lattice, impurities, and especially at the interfaces of 2D heterostructures. Therefore,

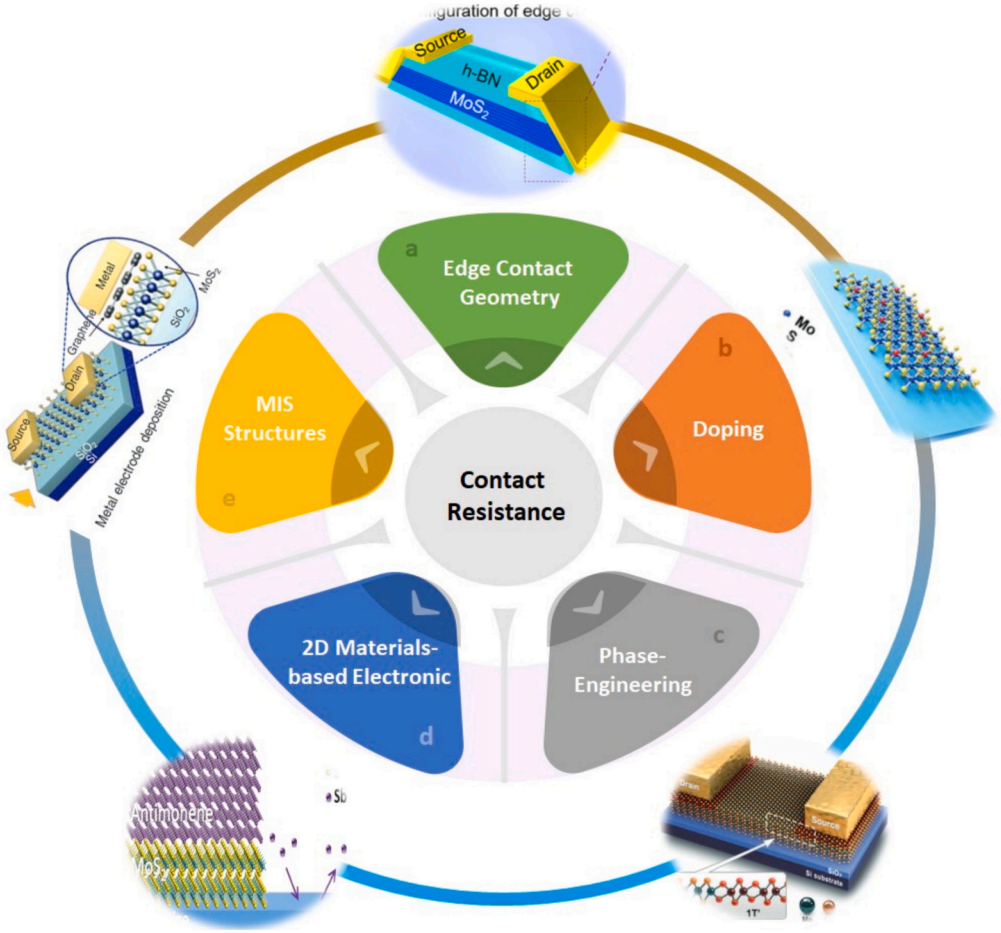

Fig. 10. Design strategies for IR PDs to diminish contact resistance. Inset: a. Edge-contacted hBN/MoS2/h-BN sandwich structure device. Reproduced with permission from ref. [239] Copyright 2019 American Chemical Society. b. Fe-doped monolayer MoS_2 device. Reproduced with permission from ref. [240] Copyright 2022 Wiley-VCH GmbH. c. A device with a 1 T'/2H phase homojunction of $MoTe_2$. Reproduced with permission from ref. [241] Copyright 2015 American Association for the Advancement of Science. d. Transistor-based on a patterned MoS2 on a sapphire substrate using β-antimonene as electrodes. Reproduced with permission from ref [242] Copyright 2018 American Chemical Society. e. Schematic illustration of graphene interlayer inserted MoS_2 FETs with metal contacts. Reproduced with permission from ref. [243] Copyright 2018 Wiley-VCH GmbH.

suppressing such scattering both within the material and at its boundaries is crucial for maximizing device performance. One effective method to achieve this is through the use of dielectric encapsulation layers. The incorporation of high-κ dielectric encapsulation layers into IR PDs based 2D materials has emerged as a promising strategy to enhance device performance by mitigating carrier scattering, improving environmental stability, and extending operational lifetime. However, this approach also introduces critical material compatibility concerns that must be addressed to preserve the intrinsic electronic and optoelectronic properties of the 2D active layers. In the case of graphene-based photodetectors, the deposition of high-κ dielectrics via methods such as e-beam evaporation, sputtering, or ALD can significantly influence device performance. These deposition techniques may induce structural defects, unintentional doping, or strain, which can degrade graphene's exceptional carrier mobility and photodetection capabilities. Thus, careful selection of dielectric materials and precise control over deposition parameters are essential to minimize disruption of graphene's electronic properties [244]. Similarly, MoS_2 photodetectors encapsulated with ALD-deposited hafnium oxide (HfO_2) benefit from enhanced environmental isolation, effectively reducing surface adsorbates and improving overall stability. Nonetheless, this encapsulation can lead to pronounced n-type doping and reduced device resistance, indicating strong interfacial interactions that may inadvertently alter the device's electrical characteristics. These effects highlight the need for tailored encapsulation strategies that maintain a delicate balance between protection and electronic neutrality [245]. For other 2D materials such as BP and TMDs, encapsulation remains essential for achieving ambient stability. However, the encapsulation method whether polymer coating, mechanical stacking, or ALD must be selected carefully, as it can impact interfacial integrity, introduce traps, or cause thermal and mechanical mismatch. Such compatibility issues can compromise long-term reliability and optoelectronic performance. Beyond these specific cases, the encapsulation of other environmentally sensitive 2D materials such as BP and a wide range of TMDs demands careful strategic consideration [246]. While encapsulation is indispensable for maintaining material integrity under ambient conditions, the choice of technique whether polymer coating, mechanical stacking, or ALD can inadvertently introduce interfacial trap states, compromise adhesion, or induce thermal mismatch stresses. These factors collectively jeopardize long-term device reliability and can significantly degrade optoelectronic performance.

To mitigate these challenges, several targeted approaches have been developed. One key strategy involves the optimization of deposition parameters including temperature, pressure, and deposition rate to minimize process-induced damage and preserve the intrinsic properties of the 2D active material. Additionally, applying surface functionalization treatments prior to encapsulation can enhance interface compatibility and suppress adverse chemical or electronic interactions. Another critical consideration is material selection and interface engineering; choosing dielectrics with appropriate band alignment, chemical

stability, and minimal charge trapping characteristics helps maintain charge carrier mobility and reduces the risk of unintentional doping [247,248]. Furthermore, the rational design of encapsulation architectures, such as multilayer or hybrid dielectric structures, can effectively balance environmental shielding with electrical neutrality, thereby sustaining performance without introducing undesirable side effects. Although high-κ dielectric encapsulation significantly improves the stability and functionality of IR PDs, achieving seamless integration with 2D materials requires a multifaceted approach [246]. Success in this domain depends on the synergistic optimization of fabrication processes, thoughtful materials engineering, and precise interface control. This holistic design philosophy is vital for fully realizing the potential of 2D materials in high-performance, next-generation optoelectronic technologies. Interestingly, Lee et al. have developed a metal-semiconductor field-effect transistor (MESFET) based on MoS_2/NiOx van der Waals Schottky junction [240]. This structure exhibits a high intrinsic mobility of 500–1200 $cm^2\ V^{-1}\ s^{-1}$ resulting in ultra-high responsivity of 5000 A W^{-1} and fast switching time of ~2 ms. It can be explained that there are only van der Waals bonds between NiOx and MoS_2, hence gate leakage does not occur at this interface. Therefore, in this case, NiOx acts as gate electrodes that can help to decrease the scattering effects. Recently, the encapsulation layers with high-κ values have been used widely to passivate the surface states of the active channel in their dielectric environments and lead to carrier mobility improvement. Encapsulating is expected to protect surface materials against oxygen absorption and moisture from the surrounding environment. The selected encapsulation materials have to exhibit significant optical transmittance, desirable chemical (high stability, strong adhesion, etc.), and mechanical (suitable thermal expansion coefficient, nominal residual mechanical stress, etc.) abilities. These properties are required to adapt to temperature cycling and avoid delamination during the operation period in severe environments with high-temperatures [241]. The existence of a high-κ dielectric film can change the dielectric environment, and modify the edge and defect states of materials [242,243]. The formation of the dielectric environment also adjusts the exciton binding energy leading to the coulomb impurities and surface polar phonon scattering reduction, and these effects will be decreased with an increase in the dielectric constants [249]. More importantly, the requirement for high-κ can significantly reduce the applied voltage, leading to a low required voltage and thus lower device power consumption. Commonly used dielectric materials for encapsulation layers can be listed including inorganic materials (HfO_2, SiO_2, Al_2O_3, hBN, Si_3N_4, etc.) and polymers (PMMA, PVDF, PVA, etc.) [249]. Encapsulation of monolayer MoS_2 in a high-κ dielectric environment to reduce Coulomb scattering and increase the temperature mobility [250,251]. Xu et al. utilized an organic crystalline film of N, N′-ditridecylperylene-3,4,9,10-tetracarboxylicdiimide (PTCDI-C_{13}) to fully encapsulate the MoS_2 surface and exhibit the huge difference in mobility of this PDs between before and after passivation (from 0.5 to 8.3 $cm^2V^{-1}\ s^{-1}$) [252].

Furthermore, the mismatch in roughness, charge impurity and defects of substrates and deposited materials can cause strong scattering states at the interfaces and thus the carrier transport can be limited [249]. Chamlagain et al. have proposed a device structure of $MoSe_2$ deposited on Parylene-C substrate and gained the mobility of 118 cm2 V-1 s-1 which is 2 times larger than the $MoSe_2$ devices on SiO_2 [253]. SiO_2 has widely been used as a usual substrate in devices based on TMDs but it has the additional surface polar optical phonon scattering which is nearly absent in parylene-C. Therefore, this phenomenon creates a difference in the mobility of these substrates and a strong dependence on the temperature of the SiO_2. Interestingly, Bhattacharjee et al. successfully suppressed the dominating scattering effects by combining the two above approaches – providing dielectric environments, and choosing/modifying an appropriate substrate [254]. They used AlN as a substrate because it has a dielectric constant of 8.5, a high optical phonon energy of 81.4 meV, and the lowest mobility degradation values of 0.88 for MoS_2 devices. These properties indicate less dependence of mobility on temperature and contact resistance, and scattering in the channel, leading to a surface optical phonon scattering reduction. Then, to observe the higher-performance of the MoS_2 devices, authors treated the substrate with sulfur to passivate the number of defect states on the surface and reduce SBH at the MoS2/metal contact interface. Also, a high-κ dielectric environment is enhanced by adding h-BN which provides the encapsulation on the devices. After the strict modification process at the substrate surface, the observed mobility is up to 72.8 $cm^2V^{-1}\ s^{-1}$, which is 1.6 times larger than MoS_2 devices based on bare AlN.

2.3.5. Role of interfaces and geometries

It is a necessary approach to research defect-free interfaces to deal with the large density of states at the contacts and there are several previous publications that reported good results in this regard. To confirm this experimental effect, M. Houssa et al. have simulated models by using DFT and the NEGF to deeply study the contact resistance of devices based on a graphene/MoS_2 heterostructure [255]. The existence of S dangling bonds make the gap states in the conduction band of MoS_2 pin the Fermi level of the material leading to high barrier height at the graphene/MoS_2 interface. The obtained contact resistance values are 5.6 Ω μm and 2.2 Ω μm, respectively which are improved by 2 orders of magnitude when compared to other Models with non-linked S atoms.

The dangling-bond-free surface of 2D materials allows for the direct stack-by-stack heterostructure through only the van der Waals force. The weak Van der Waals interaction along the out-of-plane direction is a characterization that makes 2D nanomaterials easy to exfoliate into individual layers. However, the Van der Waals interfacial force at the top-contacted interfaces acts as a tunnel barrier for carriers before the Schottky barrier, and thus it reduces charge carrier transfer leading to a high contact resistance [15]. Therefore, it is essential to take advantage of edge contacts to overcome this Van der Waals gap. Due the existence of conductivity anisotropy within multi-layered 2D materials, the edge contact brings a stronger impact to structures with in-plane and out-plane orientations than in the case of a top contact. The edge contact exhibits lower resistivity and contributes to the higher cohesive energy between metal atoms and the active material [256].

A proposed method to eliminate the intrinsic Van der Waals gap is the hybridization of the metal electrode atoms and the 2D material surface due to the ability to form covalent bonds of several specific metals [257]. For example, Popov et al. would like to search for another metal to use as electrodes which will substitute the common contact Au for MoS_2-based nano-electronic devices [258]. They realized that Sc and Zr have a large lattice mismatch despite having d orbitals which can suitably mix with the Mo_4d states. Therefore, Ti becomes an appropriate candidate due to only a 1 % mismatch with MoS_2. The average Mo—Ti bond length is 3.57 Å which is shorter than that of Mo—Au bonds (4.21 Å), leading to a larger wavefunction overlap. Also, Ti contacts modified the electronic states near the Fermi level much more than Au and it can cause the high density of delocalized states at the Fermi level of MoS_2. The optimal contact Ti has a favorable interface geometry and bonding, exhibiting a minimized or non-existent tunneling barrier between the two materials. Therefore, the interface geometry of the metal electrodes and active materials have to be considered thoroughly.

2.4. Fabrication methods and their impacts on reproducibility

The scalability and manufacturability of IR PDs are critical for their commercial success. Various fabrication methods significantly influence the reproducibility, performance, and integration of these devices. Techniques such as poly(methyl methacrylate) assisted transfer for CQDs, solution deposition for BP films, electrophoretic deposition (EPD) with ligand exchange for quantum dot films, and rapid thermal annealing with dry etching for GeSn nanowires have all demonstrated promising pathways toward scalable and cost-effective IR PDs

fabrication (Fig. 11.).

2.4.1. Colloidal quantum dot (CQD)

The fabrication of colloidal quantum dot (CQD)-based infrared detectors, particularly multispectral ones, typically involves several steps and techniques. Traditional methods such as drop casting, spin coating, and spray coating allow for the production of multiple photodetectors but suffer from limited spatial control over the deposited films. These approaches enable only "single-color" detectors within a deposited region, and even attempts to create bicolor devices by drop casting different CQD solutions on separate electrodes lack the precision needed for true multispectral detection within a single sensing element. To address these challenges, a study introduces a simple and highly efficient poly(methyl methacrylate) (PMMA)-assisted transfer technique that allows scalable fabrication of CQD-based photodetectors with multiple pixels, each responsive to different infrared spectral ranges [259]. This method enables site-selective patterning of CQDs, which is essential for developing multipixel and multispectral detectors. The process begins with the synthesis of solution-phase HgTe CQDs, which are deposited as thin films on 3-Mercaptopropyltrimethoxysilane-treated SiO_2/Si substrates through layer-by-layer spin-coating. Each layer undergoes cross-linking using an As_2S_3 solution, followed by ethanol rinsing and drying to ensure film conductivity, with film thickness controllable by multiple depositions. The CQD films are then patterned into pixel arrays using photolithography and oxygen plasma etching. A PMMA solution is applied to the patterned array and cured, forming strong van der Waals interactions that allow the CQD pixels to be lifted off. The PMMA layer with the attached pixels is carefully aligned and transferred onto a target substrate with prepatterned electrodes, achieving an alignment precision of around 1 μm. Due to its flexibility, the PMMA layer can be transferred onto both flat and curved surfaces. After transfer, the PMMA is removed by rinsing in acetone for two hours. Using this method, three-pixel photodetector arrays were fabricated, each pixel composed of HgTe CQDs with different cutoff wavelengths (e.g., 4.8, 6, and 9.5 μm), and larger 12 × 12 detector arrays were produced with a fabrication success rate exceeding 95 %. Electrode patterns were created through standard photolithography and radio-frequency sputtering of Cr and Au layers. Furthermore, the researchers demonstrated an eight-element spectral photodetector, where each element integrated three pixels made from CQDs with distinct absorption properties, enabling the reconstruction of infrared spectra from 2 to 10 μm. Importantly, the study confirmed that the PMMA-assisted transfer process caused minimal degradation to the CQD films, with conductance and photocurrent fluctuations within only 5 %, thanks to the robust cross-linking of the CQDs [259,260]. Overall, this work presents a scalable, efficient strategy for fabricating CQD-based multipixel and multispectral infrared detectors, offering precise spatial control and the integration of CQDs with varied spectral responses into a single device, paving the way for applications in multicolor focal plane cameras and microspectrometers.

2.4.2. Black phosphorus (bP) films

The fabrication of BP films, as detailed in the sources, involves a multi-step process emphasizing scalability and the production of high-quality films suitable for IR photodetector arrays. The method consists of electrochemical exfoliation of bulk bP, controlled vacuum filtration to create thin films, and the application of protective capping layers, all conducted in an oxygen-free environment using anhydrous solvents to minimize oxidation. The process begins with electrochemical (EC) exfoliation of bulk bP crystals, which precisely controls interlayer forces to reduce damage and in-plane tearing. A current is applied to the bulk bP in a two-electrode packed-bed electrochemical reactor containing a nonaqueous electrolyte of 0.1 M tetrabutylammonium (TBA) hydrogensulfate in dimethyl sulfoxide (DMSO), where TBA cations intercalate between the bP layers, increasing the interlayer gap and weakening van der Waals interactions [261]. This results in the gentle exfoliation of laterally large BP flakes with high crystallinity, with 78 % of flakes having a lateral diameter greater than 2 μm and a maximum size of approximately 10 μm—larger than flakes produced by typical liquid-phase exfoliation methods like ultrasonication. Following exfoliation, the bP dispersion undergoes multiple centrifugation steps to obtain an additive-free dispersion with optimized flake size and thickness distribution; high-speed centrifugation removes very small flakes (<3 nm), while low-speed centrifugation removes large aggregates (>50 nm), ensuring over 85 % of flakes have a thickness greater than 3 nm, with a mean thickness of 6.2 nm. This thickness is ideal for IR photodetector fabrication as it preserves a bulk-like bandgap for IR absorption while maintaining film uniformity and flexibility. Excess intercalant is removed through repeated redispersion and centrifugation. The bP thin film is then formed by controlled vacuum filtration, where the BP dispersion is added to anhydrous isopropanol (IPA) and filtered onto nitrocellulose (NC) filter paper with a 0.45 μm pore size. Film thickness

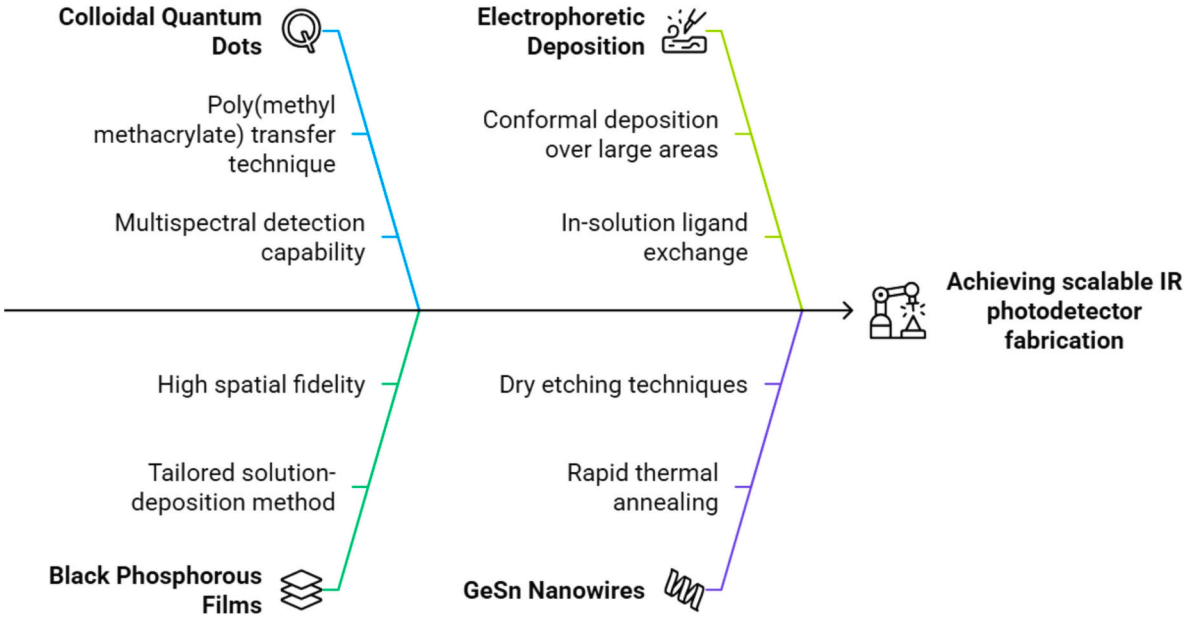

Fig. 11. Fabrication Methods and Scalability.

is controlled by adjusting the filtered dispersion volume, and vacuum filtration is favored for its scalability and ability to produce homogeneous, pinhole-minimized films. After filtration, the bP thin film is transferred onto device substrates composed of Au interdigitated electrodes on Si/SiO_2. The NC filter paper with the bP film is inverted and pressed against an IPA-wetted substrate, followed by vacuum drying and the dissolution of the filter paper in sequential anhydrous acetone baths. Except for centrifugation and vacuum drying during film transfer, all steps are conducted in a nitrogen glovebox to prevent oxidation. To protect the bP films from ambient degradation and reduce trap states, capping layers are deposited by PVD and ALD, with ALD-deposited layers (TiO_2 and Al_2O_3) showing the best performance due to fewer introduced defects and excellent conformal coatings. About 13 nm thick TiO_2 and Al_2O_3 layers were deposited at 90 °C using titanium isopropoxide (TTIP) and dimethylaluminum isopropoxide (DMAI) precursors, respectively, offering high transmission in the SWIR/MWIR region. Raman spectroscopy confirmed minimal oxidation of the bP thin film throughout the process. This tailored solution-deposition method enables the scalable fabrication of bP thin films for optoelectronic devices, demonstrated by the fabrication of a linear array of 25 BP photodetectors and successful 25 × 25 pixel IR imaging with good spatial fidelity. The fabricated BP IR photoconductors achieved specific detectivities up to 4.0×10^8 cm $Hz^{1/2}$ W^{-1} and fast rise/fall times of 30/60 τ_r under 2.2 μm illumination [260]. The larger lateral flake size from EC exfoliation and controlled vacuum filtration contribute to improved film conductivity and device performance by reducing inter-flake junction resistance, while the ALD capping layers enhance the stability and longevity of the devices.

2.4.3. Electrophoretic deposition (EPD)

Based on the information provided, the fabrication of films using Electrophoretic Deposition (EPD) involves applying an electric field to drive charged nanoparticles through a liquid medium, assembling them directly onto a conductive substrate. This method is presented as an efficient and versatile alternative to traditional deposition techniques like spin coating and drop casting, which struggle with conformal deposition on non-planar or large-area substrates. Unlike ink-jet printing, which is precise but limited to small areas, EPD can achieve conformal and selective area deposition over large scales. The source emphasizes EPD for depositing quantum dot (QD) films, addressing previous limitations caused by native ligands that hinder charge transport. In this work, in-solution ligand exchange is combined with EPD to achieve dense PbSe QD films, marking the first demonstration of one-step direct EPD assembly of QDs for electronic devices. Specifically, 4 nm PbSe QDs, initially capped with insulating oleylamine ligands, undergo ligand exchange with ammonium iodide (NH_4I) through a phase-transfer reaction, confirmed by FTIR analysis. The exchanged QDs are redispersed in 2,6-difluoropyridine (DFP), a polar solvent that stabilizes the QDs electrostatically. In the EPD setup, an electric field moves the charged QDs toward the electrode, where they lose charge and form a film. However, pure DFP suspensions showed no deposition response, necessitating solvent engineering by titrating hexane into the mixture. At a DFP:hexane ratio of 1:0.8, QDs became responsive to the field, with the optimal film quality achieved at 1:1. Deposition rates increased with higher hexane content (up to 1:1) and stronger electric fields (0.2–0.6 V mm^{-1}), with deposition times ranging from 2 to 10 min. In situ QCM measurements revealed that the EPD growth rate (~1–100 nm s^{-1}) rivals conventional semiconductor deposition methods like PVD and CVD, but without the need for vacuum systems or high temperatures. SEM imaging showed that the deposited PbSe–NH_4I QD films were compact, composed of grains averaging ~300 ± 20 nm, although GISAXS analysis indicated a lack of long-range order. EPD offers significant advantages, including fast growth rates, controllable flux, scalability, conformal and selective area deposition, and single-step fabrication without requiring post-deposition ligand exchange. However, challenges include Brownian motion, charge screening, colloidal stability management, and parasitic ionic currents, which are mitigated through solvent engineering [262,263]. The method's effectiveness was demonstrated by fabricating IR PDs with PbSe QD films conformally deposited on textured silicon substrates, achieving a responsivity of ~0.01 A W^{-1} and fast response times (4.6 ms rise and 4.7 ms decay) under IR illumination. Although the devices were tested in ambient air, potentially underestimating their performance, this study highlights EPD as a promising, scalable approach for producing QD-based optoelectronic devices.

2.4.4. GeSn nanowires

Based on the research article provided, the fabrication of GeSn vertical nanowires (NWs) involves a three-step process: molecular beam epitaxy (MBE) growth of a GeSn film, rapid thermal annealing (RTA), and inductively coupled plasma (ICP) dry etching. This method is designed as a scalable and low-cost approach to produce GeSn NWs suitable for near-infrared (NIR) or short-wavelength infrared (SWIR) nanophotonic devices. First, a GeSn film with a nominal Sn content of 6.6 % and a thickness of 200 nm was grown on a 3-in. undoped (001)-oriented Ge substrate using MBE. Prior to deposition, the substrate was degassed and deoxidized at 850 °C for 10 min and then cooled to 150 °C for GeSn growth. Ge and Sn sources were thermally evaporated from high-purity materials loaded in Knudsen effusion cells maintained at 1220 °C and 980 °C, respectively, and the growth process lasted for 3 h. Following MBE, the GeSn sample underwent RTA using a Solaris 150 Rapid Thermal Processing System, where it was rapidly heated to 550 °C at 120 °C/s in a pure N_2 atmosphere, held for 1 min, and cooled below 100 °C within 8 min. This treatment induced the formation of self-assembled Sn nanodots (NDs) on the surface due to Sn's higher surface free energy compared to Ge, promoting segregation and migration. AFM imaging confirmed increased surface roughness and ND formation after annealing, alongside a fivefold enhancement in spontaneous emission from the GeSn direct band. In the final step, ICP dry etching was carried out for 4 min using Cl_2, Ar, and O_2 gases at 10 mTorr, with ICP and RF powers set at 200 W and 100 W, respectively. During this process, the self-assembled Sn NDs served as a hard mask, protecting regions underneath while the exposed areas were etched away, resulting in the formation of vertical GeSn NWs featuring a bevel at each tip. The fabricated NWs exhibited a density of 2.8×10^9 cm^{-2} and a diameter of 25 ± 6 nm, and it was noted that tuning the RTA temperature could adjust the NW dimensions and density. Furthermore, the researchers demonstrated the potential of these NWs by fabricating a prototype photodetector [173,264,265]. In the article's introduction, other fabrication strategies are discussed, categorized into bottom-up growth and top-down processing. Bottom-up approaches, such as microwave-assisted solution–liquid–solid growth or chemical vapor deposition using Sn, Au, or AuAg catalysts, often face challenges in controlling NW orientation, size, and distribution, and the use of noble metals may degrade optical performance. Top-down methods typically rely on expensive high-resolution electron beam lithography (EBL) combined with ICP dry etching, but the high cost of EBL limits scalability. In contrast, the method proposed in the research article offers a more cost-effective and scalable solution for producing high-quality vertical GeSn NWs, addressing the limitations of conventional approaches.

In addition to scalability, reproducibility plays a vital role in ensuring consistent performance of IR PDs across multiple batches and large-area sensor arrays. For CQD-based devices, the use of lithographically patterned quantum dot films significantly enhances fabrication precision and uniformity. The PMMA-assisted transfer technique further ensures consistent film thickness and dot distribution, yielding a fabrication success rate exceeding 95 %, which is essential for reliable multispectral IR detection. Similarly, BP -based IR PDs benefit from optimized deposition methods and protective encapsulation layers, such as Al_2O_3 or hBN, which safeguard the material against environmental degradation and help maintain stable electrical performance over repeated fabrication cycles. Additionally, the electrophoretic deposition (EPD) method offers controlled and uniform film formation by

managing parameters such as thickness and NPs density. This precise control directly translates into consistent electrical and optoelectronic properties, making EPD a highly reproducible approach for scalable IR PD production.

2.4.5. Computational readout

To transcend the intrinsic material and device-level constraints of IR PDs such as thermal (Johnson) noise, dark current accumulation, and limited dynamic range research has increasingly turned to computational signal processing frameworks as a transformative approach. These frameworks leverage algorithmic intelligence, often embedded at the circuit or sensor level, to optimize signal fidelity, reduce noise artifacts, and extract meaningful information from low-photon fluxes. Among these, compressive sensing (CS) has emerged as a potent strategy to efficiently encode spectral or spatial information while minimizing redundant data acquisition. For example, a heterostructure combining MoS_2, h-BN, and $PdSe_2$ has demonstrated real-time fusion of IR and visible input, achieving dual-band data compression at the pixel level. This configuration reduces the total data bandwidth by half while preserving over 85 % classification accuracy in complex scenes. Similarly, spatial-spectral multiplexing photodiode arrays have achieved ultra-low complexity signal acquisition with significant energy savings, and grating-based mid-IR spectrometers have enabled broadband spectral reconstruction with high fidelity using a minimal number of detectors, powered by sparse recovery algorithms.

In parallel, machine learning-enhanced inference techniques are revolutionizing the signal interpretation pipeline for IR detectors. Predictive models, such as gradient-boosted trees, have shown success in estimating dark current characteristics in HgCdTe devices based on physical input parameters—allowing real-time thermal noise compensation without requiring changes to the detector structure. Meanwhile, graph neural networks (GNNs) trained on the behavior of 2D IR materials have enabled dynamic baseline correction and noise suppression, substantially improving SNR under low-signal conditions. Deep learning methods like convolutional autoencoders have further demonstrated the ability to restore degraded multispectral signals, elevating detectivity by an order of magnitude [266].

Complementary to these data-driven approaches, adaptive signal reconstruction methods allow photodetectors to self-tune in response to environmental or signal-level fluctuations. CMOS-based charge compression architectures, for instance, have enabled wide dynamic range imaging with noise levels below a single electron, supporting low-light imaging without sacrificing signal integrity. In 2D-material-based photogating systems, gate-voltage modulation of the Fermi level has enabled responsivity tuning across tens of A/W, extending linear detection range by up to 20 dB. Optimization techniques such as Bayesian parameter tuning applied to drift-diffusion simulations have further accelerated transient response in narrow-bandgap detectors, with demonstrated bandwidths above 100 GHz in long-wavelength regimes [267]. Beyond conventional denoising and reconstruction, a new frontier is emerging through the integration of neuromorphic computing principles with IR detection hardware. Traditional IR systems suffer from latency and energy bottlenecks due to off-chip processing demands. In contrast, neuromorphic photodetectors integrate sensing, memory, and decision-making directly on-chip, often inspired by the parallel architecture of biological vision systems. Devices employing MoS_2 or BP as active synaptic elements have shown capability for in-sensor learning and spike-based encoding, supporting real-time, low-power pattern recognition. These neuromorphic elements emulate essential neural behaviors such as synaptic plasticity, enabling continuous adaptation to shifting thermal environments a key asset for autonomous or wearable IR systems. Another emerging paradigm is event-based IR imaging, wherein sensors respond to temporal changes in thermal contrast rather than recording periodic frames. This leads to dramatically reduced data rates and energy consumption while enhancing temporal resolution. Such sensors are capable of detecting transient thermal anomalies, such as flickering hotspots, which are typically missed by frame-based approaches. When coupled with on-chip AI accelerators, event-driven sensors can classify scenes in near real-time, even under fluctuating backgrounds. Adding to this, physics-informed neural networks (PINNs) represent a hybrid methodology where neural models are constrained by physical laws such as the governing equations for photoconductivity, carrier diffusion, and heat transport. These models combine empirical learning with physics-based structure, improving generalization and reliability in sensor design optimization. In parallel, efforts to co-fabricate photodetectors with analog computing elements, such as resistive memory arrays and photonic crossbars, are paving the way for embedded IR signal classification, spectral decomposition, and edge-level decision-makingexecuted entirely within the photonic substrate. Together, these computational strategies redefine the fundamental limits of infrared detection. They allow IR sensors to transcend conventional trade-offs between sensitivity, speed, and power by embedding intelligence within the readout process itself. This evolution toward edge-AI-enabled IR PDs marks a significant departure from traditional designs, signaling a future dominated by compact, energy-efficient, and context-aware sensing platforms capable of real-time environmental understanding across biomedical, industrial, and aerospace domains. Despite the remarkable advancements outlined in material, device, and system-level strategies for improving IR PDs, many of these approaches face critical limitations that hinder their practical adoption at scale. For instance, while 2D materials offer tunable bandgaps and strong light–matter interactions, their synthesis is often plagued by variability in layer thickness, grain boundaries, and interfacial contamination all of which degrade reproducibility across batches. Plasmonic structures, though excellent for enhancing local field intensity and responsivity, are typically fabricated using e-beam lithography or nanoimprint techniques that are cost-intensive and poorly suited for wafer-scale production. Complex heterostructures assembled from van der Waals materials also encounter challenges in achieving defect-free stacking, thermal stability, and consistent contact resistance. These issues become more pronounced under high-throughput conditions or when attempting CMOS integration. Moreover, some performance enhancements such as increased responsivity through photogating or quantum confinement often come at the cost of slower response times or elevated dark current, compromising temporal resolution or thermal noise floor [268,269]. Similarly, metasurfaces that promise wavelength selectivity or angular response control often require nanofabrication precision beyond what current scalable methods can deliver, and their operational stability under varying environmental conditions remains underexplored.

From a systems perspective, neuromorphic and computational sensing paradigms are still in early research phases. They rely on co-integration of analog computing and photonic sensing a field that lacks standardized architectures and suffers from limited device longevity and retention in memory elements. These trade-offs highlight the importance of not just optimizing performance metrics like detectivity or responsivity, but also addressing scalability, yield, power consumption, and long-term reliability. A successful IR PDs technology must balance innovation with manufacturability and robustness to meet the demands of real-world applications ranging from biomedical sensing to aerospace surveillance. While many advanced IR photodetection strategies show exceptional performance in laboratory conditions, their practical translation to commercial technologies faces substantial obstacles (Fig. 12). For example, 2D materials offer unique advantages such as tunable bandgaps, strong optical absorption, and high carrier mobility, yet their large-scale fabrication remains inconsistent. Layer number control, defect density, and interfacial cleanliness all impact reproducibility, posing challenges for device uniformity and yield. Similarly, plasmonic structures are praised for their ability to enhance local electromagnetic fields and improve responsivity, but their fabrication often relies on high-cost, low-throughput techniques like electron-beam lithography or focused ion beam patterning, which limits

industrial scalability. Heterostructures assembled from layered materials promise tailored band alignments and ultrathin junctions, but suffer from interlayer contamination, thermal instability, and variable contact resistance issues that complicate both integration and scaling. Meanwhile, metasurfaces, though effective in engineering spectral or angular responses, demand nanoscale precision in patterning and material uniformity, which current mass-manufacturing platforms struggle to provide. Even computational readout techniques, such as AI-enhanced signal processing or neuromorphic in-sensor computing, while conceptually powerful, require co-fabrication of analog circuitry and optical interfaces areas where process compatibility and long-term stability are not yet mature.

In short, the most promising strategies in terms of performance often involve complex trade-offs in terms of fabrication difficulty, environmental sensitivity, integration overhead, or poor yield. Future research must carefully weigh these factors to determine which combinations of approaches offer not only high detectivity and bandwidth, but also scalability, energy efficiency, and robustness under real-world conditions.

2.5. Thermal-based infrared photodetectors

Thermal-based IR PDs form a vital and complementary branch of IR sensing technologies, particularly in applications that require broad spectral response, room-temperature operation, and cost-effective, scalable fabrication. Unlike photon-based detectors, which rely on the generation of electron–hole pairs via direct photon absorption, thermal detectors function by converting absorbed IR radiation into heat, which subsequently induces a measurable electrical response through a material-specific mechanism. Due to their bandgap-independent operation, thermal detectors can be designed to work across a broad spectral range, from the near-infrared to far-infrared and even terahertz domains.

2.5.1. Detection mechanisms and material platforms

Thermal IR PDs operate based on indirect sensing of IR radiation, wherein incident photons raise the temperature of an absorbing material. This temperature change is subsequently converted into an electrical signal through one of several distinct transduction mechanisms. These mechanisms differ in how they translate thermal energy into a measurable electrical output, and each offers specific advantages depending on the targeted performance metrics such as sensitivity, speed, and spectral range. The most widely adopted thermal detection mechanisms include: Thermal infrared detectors operate through a range of transduction mechanisms that convert temperature variations into measurable electrical signals. One of the most widely used mechanisms is bolometric detection, where incident infrared radiation causes a temperature rise in a thermally sensitive material, leading to a measurable change in its electrical resistance. This resistance variation is typically monitored using a Wheatstone bridge or similar circuit configuration. Bolometers are often constructed from materials with a high temperature coefficient of resistance (TCR), such as vanadium oxide (VO_x), amorphous silicon (a-Si:H), or emerging low-dimensional nanomaterials [270]. Their broadband spectral response and compatibility with large-format microbolometer arrays make them ideal for uncooled thermal imaging systems. In contrast, pyroelectric detection relies on the temperature-dependent spontaneous polarization in ferroelectric materials like lithium tantalate ($LiTaO_3$), lead zirconate titanate (PZT), and polyvinylidene fluoride (PVDF). As the material undergoes a temperature change due to IR absorption, it produces a transient electrical signal as a result of a shift in polarization [271]. These detectors are inherently AC-coupled and are best suited for applications involving modulated or dynamic thermal signals, such as flame detection or motion sensing. Lastly, thermoelectric detection, most commonly realized using thermopiles, generates a voltage based on the Seebeck effect [272]. In this case, a series of thermocouples made from dissimilar metals or semiconductors produces a cumulative voltage proportional to the temperature gradient across an absorber and a heat sink. Thermopiles offer passive operation, low intrinsic noise, and relatively fast response times, making them suitable for non-contact thermometry, gas analysis, and compact consumer electronics [270,271]. Recent progress in materials science has dramatically

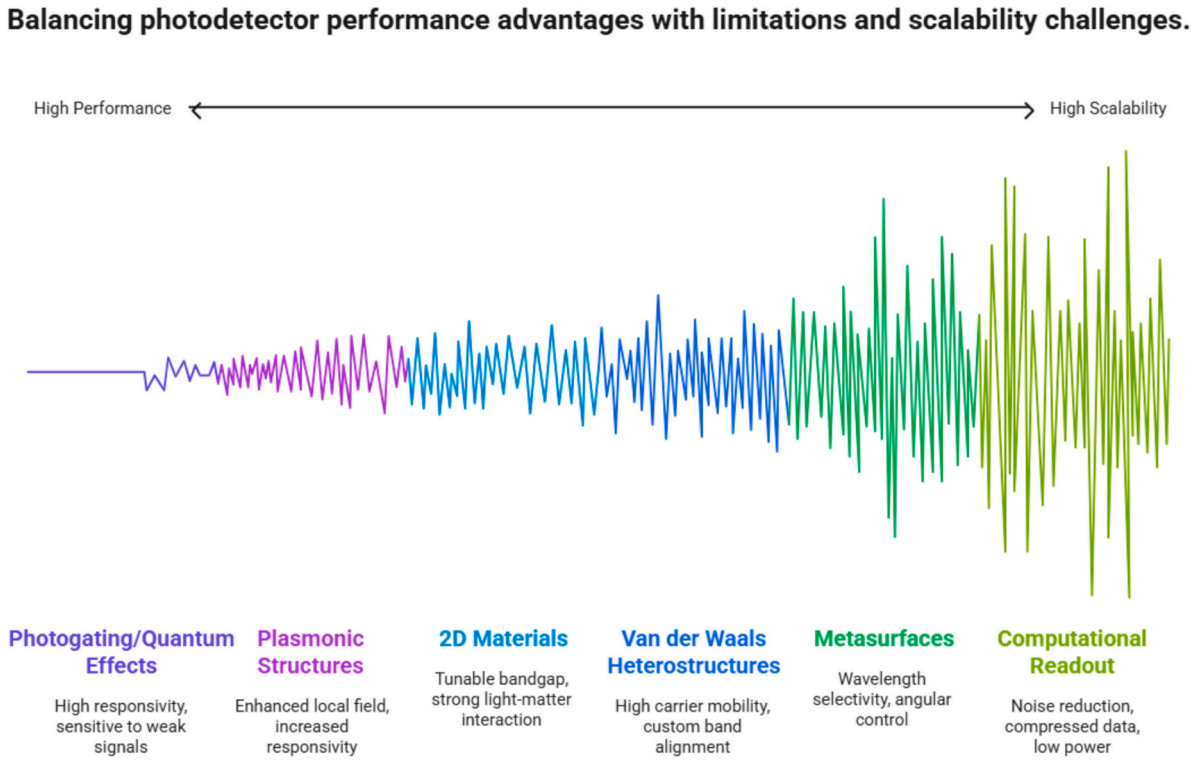

Fig. 12. Photodetector performance with limitations and Scalability challenges.

improved the functionality and application range of thermal IR detectors. In particular, 2D materials such as graphene, MoS_2, BP, and tellurium nanowires have emerged as compelling candidates for next-generation thermal detection. These materials offer extremely low thermal mass and high surface-area-to-volume ratios, which enable ultrafast thermal response and high sensitivity. Additionally, their mechanical flexibility allows integration with flexible substrates and wearable platforms.

A prime example is the use of $PdSe_2$ in photothermoelectric (PTE) detectors, which exhibit high responsivity (>13 *V/W*), rapid signal modulation, and intrinsic polarization sensitivity. These detectors capitalize on the anisotropic thermal and electrical transport properties of 2D crystals to enhance PTE conversion efficiency. Similarly, tellurium nanowires and BP heterostructures have shown excellent responsivity and broadband detection capabilities, with the added benefit of directionally dependent photoresponse. Another rapidly advancing material class is CQDs, such as HgSe, HgTe, and PbSe, which provide size-tunable bandgaps and strong IR absorption in the mid-to-long wavelength regime. Their solution processability enables low-temperature, large-area fabrication via spin-coating or inkjet printing, making them ideal for cost-sensitive and scalable uncooled IR detector applications. CQDs also show promise for integration with flexible or curved substrates, enabling novel form factors for IR sensing [270,271].

To further boost optical-to-thermal conversion, nanostructured absorbers and engineered photonic architectures have been developed. For instance, nano-fenced MoS_2 structures enhance IR absorption by creating localized thermal confinement and enhancing heat dissipation contrast. These structures not only improve responsivity but also maintain performance stability at elevated temperatures an essential feature for real-world deployment in harsh environments [273]. Moreover, the integration of MEMS technologies has transformed thermal IR detector performance. MEMS-based designs such as suspended microbridges, thermally isolated pixels, and cantilevered absorbers minimize thermal conductance to the substrate, enabling a higher temperature rise per incident photon and thus boosting detector sensitivity. These platforms form the backbone of most commercial microbolometer arrays and are increasingly being adapted to support advanced nanomaterial integration [272]. Collectively, these developments in detection mechanisms and materials platforms have significantly expanded the functional capabilities of thermal IR PDs. Through careful optimization of material properties, geometry, and thermal isolation strategies, modern thermal detectors now offer performance that approaches or even competes with that of photon-based detectors in many application domains—while maintaining the distinct advantages of broadband detection, room-temperature operation, and simplified system design.

2.5.2. Performance benchmarks and comparative highlights

Recent advancements in material engineering and device architecture have significantly improved the performance of thermal-based IR PDs, enabling room-temperature operation with impressive responsivity and detectivity. A variety of platforms reported in the literature showcase the growing potential of these detectors across different application domains. For instance, $PdSe_2$-based photothermoelectric (PTE) detectors demonstrate responsivity exceeding 13 *V/W* and are notable for their intrinsic polarization sensitivity and fast switching characteristics. Graphene-based bolometers integrated with $LiNbO_3$ substrates have exhibited an exceptionally high temperature coefficient of resistance (TCR) reaching up to 90 %/K, with μK-level thermal sensitivity, positioning them as strong candidates for ultra-sensitive thermal imaging. Nano-fenced MoS_2 devices achieve responsivity as high as 1358 mA/W and detectivity on the order of 2.8×10^{10} Jones, while also maintaining stable performance at temperatures up to 100 °C, making them suitable for self-powered, thermally robust applications. Heterostructures combining BP and WSe_2 have demonstrated broadband response and polarization sensitivity, with responsivity around 0.5 A/W and detectivity near 10^{10} Jones [271]. Tellurium nanowires, another promising 1D material system, exhibit extremely high responsivity (~6650 A/W) and broadband blackbody compatibility. Meanwhile, HgSe quantum dot films, despite lacking precise responsivity values, offer detectivity comparable to cryogenically cooled detectors (e.g., LN_2-cooled systems) while maintaining room-temperature operation [274]. Their solution-processability and tunability make them attractive for large-area, low-cost thermal sensor arrays. These benchmarks collectively illustrate how advanced materials and nanoengineered architectures are driving thermal IR detectors toward high-performance, scalable, and versatile solutions.

2.5.3. Integration with emerging technologies and comparative advantages

The functionality of thermal infrared detectors is rapidly expanding as they are increasingly integrated into emerging electronic and computational platforms, including neuromorphic systems and energy-autonomous sensors. In these contexts, thermoelectric and pyroelectric materials can be directly coupled with analog or in-memory computing elements to facilitate on-sensor processing, enabling operations such as feature extraction, classification, and environmental adaptation without the need for centralized computation. This co-integration not only reduces energy consumption but also supports real-time decision-making in compact, wearable, or distributed sensing systems. Furthermore, the ability of thermoelectric materials to convert thermal gradients into electrical energy enables the development of self-powered IR detectors, which are particularly valuable for long-duration or remote applications in space exploration, defense, and environmental monitoring. The convergence of thermal sensing and energy harvesting in a single, multifunctional platform represents a critical step toward the realization of autonomous, maintenance-free infrared detection systems.Compared to photon-based detectors, thermal detectors present several distinct advantages. These include broadband spectral sensitivity that is independent of the material's electronic bandgap, operation at ambient temperatures without the need for cryogenic cooling, and simplified, low-cost fabrication, especially suited for large-area and flexible substrates [274].

These attributes make thermal detectors particularly attractive for use in consumer electronics, smart textiles, and cost-sensitive imaging applications. However, these benefits are counterbalanced by inherent trade-offs, such as slower response times typically in the millisecond range lower specific D* due to higher thermal noise, and reduced spatial and temporal resolution, particularly in fast, dynamic imaging scenarios. Nevertheless, recent developments in low-dimensional materials, nanostructured absorbers, and thermal isolation architectures as well as the introduction of on-chip compensation and AI-based signal enhancement techniques are steadily closing the performance gap between thermal and photon-based detectors. These advancements suggest a growing role for thermal IR detectors in next-generation intelligent sensing systems, where performance, cost, and integration flexibility must be balanced.

3. Representative applications of infrared photodetectors

The principal application of IR PDs used in various industries including automotive, medical, semiconductor, food processing, and astronomy have recently adopted the use of IR PDs based cameras due to their ability to accurately measure temperature without physical contact and to monitor without causing damage. These IR cameras can monitor food quality, semiconductor chips and devices, and road conditions. IR technology's ability to monitor without physical touch or causing damage has resulted in its development for several medical purposes, such as blood vein monitors, brain injury detectors, diabetic neuropathy, thermography, and cancer cell detectors. At present, several medical instruments are being assessed to be used in medical applications and a multitude of other ones will be introduced to the market in the future decade. The IR PDs camera has numerous captivating applications, with

astronomy being particularly exciting. Moreover, cryogenic cooling has been the standard for the most sensitive IR PDs cameras up until now, but this has increased the cameras' size and maintenance costs. There are four demands for most applications. Firstly, the ability to fabricate large imaging focal plane arrays (FPA) is crucial; secondly, the need for imaging systems to be capable of cooling down to room temperature or thermal equilibrium, a feature currently unavailable for most IR PDs cameras; thirdly, the ability to integrate with silicon microcircuit technologies to create smaller and more affordable systems; and fourthly, the potential for mass production that could lead to more affordable IR PDs devices or cameras [275].

3.1. Health sector

Heat sensors were already in development before the full understanding of IR technology. The development and widespread use of various IR detector technologies, however, did not occur until the middle of the 20th century. There are several uses for IR detectors in thermal imaging. The fields of medicine, weather, search and rescue, surveillance, and climatology are among those that make use of thermal imaging for biomedical applications. For instance, by comparing the amounts of light absorbed at two wavelengths, one can determine a number of characteristics pertaining to blood flow, including pulse rate, blood pressure, and oxygen saturation. In this context, **Xu et al.** [276] developed a flexible near-IR photo-induced degradation (NIR-PPG) sensor by combining an organic PDs with excellent sensitivity and an inorganic light-emitting diode with excellent efficiency (Fig. 13a). The organic PDs that has been chosen as an active layer is made up of a DPP-DTT:PCBM bulk heterostructure that can absorb near-IR light. In addition, a double-layer gate dielectric layer allows for the realization of phototransistor-type FPDs with low operating voltage (Fig. 13b). The noise equivalent power of this device is 1.2×10^{-15} $WHz^{-1/2}$, and its NIR responsivity is up to 3.5×10^{-5} A W^{-1} (Fig. 13c). This makes it better than commercial silicon-based PDs. By putting this technology directly on the skin, researchers showed that the flexible PPG sensor could record heart rate variability continuously and accurately track changes in pulse pressure in different body positions using electrocardiogram monitoring.

There is also the use of IR PDs in the optical coherence tomography measurements of skin [275]. Here the use of wavelengths of 1300 nm is the best choice because water in the skin absorbs all other IR wavelengths whereas using visible light results in a lot of scattering from the skin's structure which severely degrades the imaging depth and quality. Note that optical coherence tomography measurements of skin are currently undergoing clinical trials for their ability to detect skin cancer and other diseases without needing to perform an excision [277], whereas all other currently clinically approved skin cancer detection methods involve an excision.

Despite the critical role that PDs play in improving the medical health status of humans, the limited spectral detection range, low stress stability, and non-degradation of standard PDs impede the development of wearable medical devices in the health sector. In this context, **Zhang et al.** [278] devised an intelligent healthcare monitoring system utilizing IR PDs technology. The system integrates a paper substrate and pure PbS via mechanical friction (Fig. 13d). The six-arm stellate dendritic shape and 1.01 eV band gap of PdS were responsible for this system's

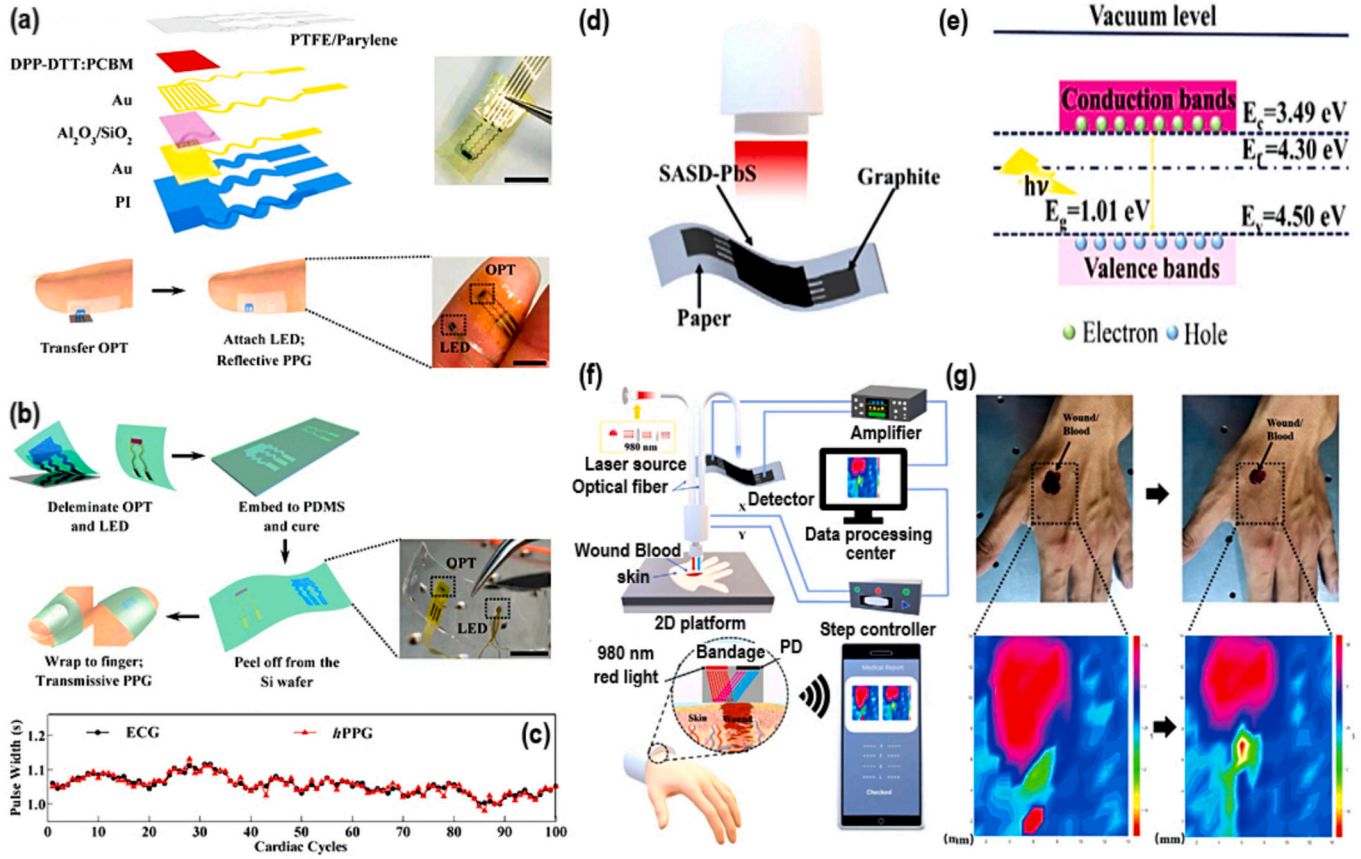

Fig. 13. (a) Representation of OPT device along with image of freestanding OPT, and epidermal hPPG sensing device. (b) Representation of process flow for assembly hPPG sensing device along with the picture of hPPG sensor. (c) The HRV tracking performance plot. (a-c) are taken with permission [276]. Copyrights @2017 WILEY-VCH. (d) Detector diagram. (e) Band structure of PbS. (f) Diagram of imaging system along with the demonstration of imaging system design accompanied by intelligent patch wound recuperation tracking imaging. (g) Rehabilitation of wounds compared using physical and imaging approaches. (d-g) are taken with permission [278]. Copyrights @2022 WILEY-VCH.

remarkable performance (Fig. 13e), which spans a broad detection spectrum from 365 to 1550 nm. Furthermore, this PD device, operating at a wavelength of 980 nm with an intensity of 50.4 μWcm^{-2}, exhibits a responsivity of 6.45 mAW^{-1}, a detectivity of 6.4 × 10^{10} Jones, a response recovery time of 0.36 s/0.41 s, and demonstrates excellent mechanical stability. Remarkably, this PD system exhibited a broader range of detection, superior ability in detecting weak signals, and a quicker response time when compared with paper-based PD system (Fig. 13**(f-g)**).

On the other hand, the manufacturing of second-near-IR (NIR-II) PDs is crucial for the creation of flexible photodetection devices that can easily integrate with 3D geometries to reliably identify and gather different types of data in real-time. But there has yet to be a technology that combines great photosensitivity, rapid photo reaction, and outstanding versatility. Considering these aspects, **Zhu et al.** [279] created IR PDs and arrays that look like skin by mixing photo-sensitive PbS quantum dots (PbS QDs) with conducting MXene ($Ti_3C_2T_x$). This allowed for efficient transport between spatially separated layers and greatly enhanced photocarrier separation at the bilayer interface. The enhancement in mechanical and optoelectronic properties is attributable to the excellent interface that was formed by the two-layer structure and strong bonding of MXene and PbS QDs. After 500 cycles of bending, the produced (NIR-II) PDs showed an impressive responsivity of 1000 mAW^{-1}, a photo-response time of 30 s, and a retention of performance of over 95 %. This work demonstrates the promising potential of inexpensive and high-performing MXene/PbS quantum dots-based material to be utilized to develop the next generation of IR PDs based systems, including optical communication, NIR-II imaging, and proximity sensing in a range of settings.

3.2. *Imaging sensors*

Among the many significant uses of IR PDs are imaging sensors. PDs, an essential component of imaging sensors, transform light into electrical signals that can be further processed and transformed into digital images. In most imaging sensors, these PDs are arranged in a grid or array, with each one responsible for collecting light from a specific area of the picture. A proportionate current is generated by PDs in reaction to light, with the intensity of the light determining the exact ratio. Each pixel's brightness and color are represented by a digital signal that is amplified from these produced currents. The digital signal is then processed by image processing algorithms to create a digital picture, which can then be saved or shown. Traditional silicon-based commercial image sensors are not very scalable or stretchy. Meeting the expectations of modern wearable technologies, including integration, miniaturization, and multi-functionality, is made tough by these limits. Organic and perovskite materials used in innovative IR PDs have the added benefit of being color-selective in addition to being flexible. Such improvements are significant since this quality is necessary for full-color selectivity in image sensing.

In order to achieve almost perfect sensing in all directions in curved and flexible organic PDs, it has been proposed to use carbon nanotubes instead of indium-tin oxide, as carbon nanotubes possess outstanding mechanical, optical, and electrical characteristics. In order to achieve optimal performance with organic PDs, it is crucial to strike a balance between their packing density and transmittance. This is because the creation of appropriate top layers depends on the presence of dense nanotube arrays. In this context, carbon nanotubes served as an electrode on a substrate that possesses both flexibility and rigidity [280]. The carbon nanotube electrode exhibits a detectivity of 2.07 × 10^{14} Jones, surpassing indium-tin oxide-based devices by a factor of 100. Additionally, it maintains an average optical transmittance of 90 %. It reduces dark current to a level that is lower than 1.0 × 10^{-12} A. The high electron injection barrier was created by the deep work function of the carbon nanotube electrode, which was determined by photoelectron yield spectroscopy (Fig. 14**(a-c)**). This investigation also considered the energy level bending caused by the electrode-semiconductor interface. The stability of organic PDs built with carbon nanotube electrodes was proven through a cyclic flex test involving 500 bending cycles.

On the other hand, solution-processed lead-halide perovskites are a highly promising material for flexible optoelectronics. The inability of perovskite materials to be used in production processes that involve polar liquids restricts the integration of ultrathin perovskite PDs. Recently, ***Wu* et al.** [281] developed a perovskite-based PDs array (10 × 10 pixels), having 2.4 μm thickness, is highly flexible, lightweight (3.12 g/m^2), and conformable. The active layer of all-inorganic $CsPbBr_3$ perovskite films may be patterned accurately in terms of pixel position, tunable morphology, and uniform size using a vacuum-assisted drop-casting patterning process (Fig. 14**(d-f)**). Employing a waterproof perylene-C film as both the substrate and the encapsulating layer effectively shields the perovskite films from polar liquid infiltration during the peel-off process. The device's encapsulation and ultra-thinness give it the ability to remain stable in the environment for a long time, endure bending and 50 % compressive strain, and maintain exceptional mechanical stability (Fig. 14**(g-m)**). The visualization of light scattering is enabled by the ultrathin flexible PDs arrays that adhere to a hemispherical support. This presents intriguing opportunities for vision-sensing devices that replicate the functionality of the retina.

On the other hand, the photoactive halide perovskites possess exceptional optoelectronic properties, customizable bandgaps, and can be easily produced on a wide scale, which makes them promising candidates for color-imaging sensors that do not require filters. Preparing patterned perovskite films using solution procedures is challenging, and evaporation methods often result in perovskite PDs with restricted performance. As a result, existing manufacturing techniques struggle to create superior-patterned perovskite films suitable for these specific applications. For instance, *Chen* et al. [282], show a way to make patterned perovskite films better by covering the substrates with a single layer of brominated (3-aminopropyl) triethoxysilane and using a better evaporation method to do it (Fig. 15**(a-b)**). The inclusion of polymer substrates improves the device's flexibility (Fig. 15**(c-e)**). Finally, sensors capable of differentiating between red, green, and blue colors are produced by combining perovskites with three separate halide components, each with a unique band gap, into a device array using the established evaporation procedure. The flexible photosensor arrays demonstrate their ability to consistently generate vibrant visuals that closely match familiar patterns (Fig. 15**(f-h)**). This research demonstrates that it is feasible to achieve filter-free color imaging by utilizing multicomponent perovskite PDs and high-performance patterned perovskites. This exhibits the potential of these detectors for advanced optoelectronic applications, including hyperspectral imaging.

Moreover, imaging of light dispersion is accomplished by means of the ultrathin PD array that conforms to the hemispherical scaffold. An improved technique for producing arrays of PDs by vacuum-evaporating perovskite photoactive layers was created by Chen et al. [282] 2D materials have emerged as promising candidates for photodetector applications owing to their atomic-scale thickness, outstanding optoelectronic properties, mechanical flexibility, and the capability to form van der Waals heterostructures without the need for lattice matching. The electromagnetic spectrum is categorized into ultraviolet (UV, 10–400 nm), visible (400–750 nm), IR (IR, 0.75–30 μm), and terahertz (30 μm–3 mm) regions, with the IR range further subdivided into near-, short-mid-, long-, and very long-wave bands**.** Fig. 15h. from the referenced source outlines a strategy to eliminate the van der Waals gap in mixed-dimensional heterostructures to enhance photodetector performance. In particular, Fig. 15**h.** presents current–time curves for a PbS/MoS_2 photodetector under illumination at wavelengths of 808, 1340, and 1550 nm. This mixed-dimensional heterostructures and introduces an innovative approach aimed at improving device performance by addressing the intrinsic van der Waals gap. This gap, which exists at the interface of van der Waals heterostructures (vdWHs), serves

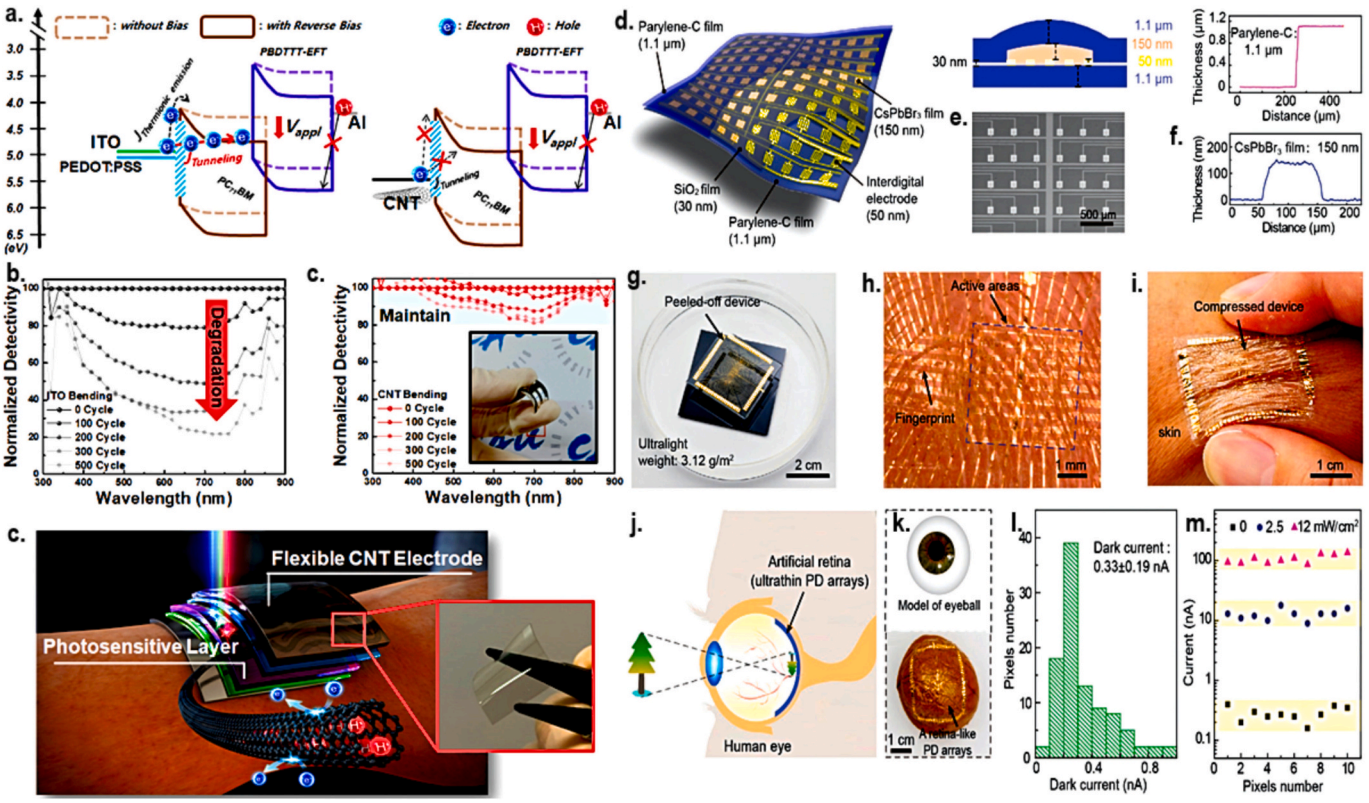

Fig. 14. Photoelectron spectroscopic responses of (a) ITO, PEDOT: PSS, CNT-based electrodes. (b) Current generation responses, and corresponding (c) Number of bending cycles, (d) The physical contact of the constructed device on hand. Taken from [280]. Copyrights © 2021 Elsevier. (d-f) Representation of ultrathin $CsPbBr_3$-based device, ultrathin $CsPbBr_3$ thickness, SEM picture of the active area, and plots between thickness and distance. (g) Picture of peeled-off device with ultra-lightweight floating on NaCl solution. (h-i) Picture of the constructed device incorporated with the finger. (j) Representation of constructed artificial vision sensing. (k) Image of eyeball and ultrathin PD arrays. (m) The dark current response @5 V bias V. e) 10 pixels picture of different illumination. Taken from [281]. Copyrights © 2021 Wiley-VCH GmbH.

as a tunneling barrier and can hinder the efficient injection of photo-generated carriers in phototransistor devices.

3.3. Optical devices

One additional significant use of IR PDs is in optical communication technologies. As they transform light into electrical impulses, PDs play a crucial role in optical communication systems. Light signals encoded with information can be received by these devices over fiber-optic cables or even free space. PDs can detect very weak signals because they are very sensitive to light. When they receive a signal, they produce a current that is directly proportionate to the strength of the light signal [15,284]. Following amplification, the current undergoes digital signal conversion, allowing for processing and transmission via the communication channel. PDs, in a nutshell, are the backbones behind optical communication systems, which can send data quickly and efficiently across great distances with almost no signal degradation. Moreover, the data processing, and human-machine interaction might be made easier with the use of flexible optical communication technology that could connect a variety of wearable devices. The use of PDs that can selectively detect wavelengths is necessary, though.

Furthermore, optical communication systems operate within a defined spectral range, typically between 300 nm and 1600 nm, with peak utilization at 850 nm, 1310 nm, and 1550 nm due to the minimal signal attenuation exhibited by optical fibers at these wavelengths [285,286]. Still, IR light is still the most used optical signal for many applications, including the Internet of Things, radar systems, data communications, and remote control, even though ultraviolet and visible light communication has come a long way in the last decade. Applications and distance requirements dictate which optical communication bands are best suited. Therefore, it is essential to minimize signal attenuation during transmission and avoid interference from ambient light while developing flexible electronic equipment. The prior research has also demonstrated the possibility of visible-light communication with wearable devices. For instance, ***Liu* et al.** [287] present an advanced optical photodetector (OPD) that employs a tandem structure to effectively reduce both the carrier transit time and the RC time constant of the device. This innovative design achieves an outstanding response speed of 146.8 ns, setting a new record in the field. The tandem structure lets voltages to be split and multi-level barriers to be added (**Fig. 16(a-d)**). This makes for a very low noise current of 7.82×10^{-14} A $Hz^{-1/2}$ and a wide detection range from 300 to 1000 nm. The effective use of the tandem OPDs as signal receivers in the optical communication system further exemplifies the precise transmission of digital signals from visible to near-IR light. Tandem OPDs are highly promising in the field of wireless transmission systems.

For instance, utilizing specifically tailored ink formulations, ***Strobel* et al.** manufactured bulk-heterojunction PDs that selectively absorb certain wavelengths [288]. They showed the results of using the produced PDs in a filter-less visible-light communication system, which allowed them to demultiplex mixed optical data and exhibit color selectivity (**Fig. 16(e-h)**). Further, based on a perovskite material made of formamide ($(BA)_2FAPb_2I_7$), ***Wang* et al.** developed flexible PDs [289] for optical communication. They suggested that the incorporation of gold nanostructures onto the substrate enhanced the light-matter interaction, likely due to the enhanced localized surface plasmon resonances (LSPRs), showing 2.3 AW^{-1} maximum responsivity, a maximum response speed of about 9 microseconds, 3.2×10^{12} Jones detectivity,

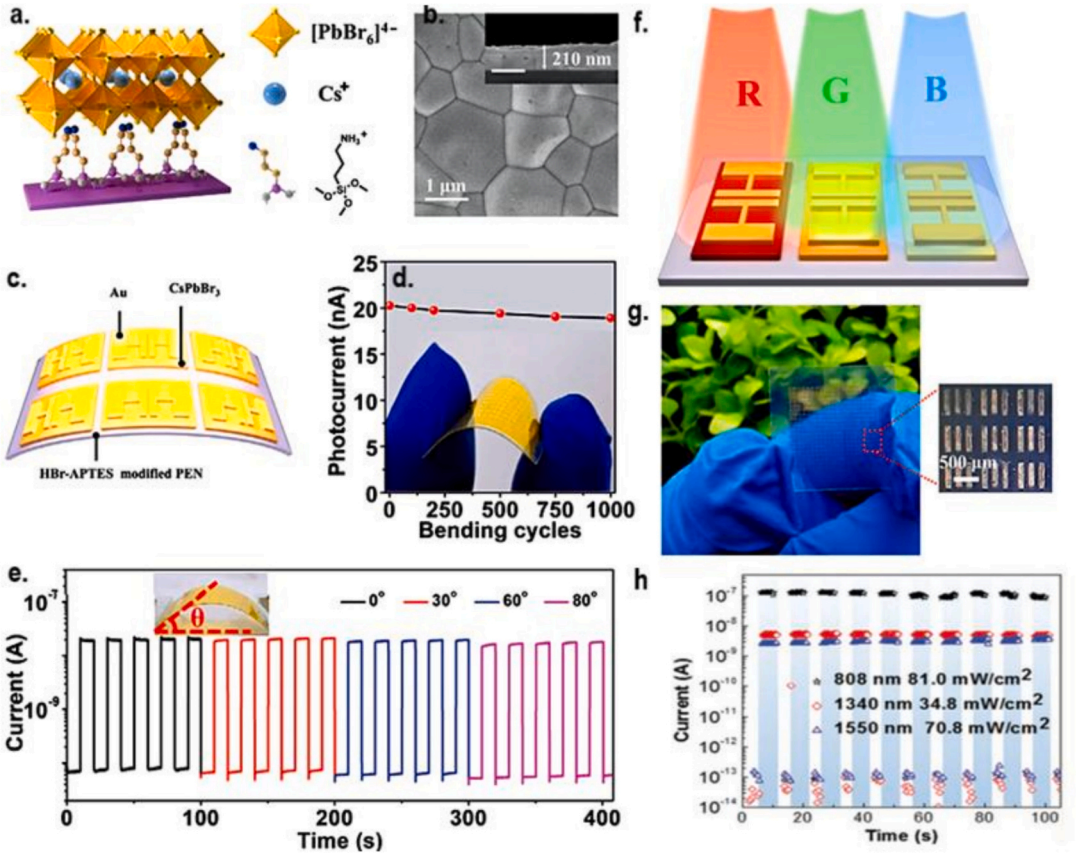

Fig. 15. (a) Crystallographic representation of the attachment of $CsPbBr_3$ perovskite with HBr-APTES-templet. (a) A SEM image of the $CsPbBr_3$ layer (c) A photo showing a built-in PDs array. (d) The built-in PDs device's photocurrent reaction. (e) PDs for time-dependent photo signals. (f) Detecting the created device's red, green, and blue lights apart. (g) A photo of the color imaging array. Taken from [282]. Copyrights© 2021 Wiley-VCH GmbH (h) Current–time curves based on PbS/MoS2 photodetector with the illumination of 808, 1340, and 1550 nm. Taken from [283] Copyrights© 2021 *Wiley*.

and stability over the thousand hours in a natural environment. In addition, the manufactured PDs was effectively used as an optical signal receiver to send ASCII-encoded data as part of a visible-light communication system. Fibrous PDs are a lightweight and flexible tool for efficient optical information transmission with high integration characteristics. They offer unique advantages in optical communication technology and have garnered significant interest in the field of wearable devices and consumer electronics. Interestingly, the integration of fibrous PDs into wearable technologies presents several complex challenges related to materials, structural design, fabrication, and long-term performance. A primary difficulty lies in reconciling the need for high optoelectronic efficiency with the mechanical flexibility required for wearable use. This necessitates the selection of materials and substrates that can sustain high performance while being sufficiently pliable to conform to the contours and movements of the human body [290]. Moreover, device architectures must be engineered to endure repetitive mechanical deformation such as bending and stretching—without compromising their operational integrity. On the manufacturing front, combining dissimilar materials with varied mechanical, thermal, and electrical properties poses additional obstacles [291]. It is critical to preserve functionality during processing while ensuring that the final device remains comfortable, lightweight, and mechanically stable. The seamless integration of fibrous PDs into fabrics or flexible platforms further demands innovative approaches to establish durable electrical connections and ensure long-term reliability under dynamic wear conditions. Environmental stability is also a major concern, as wearable PDs are routinely subjected to sweat, moisture, and mechanical stress [290]. Therefore, these devices must maintain sensitivity, a broad detection range, and robust operation throughout extended use. Addressing these multifaceted issues calls for continued advances in materials science and device engineering, including novel substrate modifications, functional material innovations, and optimized device configurations. Progress in these areas will be key to realizing the full potential of fibrous PDs in wearable systems, paving the way for next-generation applications in biomedical monitoring, smart textiles, and on-body optical communication. A compelling example of wearable IR photodetector integration is demonstrated by Kim et al., Zhang et al., and Zhou et al., who have developed fiber-shaped infrared photodetectors using PbS quantum dots and carbon nanotube (CNT) hybrid structures. These devices exhibit excellent flexibility, enabling them to be woven into fabrics or worn directly on the body. They offer broadband photodetection across the NIR to SWIR range with high responsivity and mechanical durability, making them suitable for applications in smart textiles and health monitoring. These examples illustrate how IR photodetectors can be effectively adapted into wearable form factors without compromising performance [292–294].

When compared to photodiodes and photoconductors, the three-terminal device structure of phototransistors used in fibrous PDs for optical communication makes integration more difficult. Compared to stacked or planar two-terminal PDs, fibrous PDs require more intricate preparation methods and integration techniques. The quality of the film, the contact between the vertical gates, the insulation between the layers, and the intercalation of dielectrics are all critical. The flexibility characteristic is still preferred, especially for larger areas in wearable systems, even if extremely miniature, non-flexible devices can fulfill wearable criteria. Using stiff island devices is an encouraging strategy for overcoming the lack of flexibility in non-flexible components while still taking advantage of the benefits of such structures [259,260,296].

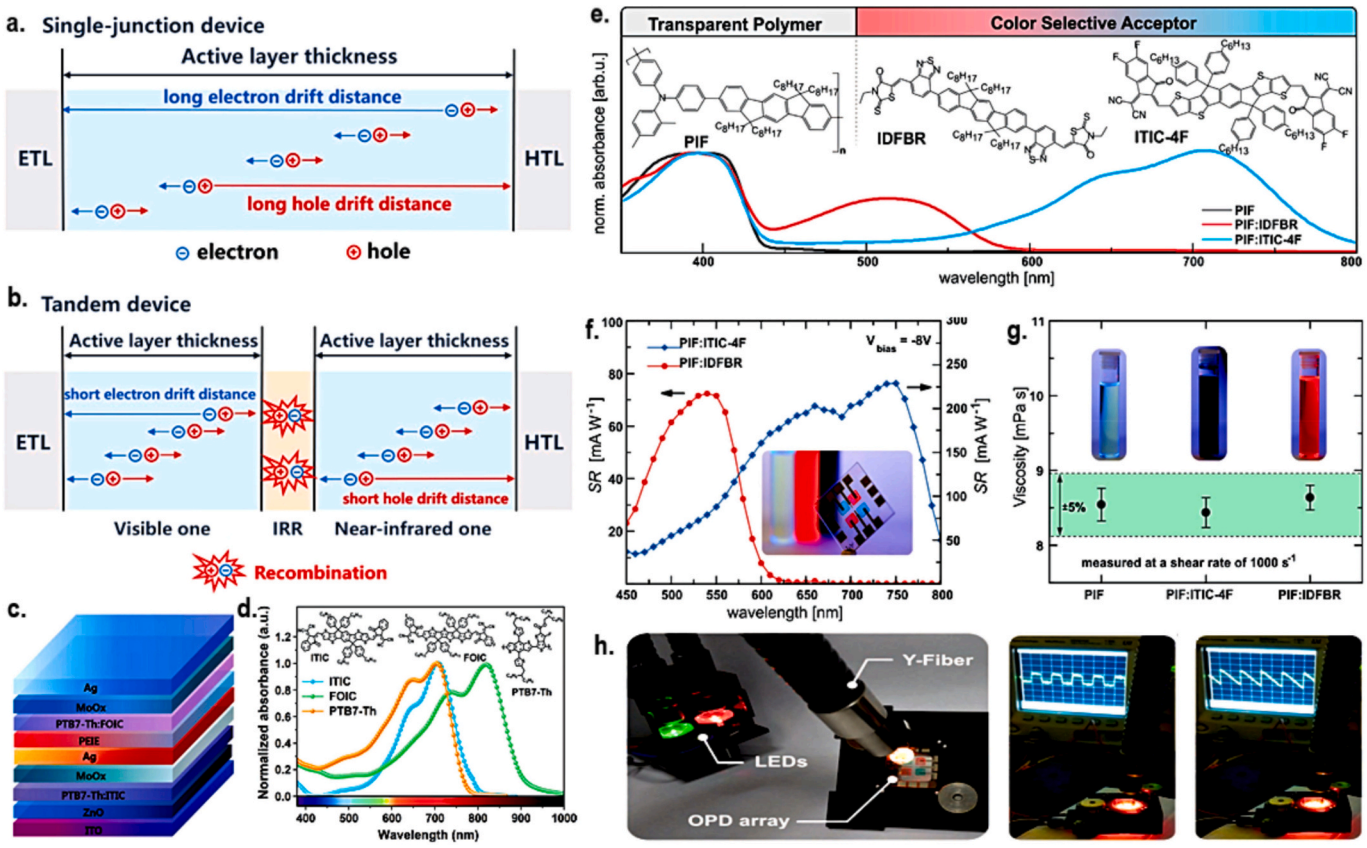

Fig. 16. A systematic illustration of (a) single-junction and (b-c) tandem devices. (d) The recorded electronic spectra of PTB7-Th, ITIC, and FOIC films. Taken from [295]. Copyrights© 2021 Wiley-VCH GmbH. (e) Electronic spectra, comprised of transparent polymer donor and different NFAs, of various materials. (f) The spectral responsivity of NFAs IDFBR (green/blue) and ITIC-4F (red) OPDs, respectively. and corresponding (g) viscosities. (h) Picture of the constructed PD-based systems. Taken from [287]. Copyrights© 2020 Wiley-VCH GmbH.

This leads us to believe that improving the functionality of cell devices will not be the end goal of future fibrous PD improvements, and research instead will focus more and more on improving the miniaturization, integration, and intelligence of fibrous PDs in flexible electronic systems. Improvements to fibrous PDs' operating stability and environmental compatibility are in the works, which should increase their usefulness and effectiveness. Recently, ***Rein* et al.** [297] successfully realized the scalable thermal drawing of electrically connected diode fibers. Initially, they construct a sizable preform, including hollow spaces that facilitate the passage of copper or tungsten wires, as well as individual diodes integrated within the framework (Fig. 17**(a-d)**). By subjecting the preform to heat and pulling it into a fiber, numerous diodes are connected in parallel within a single fiber as the conducting wires approach and establish electrical connections with the diodes. Two types of IR devices are fabricated: PDs and light-emitting diodes. The light is concentrated and aligned using a lens that is integrated into the outer layer of the fiber (Fig. 17**(e-g)**). This approach is suitable for use in clothing applications since diode fibers maintain their performance even after ten machine-wash cycles. A bidirectional optical communication link with a frequency of three megahertz is established between two fabrics that contain receiver-emitter fibers to demonstrate the practicality of this approach (Fig. 17**(h-k)**). Furthermore, the diodes' capacity to gauge heart rate implies their potential utility in physiological status monitoring systems that encompass many types of fabrics. By increasing the density and usefulness of thermally drawn textile-ready fibers, this approach holds promise for a fiber equivalent of 'Moore's law', enabling the development of increasingly sophisticated functionalities in fibers. It is also noteworthy that Figs. 17**(l–p)** collectively illustrate the impressive mechanical adaptability and environmental stability of PeQW-based fiber light-emitting diodes (Fi-LEDs), emphasizing their strong potential for wearable electronic applications. The stretchability of these devices, as depicted in Figs. 17**(l) and (m),** is achieved through a wavy (undulant) structural design, allowing elongation up to 100 % while maintaining light emission. This geometry effectively mitigates mechanical strain on the active layers by absorbing deformation. Figs. 17**(n) and (o)** present quantitative assessments of mechanical durability, demonstrating that the devices retain over 85 % of their original electroluminescence after 500 bending cycles, with thinner fibers exhibiting even greater resilience. Under tensile stress (Fig. 17**p.),** the devices maintain 85 % EL at 100 % strain, though a decline to 50 % is observed after 150 cycles at 60 % strain, indicating that stretching imposes greater mechanical degradation than bending. Thinner fibers again show improved endurance. Additionally, Fig. 17**p.** underscores the robust waterproofing performance of the PDMS-encapsulated Fi-LEDs, as evidenced by the sustained EL output after more than 1000 h of continuous water immersion [283]. This high level of moisture resistance is critical for the practical deployment of wearable devices. These findings highlight the strong potential of PeQW-based Fi-LEDs for use in flexible and wearable technologies, owing to their outstanding mechanical flexibility, durability, and resistance to environmental stress.

3.4. Environmental and gas sensing

IR PDs play a pivotal role in environmental and gas sensing by enabling the detection of trace gases such as carbon dioxide (CO_2), methane (CH_4), nitrous oxide (N_2O), and volatile organic compounds (VOCs), which have distinct infrared absorption features. These gases absorb strongly in the mid-wave infrared (MWIR, ~3–5 μm) and long-wave infrared (LWIR, ~8–14 μm) regions, making IR PDs

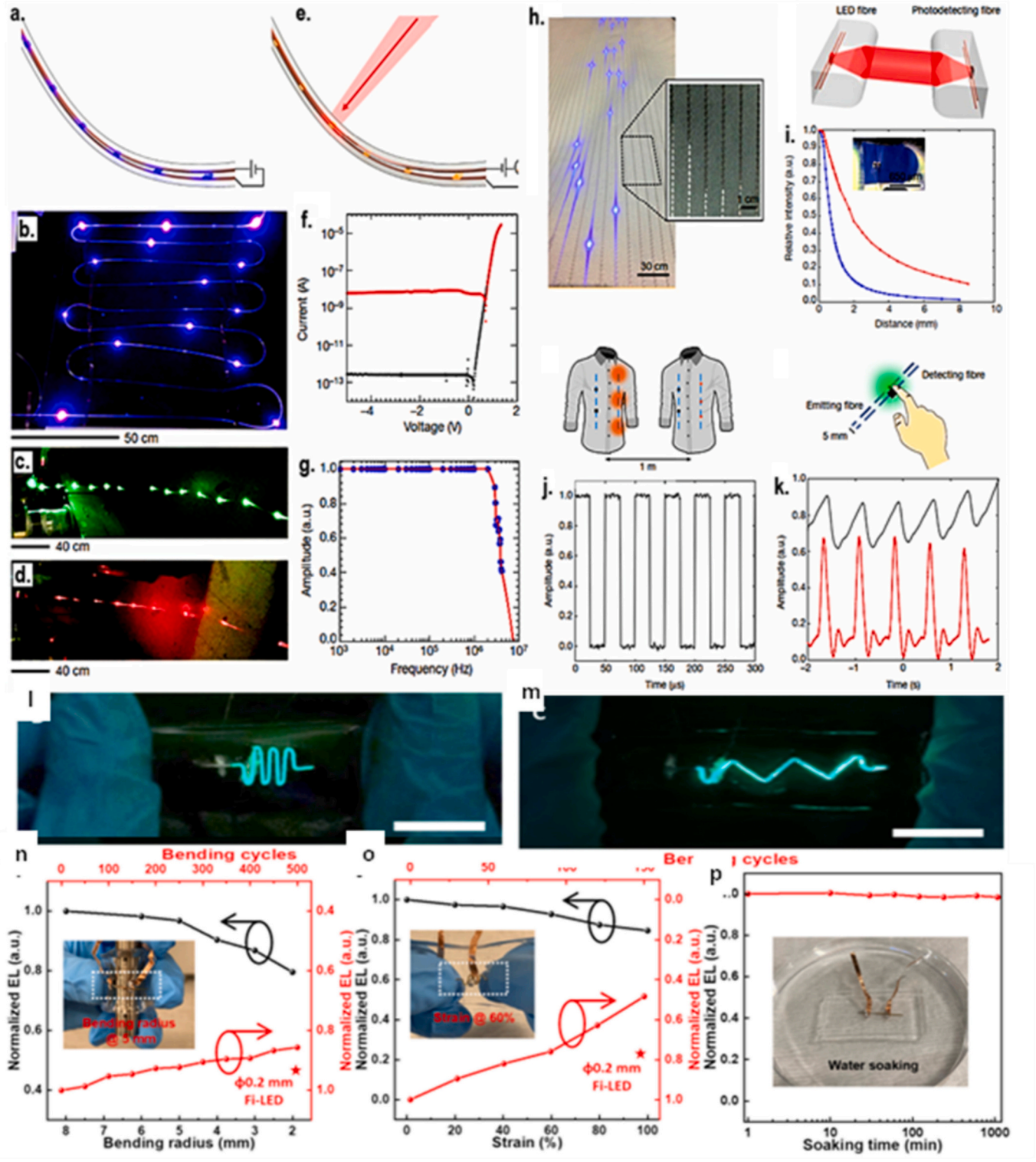

Fig. 17. (a, e) Systematic illustration of light-emitting fibers (LEF). (b-d) Pictures of LEF having InGaN blue, green, and red. (e-f) Current vs voltage, and amplitude vs frequency curves GaAs device. (h) Light-emitting and photodetecting fibers embedded in a fabric. (i) The measured current of the photodetecting fiber. (j) the experimental results of the current recorded by the photodetecting fibers incorporated into a fabric. Taken from [297] Copyrights © 2018 Springer Nature. 12(l–p) illustrate the mechanical and environmental performance of encapsulated Fi-LEDs: (l) and (m) show the stretchable device in its original undulant form and under strain; (n) and o) present quantitative assessments of bendability and stretchability, with inset images of the devices under deformation; and (p) displays the device's long-term stability during continuous water immersion. All unlabeled scale bars represent 1 cm. Taken from [283] Copyrights © 2024 AAAS.

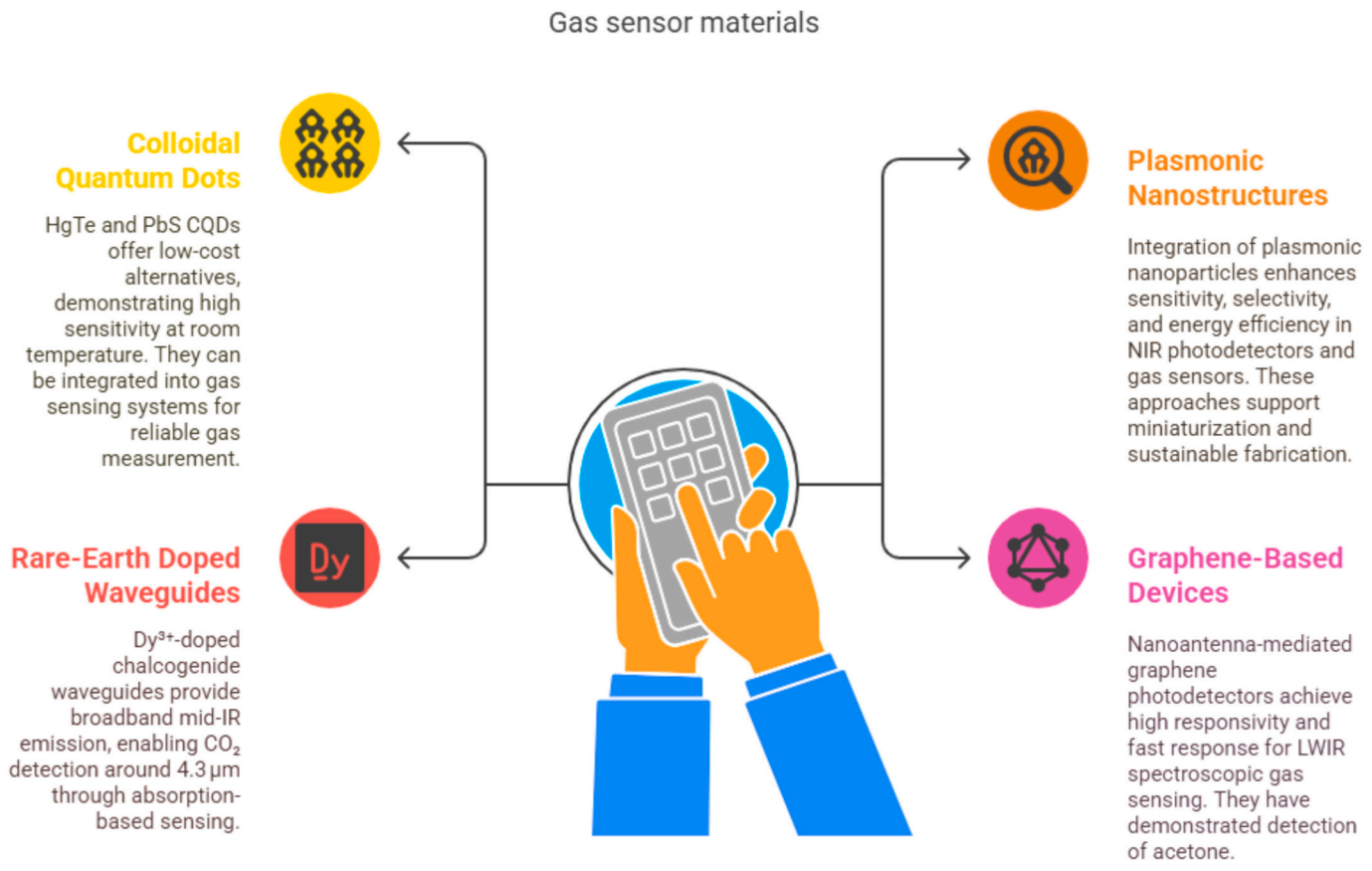

Fig. 18. Environmental and Gas Sensing Using IR PDs.

exceptionally effective for selective, sensitive, and real-time monitoring. Among the most established techniques is non-dispersive infrared (NDIR) sensing, where broadband IR light is passed through a gas sample and specific molecular absorption bands—such as 4.26 µm for CO_2 or 3.3 µm for CH_4—are measured using selective detectors like pyroelectric sensors, thermopiles, or photoconductors (PbSe/PbS). Modern NDIR systems, often miniaturized and integrated with optical filters and gas cells, are widely used in industrial emission monitoring, HVAC systems, and portable air-quality sensors due to their robustness and low power consumption [298]. Beyond NDIR, photoacoustic spectroscopy (PAS) offers even higher sensitivity by converting absorbed modulated IR radiation into acoustic signals through non-radiative relaxation. MEMS-based PAS devices can achieve sub-parts-per-billion (ppb) detection levels for gases like CH_4 and N_2O using compact dual-tube resonator designs [299]. These devices are highly suitable for portable, low-power operation in environmental monitoring and safety applications. Additionally, mid-IR photonic integration is emerging as a cutting-edge approach for on-chip gas sensing. Photonic integrated circuits (PICs) fabricated using materials like chalcogenide glass, silicon, and graphene allow for mid-IR waveguide-based absorption spectroscopy. These systems offer high sensitivity, multiplexed detection, and compactness—ideal for drone-based atmospheric sensing, smart manufacturing, and distributed environmental monitoring [300]. Significant material innovations are advancing the capabilities of IR PDs based gas sensors. CQDs, particularly HgTe and heavily doped PbS, offer solution-processable, low-cost alternatives to traditional epitaxial semiconductors. Their tunable bandgaps enable room-temperature detection of gas-specific IR absorption, and their compatibility with flexible substrates supports development of distributed, wearable sensor networks [301]. Plasmonic nanostructures, such as gold or aluminum nanoantennas, can be incorporated into IR PDs to enhance local field strength and responsivity by matching plasmonic resonances to gas absorption features. This enables ultra-sensitive detection with reduced device footprint [301]. Rare-earth doped chalcogenide waveguides, such as those incorporating Dy^{3+} or Er^{3+} ions, produce broadband mid-IR emission for absorption-based sensing. These materials are effective in the 3–5 µm region, enabling detection of greenhouse gases like CO_2 with high specificity. Furthermore, graphene and other 2D material-based IR PDs especially when coupled with plasmonic or nanoantenna architecture exhibit broadband responsivity, ultrafast carrier mobility, and high sensitivity. These properties have enabled real-time detection of VOCs and trace gases such as acetone, offering promising routes toward lightweight, flexible, and wearable environmental sensors [302]. The applications of IR PDs-based gas sensors span numerous fields (Fig. 18). In environmental monitoring, they are crucial for tracking greenhouse gas emissions and assessing air quality. In industrial settings, they provide early warnings of toxic or explosive gas leaks. In agriculture, they are used to monitor livestock environments and soil emissions. In indoor environments, smart air-quality sensors detect VOCs, CO_2, and other harmful substances. Additionally, IR PDs are being explored in medical diagnostics, such as non-invasive breath analysis for metabolic biomarkers like acetone (diabetes) or ammonia (liver function). As the demand for compact, energy-efficient, and accurate gas sensors grows, future development will likely focus on enhancing selectivity through integrated spectral filters or machine-learning-based signal analysis, improving material stability for long-term deployment, and scaling up low-cost manufacturing processes for large-area and flexible sensor deployment.

3.5. *Thermal imaging and optical communication*

Thermal imaging and optical communication are two cornerstone applications of IR PDs, both of which have seen transformative advances through the development of novel material systems and nanoscale

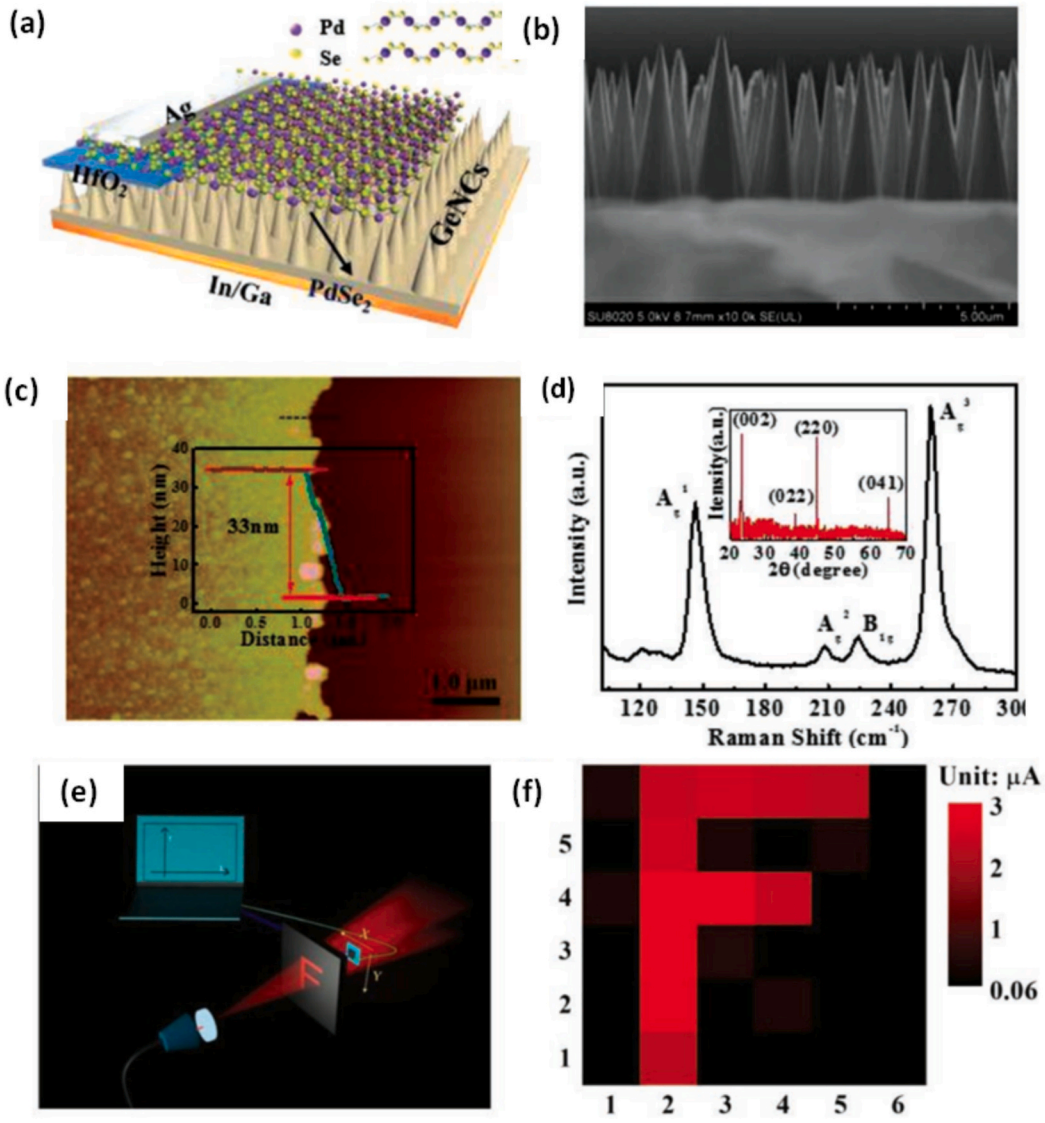

Fig. 19. Structural, material, and imaging characterization of the $PdSe_2$/GeNC IR PDs: (a) device schematic, (b) SEM of GeNCs, (c) AFM of $PdSe_2$ with height profile, (d) Raman and XRD spectra, (e) schematic of 1550 nm IR image sensing setup, (f) 2D current map of "F" image under IR illumination. Taken from [303] Copyrights© 2021 Wiley.

device architectures. These technologies are essential across a broad range of domains, including surveillance, security, industrial monitoring, telecommunications, and emerging Internet of Things (IoT) systems. A recent exemplar of progress in this field is the $PdSe_2$/GeNC-based IR PDs developed by Luo et al., which demonstrates not only enhanced thermal imaging performance but also lays the groundwork for future multifunctional optoelectronic platforms. In the context of thermal imaging, IR PDs function by capturing the infrared radiation naturally emitted from objects, enabling the visualization of temperature gradients and thermal patterns that are invisible to the naked eye. The performance of such systems depends heavily on material sensitivity, photocarrier mobility, structural design, and optical absorption. In the study by Luo et al., these parameters are addressed through the development of a hybrid heterostructure composed of a multilayer $PdSe_2$ film grown on a free-standing germanium nanocone (GeNC) array, as depicted in Fig. 19a. This schematic shows a vertically aligned array of Ge nanocones uniformly coated with $PdSe_2$, a two-dimensional group-10 TMD known for its exceptional ambient stability and tunable bandgap. The unique geometry and material choice collectively serve to enhance light–matter interaction, photocarrier generation, and signal output under infrared illumination [303]. This conceptual structure is further validated by Fig. 19 **b**, which provides a cross-sectional SEM image of the fabricated GeNCs. The nanocones are shown to have a diameter of approximately 500 nm and a height of 4 μm, arranged in a periodic array fabricated using polystyrene (PS) sphere lithography followed by noble metal-assisted HF etching. This design enables strong light-trapping effects, significantly increasing the optical path length and absorption efficiency in the infrared region a critical advantage for detecting low-intensity thermal signals. Material uniformity and surface characteristics are examined in Fig. 19 **c**, which presents an AFM image of the $PdSe_2$ layer, revealing a smooth and consistent morphology with a thickness of approximately 33 nm. This nanometer-scale control ensures consistent performance across the device and supports low-noise, high-resolution imaging. Additionally, Fig. 19d includes spectroscopic characterizations of the $PdSe_2$ film. The Raman spectra display four prominent peaks (~144, 206, 222, and 256 cm^{-1}), corresponding to distinct phonon

modes associated with Pd—Se and Se—Se interactions. These signatures confirm the high crystallinity of the film. The inset X-ray diffraction (XRD) pattern corroborates the presence of a pentagonal crystal structure with lattice parameters (a = 5.735 Å, b = 5.858 Å, c = 7.672 Å), aligning with theoretical expectations and confirming the structural integrity and phase purity of the synthesized $PdSe_2$. To translate these structural and material advantages into functional performance, the study also demonstrates the device's imaging capabilities under 1550 nm infrared illumination. Fig. 19e presents the experimental schematic for image sensing, where a software-controlled displacement platform scans the IR PDs across a predefined area illuminated by infrared light. The current output of each pixel is measured in real time and used to reconstruct a two-dimensional image. Fig. 19f shows the corresponding 2D photocurrent map, where a distinct "F" pattern is resolved. The illuminated regions exhibit a photocurrent of approximately 3 μA, whereas the un illuminated background remains at baseline dark current levels. Despite minor non-uniformity in response, the image clearly demonstrates the IR PDs spatial resolution, sensitivity, and stability under realistic conditions key attributes for integration into thermal imaging systems [303].

In the context of optical communication, IR PDs are increasingly being leveraged in innovative systems that utilize the unique properties of the infrared spectrum to enable robust and multifunctional communication platforms. A notable example is Thermal Camera Communication (TCC), a technique that employs thermographic cameras as receivers and Peltier cells as transmitters to facilitate data transmission via modulated thermal emissions. This approach is particularly effective in environments where traditional radio frequency or conventional optical communication methods are impractical, such as underwater, in smoke-filled areas, or cluttered indoor settings. TCC enables dual functionality, allowing the same IR PDs hardware to support both thermal sensing and optical data transmission, thereby simplifying system architecture and reducing energy consumption [304]. While the $PdSe_2$/GeNC-based IR PDs developed in this study was not explicitly designed for communication purposes, its demonstrated performance characteristics such as sensitivity to multiple infrared wavelengths (1350, 1550, 1650, and even 2200 nm), fast response times (rise time ~ 21.2 τ_r, decay time ~ 40.2 μs), and a 3 dB bandwidth of approximately 21 kHz suggest strong potential for modulated infrared signaling applications [303]. Furthermore, the device operates in a self-driven mode, owing to a built-in electric field at the $PdSe_2$/Ge interface, which adds energy efficiency and functional simplicity qualities that are especially valuable in mobile, wearable, or embedded communication platforms. Additionally, the ability of the IR PDs to spatially resolve infrared patterns, as demonstrated through 2D photocurrent imaging of the letter "F", supports the feasibility of thermal modulation-based communication systems, where devices not only detect IR signals but also extract meaningful spatial data. Collectively, these features indicate that the $PdSe_2$/GeNC IR PDs is well-positioned for future integration into compact, multifunctional platforms that unify thermal imaging and optical communication capabilities [304]. Self-driven infrared electrochromic devices (IR-ECDs) and pixelated micro-optics represent two of the most advanced innovations expanding the multifunctionality of IR PDs systems, particularly at the intersection of thermal management, imaging, and optical communication. IR-ECDs are capable of dynamically and reversibly modulating their infrared reflectance without the need for continuous external power, enabling rapid switching between IR-transparent and IR-reflective states. This makes them highly suitable for applications such as adaptive camouflage, energy-efficient smart windows, and tunable optical elements for infrared communication, where modulated IR signals can be transmitted or blocked in response to environmental or user-controlled stimuli [305].

Complementing this capability, pixelated micro-optics provide a novel mechanism for directional thermal emission. By engineering non-imaging micro-optic elements at the microscale, these systems can precisely control the angular distribution of emitted infrared radiation, allowing the creation of infrared displays or signal patterns that are visible only from certain viewpoints [306]. This property is particularly advantageous for privacy-preserving communication systems and secure data display, as it enables spatial confinement of information and reduces the risk of interception. Moreover, the ability to shape and direct IR emission paves the way for highly integrated systems in which both imaging and communication functions are co-localized and intelligently managed. Together, these innovations illustrate the growing trend toward convergence in IR PDs platforms where material innovations like $PdSe_2$, smart IR-modulating components like IR-ECDs, and advanced

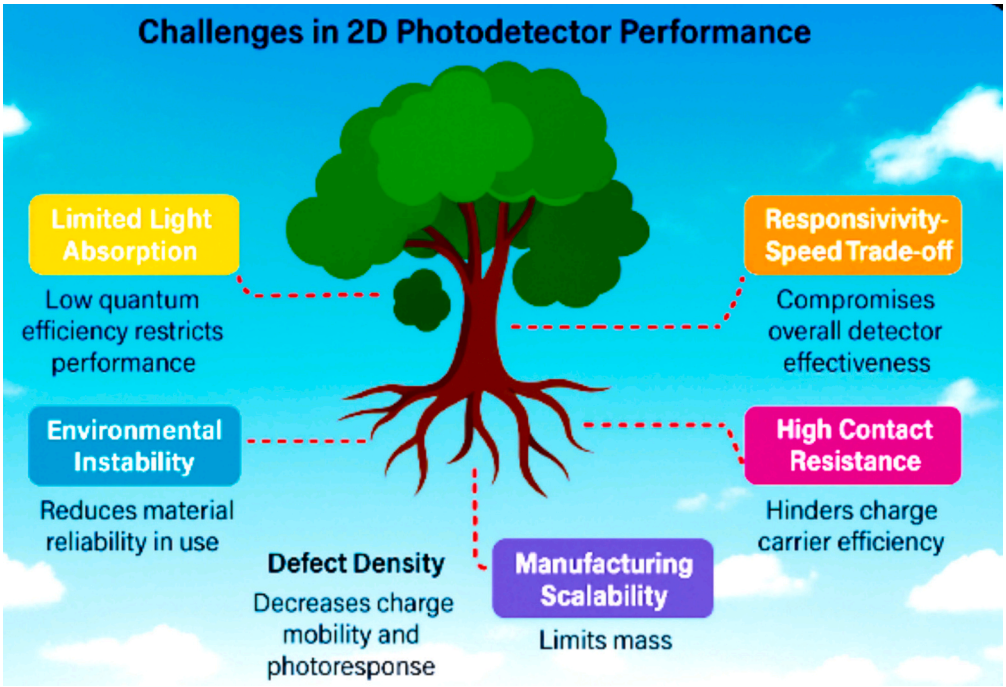

Fig. 20. Challenges in 2D Photodetectors.

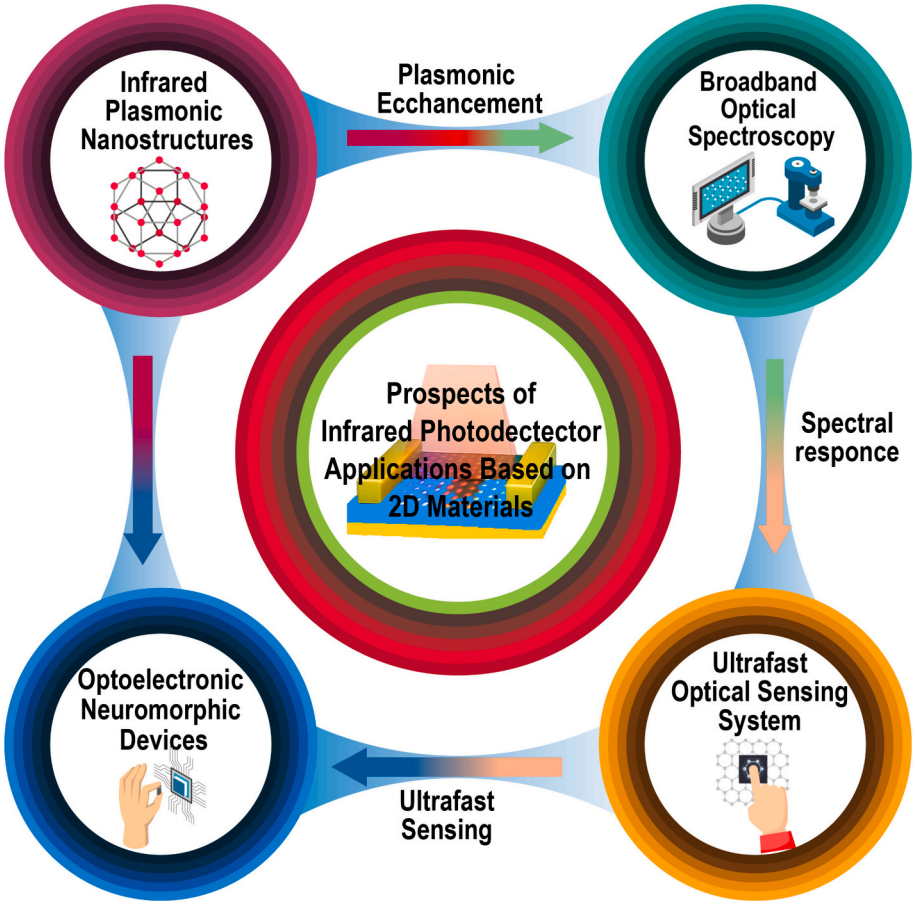

Fig. 21. The prospects of future applications associated with high-performance IR PDs.

optical architectures like pixelated emitters are brought together to enable compact, energy-efficient, and multifunctional devices. This integration is facilitating the development of next-generation systems that seamlessly blend thermal imaging, dynamic thermal control, and directional infrared communication within a unified framework [305]. As fabrication techniques and system integration strategies continue to mature, these multifunctional IR PDs are poised to transform applications across domains such as secure communication networks, smart surveillance, wearable health monitors, autonomous navigation, and IoT.

4. Conclusion, challenges, and future prospects

In summary, the IR PDs was addressed, how they function, and how to optimize a high-performance device. Our major goal in writing this review article was to cover the main topics, such as a basic explanation of PDs, methods for breaking the limit of PDs' for IR detection, and some examples of their use. Moreover, we focused on novel 2D materials and heterostructures, nanofabrication, optimization of low 2D materials, and approaches for the architecture design of 2D heterostructures that improve PDs performance. Due to their outstanding features, 2D materials and heterostructures hold considerable practical potential in optoelectronic communication systems and PDs. Despite the PDs current performance and the corresponding mechanisms, described in detail, photodetection technology based on 2D materials still requires significant work in numerous areas. These include creating new device structures, improving the transfer process, incorporating modulation, preparing high-crystal materials, and ensuring long-term stability. The development of optoelectronic devices and high-performance electronics may be facilitated by the fabrication of 2D materials with supercrystal quality and their stacked heterostructure exhibiting suitable band alignment. These devices have a wide range of potential applications, including light communication systems, thermal imaging, family safety, and temperature monitoring, to name a few. Research from a variety of fields has shown that 2D materials are already an essential part of semiconductor materials systems and might provide a solid basis for practical uses in the next few years.

Innovative fabrication and processing of micro-nanomaterials have accelerated the rate of improvement in IR PDs. From environmental sensing to military target detection and beyond, we foresee IR PDs finding more and more applications, and they might one day reach the far-IR terahertz region that is currently being explored for 6G and beyond communications. The development of better imaging technologies is a top priority for IR PDs. Because of their large-scale production ease, high responsivity at cryogenic temperatures, and versatility in the absorption wavelengths covering virtually all IR bands, bulk detectors like AlGaAs, HgCdTe, and SiGe have been extensively commercialized. However high-performance, low-dark-current and temperature-tolerant IR PDs are required for a plethora of novel applications. Thanks to advancements in nanofabrication, quantum well and quantum-dot IR PDs can now achieve higher operating temperatures and longer wavelength bands of performance than their bulk counterparts. The future of IR PDs research might be influenced by a range of sources. To improve IR PDs performance at lower prices and greater operating temperatures,

graphene and other 2D materials have been the focus of many studies in recent years. These innovative 2D materials require a large amount of space to be manufactured, are extremely sensitive to environmental variables, and have a low absorption coefficient. Nevertheless, they still hold theoretical potential to outperform many bulk-materials that currently in use thus their development for IR PDs will continue.

Despite significant advancements, 2D material-based photodetectors still face several critical challenges that limit their widespread adoption and practical deployment (Fig. 20). One of the most fundamental issues is limited light absorption. Due to their atomic-scale thickness, many 2D materials intrinsically exhibit low infrared light absorption, which directly restricts their quantum efficiency and limits overall photoresponse. Enhancing absorption through plasmonics, optical cavities, or heterostructure design remains an area of ongoing research. Another major hurdle is balancing responsivity and response speed. Photodetectors with high responsivity often rely on photoconductive gain mechanisms, which, while increasing the photocurrent, can simultaneously slow down the response time due to carrier trapping and delayed recombination. Achieving both high gain and rapid response continues to be a difficult trade-off in device engineering. Environmental instability is also a critical concern, especially for narrow-bandgap 2D materials like BP and AsP, which are suitable for mid- and long-wavelength IR detection but degrade rapidly under ambient conditions due to their sensitivity to oxygen and moisture. Developing reliable encapsulation or passivation methods is necessary for long-term stability. High contact resistance between metal electrodes and 2D semiconductors remains a limiting factor in efficient charge carrier injection and collection. Despite progress in contact engineering, forming low-resistance, reproducible, and scalable contacts continues to be a challenge, especially at scale. Additionally, defect density and scattering effects both intrinsic and substrate-induced degrade charge carrier mobility and photoresponse. Interface traps, grain boundaries, and non-uniformity in large-area growth processes contribute to charge scattering and performance inconsistency. From a manufacturing standpoint, the lack of scalable and cost-effective fabrication techniques is a major bottleneck. Many high-performance devices are fabricated through lab-scale techniques like mechanical exfoliation or complex epitaxial growth, which are not easily adaptable for industrial-scale production. Developing wafer-scale, solution-processed, or roll-to-roll methods for high-quality 2D material integration remains a pressing need. Lastly, integration with existing CMOS technologies poses compatibility issues due to mismatched lattice structures, thermal budgets, and processing protocols. Bridging this gap is essential for commercializing 2D photodetectors in mainstream optoelectronic systems. Overcoming these challenges requires a comprehensive approach that integrates materials innovation, advanced device architecture design, and the development of scalable fabrication techniques. These strategies are essential for unlocking the full potential of 2D material-based photodetectors. Despite significant research progress and numerous promising results, current 2D photodetector technologies still fall short of matching the performance and reliability of commercial photodetectors. Continued efforts are needed to fine-tune device configurations and accelerate the transition from lab-scale demonstrations to practical, real-world applications. Nonetheless, the field presents a wide array of promising directions for future research and development in low-dimensional photodetector systems. Absolute absorption is lower in graphene and other 2D materials with atomic-scale thickness than in commercial optical materials. The high exciton binding energy is caused by a mild electrostatic shielding effect and intense coulomb interaction enhances Auger scattering even further. Thus, quantum efficiency has its limits. The quantum efficiency of PDs composed of low-dimensional materials has been the subject of multiple studies. New 2D materials with desirable features, including 2D perovskites, with low exciton binding energy and extended diffusion lengths for photogenerated carriers should be investigated soon. A strong optical absorption coefficient and strong charge carrier mobility in typical, nonlayered 2D materials necessitate further investigation. Semiconductors of groups III-V and II-VI are included in this. Particularly challenging is the lack of effective solution-based technologies for the economically viable production of 2D III-V materials. Bandgaps are often rather significant in 2D materials. Materials with a narrow bandgap, such as BP and AsP, are unfortunately prone to instability. Exploring new stable 2D materials with a small bandgap for detection in the mid-IR and far-IR areas is highly desirable. One common method to enhance photodetection performance is to create photodiodes and hybrid phototransistors. However, in most cases, it is not feasible to have both high quantum efficiencies and a fast response time. Additional research is required to construct a novel heterostructure with high quantum efficiencies and rapid response times. Making cost-effective, uniform single-crystalline films on a wafer scale using solution-based technologies is still an attractive prospect. The mechanical flexibility and robustness of low-dimensional materials make them promising candidates for large-area wearable flexible optoelectronic systems. Common optoelectronic materials and complementary metal-oxide semiconductor integrated circuits have very different lattice and temperature structures, which makes their integration extremely challenging. Furthermore, 2D materials display little binding to neighboring materials via Van der Waals interactions and are very compatible with complementary metal-oxide semiconductors (CMOS) integrated circuits. Therefore, affordable imaging arrays using IR PDs is a long-term objective. While significant strides have been made in overcoming the traditional limits of IR PDs, widespread adoption depends on solving practical challenges related to scale, reproducibility, cost, and integration. A holistic approach that balances performance with manufacturability and robustness will be key to transitioning laboratory breakthroughs into commercial platforms.

In conclusion, numerous challenges remain in overcoming the detection limits of IR PDs. These challenges include material limitations, device engineering complexities, and optimization of performance metrics such as sensitivity, responsivity, and noise reduction. However, advancements in the design and manufacturing processes, particularly those leveraging 2D heterostructure-based nanomaterials, hold great promise for addressing these issues. The unique properties of these materials, such as their exceptional tunability, scalability, and compatibility with novel architectures, are poised to revolutionize the field of IR detection. Looking forward, the prospects for high-performance IR PDs are incredibly promising across a wide range of cutting-edge applications. For instance, their integration into optical spectrometer systems could enable more precise and efficient spectral analysis for scientific and industrial purposes. In ultrafast optical sensing systems, IR PDs may achieve unprecedented speed and accuracy, enhancing technologies such as LiDAR, remote sensing, and real-time monitoring. Furthermore, advancements in optical synaptic systems inspired by neuromorphic computing could benefit from the unique characteristics of IR PDs, paving the way for next-generation artificial intelligence and memory devices. Where, neuromorphic IR PDs are designed to mimic brain-like computation by processing and adapting to optical signals directly at the sensor level, thereby reducing latency and energy consumption in data-intensive applications. This paradigm shift is enabled by recent breakthroughs in ferroelectric 2D semiconductors such as α-In_2Se_3 and $CuInP_2S_6$, which offer reconfigurable polarization states and exhibit both volatile and non-volatile memory characteristics. These materials support synaptic behaviors and logic switching, making them ideal candidates for in-sensor and in-memory computing [203,307,308]. Devices based on α-In_2Se_3, for example, have demonstrated high photoresponse sensitivity (up to 98 mA/W at 1800 nm), fast response times, and high carrier mobility, while maintaining compatibility with broadband optical detection from the visible to short-wavelength infrared (SWIR) regimes. Moreover, hybrid heterostructures that combine ferroelectric 2D semiconductors with IR-active layers such as black phosphorus or transition metal dichalcogenides (e.g., WS_2, $MoTe_2$) further enhance spectral range and responsivity. These hybrid systems enable programmable, adaptive photodetection behaviors by leveraging built-in electric

fields and strong interfacial coupling. As a result, such material combinations not only improve photodetector performance but also lay the groundwork for intelligent IR sensing platforms capable of complex tasks such as real-time learning, recognition, and decision-making at the edge. Additionally, IR PDs integrated into plasmonic systems have the potential to unlock new possibilities in manipulating light at the nanoscale, enabling breakthroughs in areas like subwavelength imaging, energy harvesting, and advanced optical communications. These advancements collectively underscore the transformative potential of IR PDs, suggesting that ongoing research and innovation will continue to push the boundaries of their capabilities in diverse and impactful ways (Fig. 21). IR PDs is undergoing a pivotal transformation, fueled by simultaneous progress in material development, device architecture, and computational processing. This review has outlined an array of emerging strategies aimed at overcoming the intrinsic limitations of conventional IR PDs. These strategies span a wide range from bandgap engineered 2D materials and vertically stacked heterostructures to plasmonically enhanced interfaces and intelligent, algorithm-driven readout systems. Despite this breadth of innovation, developing scalable, robust, and high-performance IR detector platforms remains a formidable challenge. On the materials front, ultrathin semiconductors like MoS_2, $PdSe_2$, and Bi_2O_2Se have attracted attention for their tunable optical characteristics and suitability for multi-wavelength sensing. However, their real-world adoption is constrained by difficulties in achieving uniform, large-area growth, ensuring stability in operational environments, and integrating them with standard CMOS fabrication processes. Addressing these concerns calls for advanced, low-temperature synthesis techniques, improved control of interface quality, and long-term passivation solutions.

In terms of device design, innovations such as photogating elements, metasurface-based absorbers, and hybrid-layer structures have yielded notable improvements in key parameters like detectivity and spectral responsiveness. Yet, the reliance on precise nanofabrication remains a barrier to mass production. The future of scalable device engineering will depend on streamlined architectures and cost-effective manufacturing approaches, such as solution-based processes and imprint lithography. System level integration presents its own set of challenges. Future IR PDs must be compatible with flexible substrates, maintain performance across a range of environmental conditions, and support high-throughput assembly with minimal variability. Reliable packaging, effective thermal management, and mechanical robustness are essential to transition from proof-of-concept devices to deployable technologies in areas like aerospace, biomedical monitoring, and autonomous systems. One of the most promising directions lies in computational photodetection. By embedding signal processing capabilities directly into the sensing architecture, methods such as neuromorphic computing, compressed sensing, and machine learning-based filtering are redefining how IR detectors handle data. These approaches reduce dependence on material performance alone, yet still face hurdles such as analog hardware integration and power efficiency. In conclusion, the future of IR PDs depends on the successful convergence of innovations in materials, device structures, signal processing, and system engineering. A collaborative, cross-disciplinary approach focused on co-design and scalability will be key to transforming current laboratory advances into widely adopted, high-performance sensing platforms. These systems will play a critical role in shaping next-generation technologies across a variety of sectors, from healthcare and environmental analysis to space exploration and intelligent electronics.

CRediT authorship contribution statement

Phuong V. Pham: Writing – review & editing, Writing – original draft, Supervision, Project administration, Methodology, Investigation, Funding acquisition, Conceptualization. **S. Cathrin Lims:** Writing – review & editing, Writing – original draft, Software. **Anuj Kumar:** Writing – review & editing, Writing – original draft. **Rajesh K. Ulaganathan:** Writing – review & editing. **Rayko I. Stantchev:** Writing – review & editing. **Raman Sankar:** Writing – review & editing.

Declaration of competing interest

The authors declare the following financial interests/personal relationships which may be considered as potential competing interests: Phuong V. Pham reports was provided by National Sun Yat-sen University. If there are other authors, they declare that they have no known competing financial interests or personal relationships that could have appeared to influence the work reported in this paper.

Acknowledgements

This work is supported by the National Science and Technology Council, Taiwan (Grant No.: NSTC-112-2112-M-110-004-MY3 and NSTC-114-2112-M-110-015). R.S. acknowledges support from NSTC of Taiwan under No. 111-2124-M-001-007, 113-2112-M-001-045-MY3, and Academia Sinica Project No. AS-iMATE-113-12.

Data availability

Data will be made available on request.

References

[1] D. Kong, et al., Recent progress in InGaN-based photodetectors for visible light communication, J. Mater. Chem. C 10 (2022) 14080–14090.
[2] D. Schall, et al., Record high bandwidth integrated graphene photodetectors for communication beyond 180 Gb/s, in: *Optical Fiber Communication Conference* M2I-4, Optica Publishing Group, 2018.
[3] C. Bao, et al., High performance and stable all-inorganic metal halide perovskite-based photodetectors for optical communication applications, Adv. Mater. 30 (2018) 1803422.
[4] T. Agostinelli, et al., A polymer/fullerene based photodetector with extremely low dark current for x-ray medical imaging applications, Appl. Phys. Lett. 93 (2008).
[5] E. Thrush, et al., Integrated semiconductor vertical-cavity surface-emitting lasers and PIN photodetectors for biomedical fluorescence sensing, IEEE J. Quantum Electron. 40 (2004) 491–498.
[6] S. Rezaei-Mazinani, et al., Monitoring intrinsic optical signals in brain tissue with organic photodetectors, Adv. Mater. Technol. 3 (2018) 1700333.
[7] P. Vashishtha, L. Goswami, S.K. Jain, N. Aggarwal, G. Gupta, GaN-djoser pyramidal self powered UV photodetector for optical signal detection in rugged environments, J. Alloys Compd. 930 (2023) 167267.
[8] X. Hou, et al., High-performance harsh-environment-resistant GaOX solar-blind photodetectors via defect and doping engineering, Adv. Mater. 34 (2022) 2106923.
[9] G.H. Rieke, Infrared detector arrays for astronomy, Annu. Rev. Astron. Astrophys. 45 (2007) 77–115.
[10] I. Medina, et al., Reflection of near-infrared light confers thermal protection in birds, Nat. Commun. 9 (2018) 3610.
[11] K. Miah, D.K. Potter, A review of hybrid fiber-optic distributed simultaneous vibration and temperature sensing technology and its geophysical applications, Sensors 17 (2017) 2511.
[12] D. Kesztyüs, S. Brucher, C. Wilson, T. Kesztyüs, Use of infrared thermography in medical diagnosis, screening, and disease monitoring: A scoping review, Medicina (B. Aires). 59 (2023) 2139.
[13] C.P. Shirley, J.I.J. Raja, S.V. Evangelin Sonia, I. Titus, Recognition and monitoring of gas leakage using infrared imaging technique with machine learning, Multimed. Tools Appl. 83 (2024) 35413–35426.
[14] W. Ouyang, J. Chen, Z. Shi, X. Fang, Self-powered UV photodetectors based on ZnO nanomaterials, Appl. Phys. Rev. 8 (2021).
[15] P.V. Pham, et al., 2D Heterostructures for ubiquitous electronics and optoelectronics: principles, opportunities, and challenges, Chem. Rev. 122 (2022) 6514–6613.
[16] V.P. Pham, H.-S. Jang, D. Whang, J.-Y. Choi, Direct growth of graphene on rigid and flexible substrates: Progress, applications, and challenges, Chem. Soc. Rev. 46 (2017) 6276–6300.
[17] R. Chai, et al., Non-layered ZnSb nanoplates for room temperature infrared polarized photodetectors, J. Mater. Chem. C 8 (2020) 6388–6395.
[18] P. Wu, Y. Dai, Y. Ye, Y. Yin, L. Dai, Fast-speed and high-gain photodetectors of individual single crystalline Zn 3 P 2 nanowires, J. Mater. Chem. 21 (2011) 2563–2567.
[19] G. Chen, et al., Single-crystalline p-type Zn3As2 nanowires for field-effect transistors and visible-light photodetectors on rigid and flexible substrates, Adv. Funct. Mater. 23 (2013) 2681–2690.

[20] M. Yang, et al., Enhanced performance of wideband room temperature photodetector based on Cd3As2 thin film/pentacene heterojunction, ACS Photonics 5 (2018) 3438–3445.
[21] Y. Yang, et al., Photodetection and infrared imaging based on Cd3As2 epitaxial vertical Heterostructures, ACS Nano 16 (2022) 12244–12252.
[22] T. Journot, V. Bouchiat, B. Gayral, J. Dijon, B. Hyot, Self-assembled UV photodetector made by direct epitaxial GaN growth on graphene, ACS Appl. Mater. Interfaces 10 (2018) 18857–18862.
[23] J. Wu, et al., Monolithically integrated InAs/GaAs quantum dot mid-infrared photodetectors on silicon substrates, Acs Photonics 3 (2016) 749–753.
[24] D.Z. Ting, et al., InAs/InAsSb type-II strained-layer superlattice infrared photodetectors, Micromachines 11 (2020) 958.
[25] G. Yu, Z. Liu, X. Xie, X. Ouyang, G. Shen, Flexible photodetectors with single-crystalline GaTe nanowires, J. Mater. Chem. C 2 (2014) 6104–6110.
[26] C. Xiao, Y. Wang, T. Yang, Y. Luo, M. Zhang, Preparation of ZnO/ZnSe heterostructure parallel arrays for photodetector application, Appl. Phys. Lett. 109 (2016).
[27] P. Hu, et al., Highly responsive ultrathin GaS nanosheet photodetectors on rigid and flexible substrates, Nano Lett. 13 (2013) 1649–1654.
[28] C.-H. Ho, Y.-H. Chen, J.-H. Ho, Optical and photodetector properties of stripe-like InS crystal, RSC Adv. 6 (2016) 97445–97448.
[29] Z. Yang, et al., Large-scale synthesis of two-dimensional indium telluride films for broadband photodetectors, Mater. Des. 233 (2023) 112218.
[30] J. Gohil, V. Jethwa, H.S. Jagani, A.G. Dalvaniya, V.M. Pathak, Self-powered photodetector based on direct vapour transfer (DVT) method grown tin selenide (SnSe) crystals, J. Alloys Compd. 941 (2023) 168907.
[31] S.V. Averin, L.Y. Zakharov, V.A. Zhitov, V.M. Kotov, ZnSe and ZnCdSe/ZnSe photodetectors for visible spectral range: comparative parameters, J. Commun. Technol. Electron. 67 (2022) 911–917.
[32] X. Fang, et al., High-performance blue/ultraviolet-light-sensitive ZnSe-Nanobelt photodetectors, Adv. Mater. 21 (2009) 5016–5021.
[33] S.A. McDonald, et al., Solution-processed PbS quantum dot infrared photodetectors and photovoltaics, Nat. Mater. 4 (2005) 138–142.
[34] F. Lu, et al., Gas-dependent photoresponse of SnS nanoparticles-based photodetectors, J. Mater. Chem. C 3 (2015) 1397–1402.
[35] P. Ramasamy, D. Kwak, D.-H. Lim, H.-S. Ra, J.-S. Lee, Solution synthesis of GeS and GeSe nanosheets for high-sensitivity photodetectors, J. Mater. Chem. C 4 (2016) 479–485.
[36] T. He, et al., Extrinsic photoconduction induced short-wavelength infrared photodetectors based on Ge-based chalcogenides, Small 17 (2021) 2006765.
[37] J. Zhang, et al., Single-crystal Sb2S3 tube prepared by chemical vapor deposition for a 1 cm photodetector application, ACS Appl. Electron. Mater. 4 (2022) 2455–2462.
[38] L. Li, et al., Sb2O3 nanobelt networks for excellent visible-light-range photodetectors, Nanotechnology 22 (2011) 165704.
[39] T. Zhai, et al., Single-crystalline Sb2Se3 nanowires for high-performance field emitters and photodetectors, Adv. Mater. 22 (2010) 4530–4533.
[40] W. Zheng, et al., Patterning two-dimensional chalcogenide crystals of Bi2Se3 and In2Se3 and efficient photodetectors, Nat. Commun. 6 (2015) 6972.
[41] W. Wang, et al., Highly sensitive low-bandgap perovskite photodetectors with response from ultraviolet to the near-infrared region, Adv. Funct. Mater. 27 (2017) 1703953.
[42] Y. Guo, C. Liu, H. Tanaka, E. Nakamura, Air-stable and solution-processable perovskite photodetectors for solar-blind UV and visible light, J. Phys. Chem. Lett. 6 (2015) 535–539.
[43] X. Li, et al., Constructing fast carrier tracks into flexible perovskite photodetectors to greatly improve responsivity, ACS Nano 11 (2017) 2015–2023.
[44] Y. Li, et al., High-performance perovskite photodetectors based on solution-processed all-inorganic CsPbBr 3 thin films, J. Mater. Chem. C 5 (2017) 8355–8360.
[45] B. Wang, et al., Molecular doping of near-infrared organic photodetectors for photoplethysmogram sensors, J. Mater. Chem. C 9 (2021) 3129–3135.
[46] G. Azzellino, et al., Fully inkjet-printed organic photodetectors with high quantum yield, Adv. Mater. 25 (2013) 6829–6833.
[47] J. Miao, F. Zhang, M. Du, W. Wang, Y. Fang, Photomultiplication type organic photodetectors with broadband and narrowband response ability, Adv Opt Mater 6 (2018) 1800001.
[48] Z. Zhao, et al., Highly sensitive narrowband photomultiplication-type organic photodetectors prepared by transfer-printed technology, Adv. Funct. Mater. 31 (2021) 2106009.
[49] M. Kielar, O. Dhez, G. Pecastaings, A. Curutchet, L. Hirsch, Long-term stable organic photodetectors with ultra low dark currents for high detectivity applications, Sci. Rep. 6 (2016) 39201.
[50] T. Vandermeeren, et al., A PDTPQx: PC61BM blend with pronounced charge-transfer absorption for organic resonant cavity photodetectors–direct arylation polymerization vs. Stille polycondensation, Dyes Pigments 200 (2022) 110130.
[51] C. Kim, et al., Highly responsive near-infrared photodetector with low dark current using graphene/germanium Schottky junction with Al2O3 interfacial layer, Nanophotonics 10 (2021) 1573–1579.
[52] A. Hassan, Y. Jin, M. Irfan, Y. Jiang, Acceptor-modulated optical enhancements and band-gap narrowing in ZnO thin films, AIP Adv. 8 (2018).
[53] S. Jalaei, J. Karamdel, H. Ghalami-Bavil-Olyaee, Mid-infrared photodetector based on selenium-doped black phosphorus, Phys. Status Solidi 217 (2020) 2000483.
[54] A. Walsh, J.L.F. Da Silva, S.-H. Wei, Origins of band-gap renormalization in degenerately doped semiconductors, Phys. Rev. B—Condensed Matter Mater. Phys. 78 (2008) 75211.
[55] P. Bhattacharya, R. Fornari, H. Kamimura, Comprehensive Semiconductor Science and Technology, Newnes, 2011.
[56] P.V. Pham, et al., Layer-by-layer thinning of two-dimensional materials, Chem. Soc. Rev. 53 (2024) 5190–5226.
[57] K. Zheng, et al., Optoelectronic characteristics of a near infrared light photodetector based on a topological insulator Sb 2 Te 3 film, J. Mater. Chem. C 3 (2015) 9154–9160.
[58] W. Macherzyński, et al., Influence of thermal treatment on the formation of ohmic contacts based on Ti/Al/Ni/Au metallization to n-type AlGaN/GaN heterostructures, Mater. Sci. 30 (2012) 342–347.
[59] A.C. Schmitz, et al., Metal contacts to n-type GaN, J. Electron. Mater. 27 (1998) 255–260.
[60] R.Q. Yang, Shot and Johnson noises in interband cascade infrared photodetectors, Appl. Phys. Lett. 121 (2022).
[61] Y. Zhou, J. Chen, Z. Xu, L. He, High quantum efficiency mid-wavelength interband cascade infrared photodetectors with one and two stages, Semicond. Sci. Technol. 31 (2016) 85005.
[62] W. Bowden, A. Vianello, R. Hobson, A low-noise resonant input transimpedance amplified photodetector, Rev. Sci. Instrum. 90 (2019).
[63] V.P. Pham, G.Y. Yeom, Recent advances in doping of molybdenum disulfide: industrial applications and future prospects, Adv. Mater. 28 (2016) 9024–9059.
[64] Y. Gao, L. Liu, W. Ta, J. Song, Effect of surfaces similarity on contact resistance of fractal rough surfaces under cyclic loading, AIP Adv. 8 (2018).
[65] S. Banerjee, L. Cao, Y.S. Ang, L.K. Ang, P. Zhang, Reducing contact resistance in two-dimensional-material-based electrical contacts by roughness engineering, Phys. Rev. Appl. 13 (2020) 64021.
[66] F. Pennec, et al., Impact of the surface roughness description on the electrical contact resistance of ohmic switches under low actuation forces, IEEE Trans. Components, Packag. Manuf. Technol. 2 (2012) 85–94.
[67] J. Yao, G. Yang, 2D material broadband photodetectors, Nanoscale 12 (2020) 454–476.
[68] E.H. Hwang, S. Das Sarma, Acoustic phonon scattering limited carrier mobility in two-dimensional extrinsic graphene, Phys. Rev. B—Condensed Matter Mater. Phys. 77 (2008) 115449.
[69] J.-H. Chen, W.G. Cullen, C. Jang, M.S. Fuhrer, E.D. Williams, Defect scattering in graphene, Phys. Rev. Lett. 102 (2009) 236805.
[70] H. Rabiee-Golgir, et al., Ultra-thin super absorbing photon trapping materials for high-performance infrared detection, in: Infrared Technology and Applications XLV 11002, 2019, pp. 159–165. SPIE.
[71] T.J. De Lyon, et al., MBE growth and transfer of HgCdTe epitaxial films from InSb substrates, J. Electron. Mater. 39 (2010) 1058–1062.
[72] J.D. Caldwell, et al., Atomic-scale photonic hybrids for mid-infrared and terahertz nanophotonics, Nat. Nanotechnol. 11 (2016) 9–15.
[73] A. Olafsson, et al., Imaging infrared plasmon hybridization in doped semiconductor nanocrystal dimers, J. Phys. Chem. Lett. 12 (2021) 10270–10276.
[74] I. Tiginyanu, et al., Strong light scattering and broadband (UV to IR) photoabsorption in stretchable 3D hybrid architectures based on aerographite decorated by ZnO nanocrystallites, Sci. Rep. 6 (2016) 32913.
[75] M.A. Iqbal, et al., Technological evolution of image sensing designed by nanostructured materials, ACS Mater. Lett. 5 (2023) 1027–1060.
[76] V.P. Pham, et al., Low damage pre-doping on CVD graphene/cu using a chlorine inductively coupled plasma, Carbon N. Y. 95 (2015) 664–671.
[77] T. Shen, F. Li, Z. Zhang, L. Xu, J. Qi, High-performance broadband photodetector based on monolayer MoS2 hybridized with environment-friendly CuInSe2 quantum dots, ACS Appl. Mater. Interfaces 12 (2020) 54927–54935.
[78] Y. Tao, et al., Bright monolayer tungsten disulfide via exciton and Trion chemical modulations, Nanoscale 10 (2018) 6294–6299.
[79] M.H. Nawaz, et al., Flatland of graphene's derivatives: classification, synthesis, mechanisms, role of defects, applications, and prospectives, Coord. Chem. Rev. 528 (2025) 216421.
[80] K.G. Saw, N.M. Aznan, F.K. Yam, S.S. Ng, S.Y. Pung, New insights on the burstein-moss shift and band gap narrowing in indium-doped zinc oxide thin films, PLoS One 10 (2015) e0141180.
[81] Y. Xia, et al., Tuning electrical and optical properties of MoSe2 transistors via elemental doping, Adv. Mater. Technol. 5 (2020) 2000307.
[82] Y. Zhao, et al., High response and broadband photodetection by monolayer MoSe2 with vanadium doping and Mo vacancies, Appl. Surf. Sci. 564 (2021) 150399.
[83] R. Pokharel, et al., Epitaxial high-yield intrinsic and Te-doped dilute nitride GaAsSbN nanowire heterostructure and ensemble photodetector application, ACS Appl. Electron. Mater. 2 (2020) 2730–2738.
[84] S. Devkota, et al., A study of n-doping in self-catalyzed GaAsSb nanowires using GaTe dopant source and ensemble nanowire near-infrared photodetector, Nanotechnology 31 (2020) 505203.
[85] M. Wang, et al., Silicon-based intermediate-band infrared photodetector realized by Te hyperdoping, Adv Opt Mater 9 (2021) 2001546.
[86] Q. Hao, et al., Visible to near-infrared photodetector with novel optoelectronic performance based on graphene/S-doped InSe heterostructure on h-BN substrate, Nanoscale 12 (2020) 19259–19266.
[87] R. Kumar, M.A. Khan, A.V. Anupama, S.B. Krupanidhi, B. Sahoo, Infrared photodetectors based on multiwalled carbon nanotubes: insights into the effect of nitrogen doping, Appl. Surf. Sci. 538 (2021) 148187.

[88] L. Tang, et al., Deep ultraviolet to near-infrared emission and photoresponse in layered N-doped graphene quantum dots, ACS Nano 8 (2014) 6312–6320.
[89] R. Guo, et al., Manganese doped eco-friendly CuInSe2 colloidal quantum dots for boosting near-infrared photodetection performance, Chem. Eng. J. 403 (2021) 126452.
[90] M. Yang, et al., Ultrahigh stability 3D TI Bi2Se3/MoO3 thin film heterojunction infrared photodetector at optical communication waveband, Adv. Funct. Mater. 30 (2020) 1909659.
[91] J. Kim, et al., Rhenium diselenide (ReSe2) near-infrared photodetector: performance enhancement by selective p-doping technique, Adv. Sci. 6 (2019) 1901255.
[92] M.-W. Kim, et al., Ultrafast infrared photoresponse from heavily hydrogen-doped VO2 single crystalline nanoparticles, Nano Lett. 20 (2020) 2733–2740.
[93] S. KiáLai, S. Lau, Solution processable high-performance infrared organic photodetector by iodine doping, RSC Adv. 6 (2016) 45166–45171.
[94] P. Maity, S.V. Singh, S. Biring, B.N. Pal, A.K. Ghosh, Selective near-infrared (NIR) photodetectors fabricated with colloidal CdS: co quantum dots, J. Mater. Chem. C 7 (2019) 7725–7733.
[95] M. Amiri, N. Alizadeh, Highly photosensitive near infrared photodetector based on polypyrrole nanoparticle incorporated with CdS quantum dots, Mater. Sci. Semicond. Process. 111 (2020) 104964.
[96] A.I. Yakimov, et al., Influence of delta-doping on the performance of Ge/Si quantum-dot mid-infrared photodetectors, J. Appl. Phys. 112 (2012).
[97] H. Jang, et al., High-performance near-infrared photodetectors based on surface-doped InSe, Adv. Funct. Mater. 31 (2021) 2006788.
[98] X. Yu, S. Zhang, H. Zeng, Q.J. Wang, Lateral black phosphorene P–N junctions formed via chemical doping for high performance near-infrared photodetector, Nano Energy 25 (2016) 34–41.
[99] B.H. Xie, et al., Preparation and enhanced infrared response properties of ordered W-doped VO2 nanowire array, Appl. Surf. Sci. 436 (2018) 1061–1066.
[100] M.G. Kwon, et al., Performance enhancement of graphene/Ge near-infrared photodetector by modulating the doping level of graphene, Apl Photonics 7 (2022).
[101] A. Pfenning, et al., P-type doped AlAsSb/GaSb resonant tunneling diode photodetector for the mid-infrared spectral region, Adv Opt Mater 6 (2018) 1800972.
[102] L. Ye, H. Li, Z. Chen, J. Xu, Near-infrared photodetector based on MoS2/black phosphorus heterojunction, ACS Photonics 3 (2016) 692–699.
[103] M. Peng, et al., One-step synthesized PbSe nanocrystal inks decorated 2D MoS 2 heterostructure for high stability photodetectors with photoresponse extending to near-infrared region, J. Mater. Chem. C 10 (2022) 2236–2244.
[104] U.N. Noumbé, et al., Reconfigurable 2D/0D p–n graphene/HgTe nanocrystal heterostructure for infrared detection, ACS Nano 14 (2020) 4567–4576.
[105] M. Vemula, S. Veeralingam, S. Badhulika, Hybrid 2D/0D SnSe2-SnO2 vertical junction based high performance broadband photodetector, J. Alloys Compd. 883 (2021) 160826.
[106] J. Miao, et al., High-responsivity graphene/InAs nanowire heterojunction near-infrared photodetectors with distinct photocurrent on/off ratios, small 11 (2015) 936–942.
[107] N. Chaudhary, M. Khanuja, Architectural design of photodetector based on 2D (MoS2 nanosheets)/1D (WS2 nanorods) heterostructure synthesized by facile hydrothermal method, J. Electrochem. Soc. 166 (2019) B1276.
[108] Y. Liu, et al., Highly efficient and air-stable infrared photodetector based on 2D layered graphene–black phosphorus heterostructure, ACS Appl. Mater. Interfaces 9 (2017) 36137–36145.
[109] L. Ye, et al., Highly polarization sensitive infrared photodetector based on black phosphorus-on-WSe2 photogate vertical heterostructure, Nano Energy 37 (2017) 53–60.
[110] Y. Chen, et al., Momentum-matching and band-alignment van der Waals heterostructures for high-efficiency infrared photodetection, Sci. Adv. 8 (2022) eabq1781.
[111] K. Zhang, et al., Ultrasensitive near-infrared photodetectors based on a graphene–MoTe2–graphene vertical van der Waals heterostructure, ACS Appl. Mater. Interfaces 9 (2017) 5392–5398.
[112] S. Gao, et al., Graphene/MoS2/graphene vertical heterostructure-based broadband photodetector with high performance, Adv. Mater. Interfaces 8 (2021) 2001730.
[113] D. Wu, et al., Highly polarization-sensitive, broadband, self-powered photodetector based on graphene/PdSe2/germanium heterojunction, ACS Nano 13 (2019) 9907–9917.
[114] B. Yang, et al., Visible and infrared photodiode based on γ-InSe/Ge van der Waals heterojunction for polarized detection and imaging, Nanoscale 15 (2023) 3520–3531.
[115] W. Du, et al., Overall high-performance near-infrared photodetector based on CVD-grown MoTe2 and graphene vertical vdWs heterostructure, Appl. Sci. 12 (2022) 3622.
[116] H. Zhang, et al., Near-infrared photodetection based on topological insulator PN heterojunction of SnTe/Bi2Se3, Appl. Surf. Sci. 509 (2020) 145290.
[117] T. Yang, et al., Broadband photodetection of 2D Bi2O2Se–MoSe2 heterostructure, J. Mater. Sci. 54 (2019) 14742–14751.
[118] H.J. Jin, C. Park, K.J. Lee, G.H. Shin, S. Choi, Ultrasensitive WSe2/α-In2Se3 NIR photodetector based on ferroelectric gating effect, Adv. Mater. Technol. 6 (2021) 2100494.
[119] J. Yao, et al., A high-performance short-wave infrared phototransistor based on a 2D tellurium/MoS 2 van der Waals heterojunction, J. Mater. Chem. C 9 (2021) 13123–13131.
[120] Z. Zhang, et al., Type II homo-type Bi2O2Se nanosheet/InSe nanoflake heterostructures for self-driven broadband visible–near-infrared photodetectors, ACS Appl. Nano Mater. 6 (2023) 4573–4583.
[121] R. Xiao, et al., High performance Van der Waals graphene–WS2–Si heterostructure photodetector, Adv. Mater. Interfaces 6 (2019) 1901304.
[122] D. Wu, et al., Fabrication of 2D PdSe2/3D CdTe mixed-dimensional van der Waals heterojunction for broadband infrared detection, ACS Appl. Mater. Interfaces 13 (2021) 41791–41801.
[123] D. Wu, et al., Ultrabroadband and high-detectivity photodetector based on WS2/Ge heterojunction through defect engineering and interface passivation, ACS Nano 15 (2021) 10119–10129.
[124] Z. Wang, et al., Construction of mixed-dimensional WS 2/Si heterojunctions for high-performance infrared photodetection and imaging applications, J. Mater. Chem. C 8 (2020) 6877–6882.
[125] D. Wu, et al., A defect-induced broadband photodetector based on WS 2/pyramid Si 2D/3D mixed-dimensional heterojunction with a light confinement effect, Nanoscale 13 (2021) 13550–13557.
[126] H. Jiao, et al., HgCdTe/black phosphorus van der Waals heterojunction for high-performance polarization-sensitive midwave infrared photodetector, Sci. Adv. 8 (2022) eabn1811.
[127] L. Marsal, et al., Zero-dimensional excitons in CdTe/ZnTe nanostructures, J. Appl. Phys. 91 (2002) 4936–4943.
[128] S. Yip, L. Shen, J.C. Ho, Recent advances in flexible photodetectors based on 1D nanostructures, J. Semicond. 40 (2019) 111602.
[129] T. Zhai, et al., A comprehensive review of one-dimensional metal-oxide nanostructure photodetectors, Sensors 9 (2009) 6504–6529.
[130] E.P. Randviir, D.A.C. Brownson, C.E. Banks, A decade of graphene research: production, applications and outlook, Mater. Today 17 (2014) 426–432.
[131] T. Hu, et al., Two-dimensional nanomaterials: fascinating materials in biomedical field, Sci. Bull. 64 (2019) 1707–1727.
[132] F.M. de Souza, et al., 2D heterostructure-based sweat and heat sensors, ACS Appl. Electron. Mater. 7 (2025) 2173–2207.
[133] X. Gan, et al., Chip-integrated ultrafast graphene photodetector with high responsivity, Nat. Photonics 7 (2013) 883–887.
[134] M. Long, P. Wang, H. Fang, W. Hu, Progress, challenges, and opportunities for 2D material based photodetectors, Adv. Funct. Mater. 29 (2019) 1803807.
[135] A.K. Geim, I.V. Grigorieva, Van der Waals heterostructures, Nature 499 (2013) 419–425.
[136] X. Wang, F. Xia, Stacked 2D materials shed light, Nat. Mater. 14 (2015) 264–265.
[137] L. Britnell, et al., Strong light-matter interactions in heterostructures of atomically thin films, Science **340** (2013) 1311–1314. *80-*..
[138] J.B. Oostinga, H.B. Heersche, X. Liu, A.F. Morpurgo, L.M.K. Vandersypen, Gate-induced insulating state in bilayer graphene devices, Nat. Mater. 7 (2008) 151–157.
[139] A.K. Geim, K.S. Novoselov, The rise of graphene, Nat. Mater. 6 (2007) 183–191.
[140] B. Chitara, L.S. Panchakarla, S.B. Krupanidhi, C.N.R. Rao, Infrared photodetectors based on reduced graphene oxide and graphene nanoribbons, Adv. Mater. 23 (2011) 5419–5424.
[141] M.E. Pumarol, et al., Direct nanoscale imaging of ballistic and diffusive thermal transport in graphene nanostructures, Nano Lett. 12 (2012) 2906–2911.
[142] J. Liu, et al., Ultrathin high-quality SnTe nanoplates for fabricating flexible near-infrared photodetectors, ACS Appl. Mater. Interfaces 12 (2020) 31810–31822.
[143] P. Namboothiri, K.J. Vishnumaya, P.V. Pham, K.K. Supin, M. Vasundhara, Impact of Mg substitution in LaMnO 3 manganites on their structural integrity and magnetic behavior, RSC Adv. 15 (2025) 8561–8571.
[144] S. Ogawa, S. Fukushima, M. Shimatani, Hexagonal boron nitride for photonic device applications: a review, Materials (Basel). 16 (2005), 2023.
[145] G. Cassabois, P. Valvin, B. Gil, Hexagonal boron nitride is an indirect bandgap semiconductor, Nat. Photonics 10 (2016) 262–266.
[146] B. Chao, et al., Donor–acceptor pyrrolo [3, 2-b] pyrrolyl-and dibenzothiophene-containing microporous polymeric frameworks for photocatalytic organic pollutant degradation, ACS Appl. Polym. Mater. 7 (2025) 998–1011.
[147] T. Iqbal, et al., Exploring the photocatalytic efficacy of ZnO nanostructures for simultaneous treatment of MB dye and Glucophage pharmaceuticals: experimental and theoretical investigations, Eur. Phys. J. Plus 140 (2025) 1–13.
[148] L. Zeng, et al., High-responsivity UV-vis photodetector based on transferable WS2 film deposited by magnetron sputtering, Sci. Rep. 6 (2016) 20343.
[149] E.P. Mukhokosi, S.B. Krupanidhi, K.K. Nanda, Band gap engineering of hexagonal SnSe2 nanostructured thin films for infra-red photodetection, Sci. Rep. 7 (2017) 15215.
[150] X.-W. Tong, et al., Direct tellurization of Pt to synthesize 2D PtTe2 for high-performance broadband photodetectors and NIR image sensors, ACS Appl. Mater. Interfaces 12 (2020) 53921–53931.
[151] N.B. Singh, S.K. Shukla, Properties of two-dimensional nanomaterials, in: Two-Dimensional Nanostructures for Biomedical Technology, Elsevier, 2020, pp. 73–100.
[152] M. Wang, et al., New approach to low-power-consumption, high-performance photodetectors enabled by nanowire source-gated transistors, Nano Lett. 22 (2022) 9707–9713.
[153] G. Wang, et al., Tunable contacts of Bi2O2Se nanosheets MSM photodetectors by metal-assisted transfer approach for self-powered near-infrared photodetection, Small 20 (2024) 2306363.
[154] X. Ren, et al., Self-powered broadband photodetectors based on Bi2O2Se with asymmetric contact areas, Chem. Eng. J. 496 (2024) 153937.
[155] M. Wang, et al., Toward low-power-consumption source-gated phototransistor, Appl. Phys. Lett. 124 (2024).

[156] P. Li, et al., Tunable synaptic behaviors of solution-processed InGaO films for artificial visual systems, Mater. Horizons 11 (2024) 4979–4986.
[157] Z. Lai, et al., High-performance flexible self-powered photodetectors utilizing spontaneous electron and hole separation in quasi-2D halide perovskites, Small 17 (2021) 2100442.
[158] J. Zhang, et al., All-solution-processed InGaO/PbI2 heterojunction for self-powered omnidirectional near-ultraviolet Photodetection and imaging, Adv Opt Mater 12 (2024) 2302665.
[159] F. Cao, et al., A dual-functional perovskite-based photodetector and memristor for visual memory, Adv. Mater. 35 (2023) 2304550.
[160] J. Wan, et al., Toward high-performance self-powered near-ultraviolet Photodetection by constructing a unipolar heterojunction, ACS Appl. Mater. Interfaces 16 (2024) 41157–41164.
[161] J. Zha, et al., Infrared photodetectors based on 2D materials and nanophotonics, Adv. Funct. Mater. 32 (2022) 2111970.
[162] F. Liu, et al., Lattice-mismatch-free construction of III-V/chalcogenide core-shell heterostructure nanowires, Nat. Commun. 14 (2023) 7480.
[163] M. Xu, et al., Nickel doping in tin disulfide enables visible photodetectors with extended detection range and high responsivity, ACS Appl. Mater. Interfaces 17 (2025) 17045–17054.
[164] Y. Yin, et al., Substrate-free chemical vapor deposition of large-scale III–V nanowires for high-performance transistors and broad-Spectrum photodetectors, Adv Opt Mater 10 (2022) 2102291.
[165] Z. Li, et al., Broadband GaAsSb nanowire array photodetectors for filter-free multispectral imaging, Nano Lett. 21 (2021) 7388–7395.
[166] J. Sun, et al., Stoichiometric effect on electrical and near-infrared photodetection properties of full-composition-range GaAs 1− x Sb x nanowires, Nano Res (2021) 1–8.
[167] K. Zhang, et al., Near-infrared polarimetric image sensors based on ordered sulfur-passivation GaSb nanowire arrays, ACS Nano 16 (2022) 8128–8140.
[168] D. Liu, et al., Schottky-contacted high-performance GaSb nanowires photodetectors enabled by lead-free all-inorganic perovskites decoration, Small 18 (2022) 2200415.
[169] V.P. Pham, K.N. Kim, M.H. Jeon, K.S. Kim, G.Y. Yeom, Cyclic chlorine trap-doping for transparent, conductive, thermally stable and damage-free graphene, Nanoscale 6 (2014) 15301–15308.
[170] V.P. Pham, et al., Chlorine-trapped CVD bilayer graphene for resistive pressure sensor with high detection limit and high sensitivity, 2D Mater. 4 (2017) 25049.
[171] U. Farooq, et al., Photodetection tuning with high absorptivity using stacked 2D heterostructure films, Nanomaterials 12 (2022) 712.
[172] M.A. Iqbal, et al., Nanostructures/graphene/silicon junction-based high-performance photodetection systems: progress, challenges, and future trends, Adv. Mater. Interfaces 10 (2023) 2202208.
[173] K.A.A. Min-Dianey, T.K. Le, J.R. Choi, P.V. Pham, Advanced optical detection through the use of a deformably transferred nanofilm, Nanomaterials 11 (816) (2021).
[174] A. Kumar, et al., Unlocking the potential of borophene: recent progress in synthesis, properties, and applications, Coord. Chem. Rev. 523 (2025) 216246.
[175] S.C. Lims, et al., Exploring the photocatalytic breakdown of organic pollutants using intercalated ZnO/SiO2 nanocomposites, Mater. Chem. Phys. 329 (2025) 130050.
[176] P.V. Pham, et al., Transfer of 2D films: from imperfection to perfection, ACS Nano 18 (2024) 14841–14876.
[177] W. Ahmad, et al., Strong interlayer transition in few-layer InSe/PdSe2 van der Waals heterostructure for near-infrared photodetection, Adv. Funct. Mater. 31 (2021) 2104143.
[178] E. Wu, et al., In situ fabrication of 2D WS2/Si type-II heterojunction for self-powered broadband photodetector with response up to mid-infrared, ACS Photonics 6 (2019) 565–572.
[179] W. Yu, et al., Near-infrared photodetectors based on MoTe2/graphene heterostructure with high responsivity and flexibility, Small 13 (2017) 1700268.
[180] J. Zhang, et al., Characterization of atomic defects on the photoluminescence in two-dimensional materials using transmission electron microscope, InfoMat 1 (2019) 85–97.
[181] S. Ghosh, et al., Dark current analysis on GeSn pin photodetectors, Sensors 23 (2023) 7531.
[182] M. Long, et al., Palladium diselenide long-wavelength infrared photodetector with high sensitivity and stability, ACS Nano 13 (2019) 2511–2519.
[183] J. Kublitski, et al., Reverse dark current in organic photodetectors and the major role of traps as source of noise, Nat. Commun. 12 (2021) 551.
[184] Y. Le Thi, Y. Kamakura, N. Mori, Simulation of dark current characteristics of type-II InAs/GaSb superlattice mid-wavelength infrared p–i–n photodetector, Jpn. J. Appl. Phys. 58 (2019) 44002.
[185] B.T. Marozas, et al., Surface dark current mechanisms in III-V infrared photodetectors, Opt Mater Express 8 (2018) 1419–1424.
[186] A. Kumar, M. Ubaidullah, P.V. Pham, R.K. Gupta, Three-dimensional macro-structures of graphene-based materials for emerging heterogeneous electrocatalysis: concepts, syntheses, principles, applications, and perspectives, Chem. Eng. J. 499 (2024) 156664.
[187] S.P. Ratnayake, et al., Carbon quantum dots-decorated nano-zirconia: a highly efficient photocatalyst, Appl. Catal. A Gen. 570 (2019) 23–30.
[188] M.G. Mohamed, et al., Design and synthesis of bifunctional conjugated microporous polymers containing tetraphenylethene and bisulfone units for energy storage and fluorescent sensing of p-nitrophenol, Colloids Surfaces A Physicochem. Eng. Asp. 680 (2024) 132675.
[189] H.-B. Do, et al., Recycling of reduced graphene oxide from graphite rods in disposable zinc battery applicable to optical sensing, Ceram. Int. 50 (2024) 43754–43762.
[190] T.-H. Mai, et al., 2D heterostructures in photocatalysis for emerging applications: current status, challenges, and prospectives, J. Catal. 439 (2024) 115744.
[191] K.A.A. Min-Dianey, et al., The ripple effect of graphite nanofilm on stretchable polydimethylsiloxane for optical sensing, Nanomaterials 11 (2021) 2934.
[192] X. Liu, et al., Infrared photodetector based on the photothermionic effect of graphene-nanowall/silicon heterojunction, ACS Appl. Mater. Interfaces 11 (2019) 17663–17669.
[193] S. Yang, et al., Gate dielectrics integration for 2D electronics: challenges, advances, and outlook, Adv. Mater. 35 (2023) 2207901.
[194] T.H. Mai, et al., Efficient photoanode with a MoS2/TiO2/au nanoparticle heterostructure for ultraviolet-visible photoelectrocatalysis, Nanotechnology 35 (2024).
[195] K. Dharmalingam, et al., Novel MoS2-In2O3-WS2 (2D/3D/2D) ternary heterostructure nanocomposite material: efficient photocatalytic degradation of antimicrobial agents under visible-light, Environ. Res. 261 (2024) 119759.
[196] M. Liaqat, et al., Synthesis of heterojunction BiVO4/MnO2 graphene ternary nanocomposites with enhanced photocatalytic activities through degradation of rhodamine B and tetracycline hydrochloride, Chin. J. Phys. 91 (2024) 406–420.
[197] M. Yousaf, et al., Exploring innovative antibacterial properties of porous ALT (Al2O3/TiO2) composite, Mater. Chem. Phys. 325 (2024) 129736.
[198] X. Wang, et al., Ultrasensitive and broadband MoS2 photodetector driven by ferroelectrics, Adv. Mater. 27 (2015) 6575–6581.
[199] F. Yang, et al., Emerging opportunities for ferroelectric field-effect transistors: integration of 2D materials, Adv. Funct. Mater. 34 (2024) 2310438.
[200] S. Wu, et al., Ultra-sensitive polarization-resolved black phosphorus homojunction photodetector defined by ferroelectric domains, Nat. Commun. 13 (2022) 3198.
[201] L. Guo, et al., Ferro-pyro-phototronic effect in monocrystalline 2D ferroelectric perovskite for high-sensitive, self-powered, and stable ultraviolet photodetector, ACS Nano 16 (2022) 1280–1290.
[202] L. Guo, et al., A self-powered UV photodetector with ultrahigh responsivity based on 2D perovskite ferroelectric films with mixed spacer cations, Adv. Mater. 35 (2023) 2301705.
[203] C. Jia, et al., Ferroelectrically modulated and enhanced photoresponse in a self-powered α-In2Se3/Si heterojunction photodetector, ACS Nano 17 (2023) 6534–6544.
[204] C. Zhou, Y. Chai, Ferroelectric-gated two-dimensional-material-based electron devices, Adv. Electron. Mater. 3 (2017) 1600400.
[205] Z. Luo, M. Yang, Y. Liu, M. Alexe, Emerging opportunities for 2D semiconductor/ferroelectric transistor-structure devices, Adv. Mater. 33 (2021) 2005620.
[206] H. Jiao, et al., Ferroelectric field effect transistors for electronics and optoelectronics, Appl. Phys. Rev. 10 (2023).
[207] S. Zhang, et al., Highly sensitive InSb nanosheets infrared photodetector passivated by ferroelectric polymer, Adv. Funct. Mater. 30 (2020) 2006156.
[208] G.A. Sundaram, A.F.M. EL-Mahdy, P.V. Pham, S. Kunjiappan, A.S.K. Kumar, Synergistic innovations: organometallic frameworks on graphene oxide for sustainable eco-energy solutions, ChemEngineering 8 (2024) 61.
[209] R. Srivastava, et al., Robust amorphous iron (II) diphosphate on nickel foam: aggrandizing electronic structure for efficient catalytic activity towards oxygen evolution and urea oxidation, Int. J. Hydrog. Energy 62 (2024) 451–461.
[210] M. Malhotra, et al., Fe-based MOFs as promising adsorbents and photocatalysts for re-use water contained arsenic: strategies and challenges, Chemosphere 357 (2024) 141786.
[211] D.N. Giang, et al., A visible-light photodetector based on heterojunctions between CuO nanoparticles and ZnO nanorods, Beilstein J. Nanotechnol. 14 (2023) 1018–1027.
[212] V.Y. Zheleznov, et al., Modification of a germanium surface exposed to radiation of a nanosecond ultraviolet laser, Russ. Microelectron. 50 (2021) 649–656.
[213] W. Chen, et al., Ultrahigh sensitive near-infrared photodetectors based on MoTe 2/germanium heterostructure, Nano Res 13 (2020) 127–132.
[214] T. Guo, et al., High-performance WO 3− x-WSe 2/SiO 2/n-Si heterojunction near-infrared photodetector via a homo-doping strategy, J. Mater. Chem. C 6 (2018) 5821–5829.
[215] A.M. Parambil, et al., Biogenic fluorescent carbon dots modulated fabrication of concatenate logic library and pattern-mediated molecular keypad lock for chemical sensing application, Chem. Eng. J. 463 (2023) 142354.
[216] P.V. Pham, T.-H. Mai, H.-B. Do, V.K. Ponnusamy, F.-C. Chuang, Integrated graphene heterostructures in optical sensing, Micromachines 14 (2023) 1060.
[217] M. Malik, M.A. Iqbal, J.R. Choi, P.V. Pham, 2D materials for efficient photodetection: overview, mechanisms, performance and UV-IR range applications, Front. Chem. 10 (2022) 905404.
[218] J.S. Parramon, T. Švarc, P. Majerič, Ž. Jelen, R. Rudolf, Optical characteristics of directly deposited gold nanoparticle films, Surfaces 7 (2024) 369–379.
[219] J. Guo, et al., Near-infrared photodetector based on few-layer MoS2 with sensitivity enhanced by localized surface plasmon resonance, Appl. Surf. Sci. 483 (2019) 1037–1043.
[220] P.K. Venuthurumilli, P.D. Ye, X. Xu, Plasmonic resonance enhanced polarization-sensitive photodetection by black phosphorus in near infrared, ACS Nano 12 (2018) 4861–4867.
[221] G. Huang, et al., Elevating surface-enhanced infrared absorption with quantum mechanical effects of plasmonic nanocavities, Nano Lett. 22 (2022) 6083–6090.

[222] J. Deng, et al., Absorption enhancement in all-semiconductor plasmonic cavity integrated THz quantum well infrared photodetectors, Opt. Express 28 (2020) 16427–16438.
[223] J. Tong, L.Y.M. Tobing, Y. Luo, D. Zhang, D.H. Zhang, Single plasmonic structure enhanced dual-band room temperature infrared photodetection, Sci. Rep. 8 (2018) 1548.
[224] Z. Chen, et al., Synergistic effects of plasmonics and electron trapping in graphene short-wave infrared photodetectors with ultrahigh responsivity, ACS Nano 11 (2017) 430–437.
[225] Y. Liu, et al., Plasmon resonance enhanced multicolour photodetection by graphene, Nat. Commun. 2 (2011) 579.
[226] C.-Y. Hsu, Z. Pei, J.-M. Liu, High-efficiency broadband infrared thin-film germanium photodetector enhanced by a resonant cavity and a nano-slit metasurface, IEEE Access 12 (2024) 156904–156914.
[227] J. Guan, et al., Light–matter interactions in hybrid material metasurfaces, Chem. Rev. 122 (2022) 15177–15203.
[228] J. Kim, et al., Dynamic control of nanocavities with tunable metal oxides, Nano Lett. 18 (2018) 740–746.
[229] K.C. Maurya, A.I.K. Pillai, M. Garbrecht, B. Saha, Simultaneous optical resonances at visible and mid-infrared frequencies with epitaxial TiN/Al0. 72Sc0. 28N/TiN metal/polar-dielectric/metal multilayers, Mater. Today Phys. 27 (2022) 100797.
[230] M. Stössel, J. Staudigel, F. Steuber, J. Simmerer, A. Winnacker, Impact of the cathode metal work function on the performance of vacuum-deposited organic light emitting-devices, Appl. Phys. A Mater. Sci. Process. 68 (1999) 387–390.
[231] A.S.K. Kumar, et al., Exploration of magnetic zeolite thin film derived from coal fly ash an efficient sorbent: application to water treatment, J. Environ. Manag. 374 (2025) 123972.
[232] H.-A. Chen, et al., Single-crystal antimonene films prepared by molecular beam epitaxy: selective growth and contact resistance reduction of the 2D material heterostructure, ACS Appl. Mater. Interfaces 10 (2018) 15058–15064.
[233] J. Jung, et al., Effect of graphene doping level near the metal contact region on electrical and photoresponse characteristics of graphene photodetector, Sensors 20 (2020) 4661.
[234] K. Bhargava, M. Shukla, V. Singh, Comparative analysis of contact resistance and photoresponse in poly (3-hexylthiophene) and poly (3-octylthiophene) based organic field-effect transistors, Synth. Met. 233 (2017) 15–21.
[235] D. Yue, et al., Homogeneous in-plane WSe 2 P–N junctions for advanced optoelectronic devices, Nanoscale 15 (2023) 4940–4950.
[236] Y. Lai, I. Wang, T. Hou, Giant Photoresponsivity and external quantum efficiency in a contact-engineered broadband a-IGZO phototransistor, Adv. Funct. Mater. 32 (2022) 2200282.
[237] J. Kim, et al., Improved contact resistance by a single atomic layer tunneling effect in WS2/MoTe2 heterostructures, Adv. Sci. 8 (2021) 2100102.
[238] M.A. Khan, et al., Tunable electron and hole injection enabled by atomically thin tunneling layer for improved contact resistance and dual channel transport in MoS2/WSe2 van der Waals heterostructure, ACS Appl. Mater. Interfaces 10 (2018) 23961–23967.
[239] P. Miró, M. Audiffred, T. Heine, An atlas of two-dimensional materials, Chem. Soc. Rev. 43 (2014) 6537–6554.
[240] H.S. Lee, et al., Metal semiconductor field-effect transistor with MoS2/conducting NiO x van der Waals Schottky interface for intrinsic high mobility and photoswitching speed, ACS Nano 9 (2015) 8312–8320.
[241] M. Cao, et al., Recent advances in UV-cured encapsulation for stable and durable perovskite solar cell devices, Polymers (Basel). 15 (2023) 3911.
[242] X. Yu, et al., A high performance, visible to mid-infrared photodetector based on graphene nanoribbons passivated with HfO 2, Nanoscale 8 (2016) 327–332.
[243] W. Feng, W. Zheng, W. Cao, P. Hu, Back gated multilayer InSe transistors with enhanced carrier mobilities via the suppression of carrier scattering from a dielectric interface, Adv. Mater. 26 (2014) 6587–6593.
[244] V.X. Ho, Y. Wang, M.P. Cooney, QN, V., Graphene-based photodetector at room temperature, in: Optical Sensing, Imaging, and Photon Counting: From X-Rays to THz 10729, 2018, pp. 7–13. SPIE.
[245] D. Kufer, G. Konstantatos, Highly sensitive, encapsulated MoS2 photodetector with gate controllable gain and speed, Nano Lett. 15 (2015) 7307–7313.
[246] W. Huang, et al., Encapsulation strategies on 2D materials for field effect transistors and photodetectors, Chin. Chem. Lett. 33 (2022) 2281–2290.
[247] P.V. Pham, A library of doped-graphene images via transmission electron microscopy, C 4 (34) (2018).
[248] P.V. Pham, Cleaning of graphene surfaces by low-pressure air plasma, R. Soc. Open Sci. 5 (2018) 172395.
[249] Y. Sun, R. Wang, K. Liu, Substrate induced changes in atomically thin 2-dimensional semiconductors: fundamentals, engineering, and applications, Appl. Phys. Rev. 4 (2017).
[250] B. Radisavljevic, A. Kis, Mobility engineering and a metal–insulator transition in monolayer MoS2, Nat. Mater. 12 (2013) 815–820.
[251] N. Gayathri Devi, T.H. Mai, R.K. Gupta, P.V. Pham, Art etching of graphene, Nanoscale Horiz. (2024) 1230–1249, https://doi.org/10.1039/d4nh00077c.
[252] X. Xu, et al., Efficient passivation of monolayer MoS2 by epitaxially grown 2D organic crystals, Sci. Bull. 64 (2019) 1700–1706.
[253] B. Chamlagain, et al., Mobility improvement and temperature dependence in MoSe2 field-effect transistors on parylene-C substrate, ACS Nano 8 (2014) 5079–5088.
[254] S. Bhattacharjee, et al., Nitride dielectric environments to suppress surface optical phonon dominated scattering in high-performance multilayer MoS2 FETs, Adv. Electron. Mater. 3 (2017) 1600358.
[255] M. Houssa, et al., Contact resistance at graphene/MoS2 lateral heterostructures, Appl. Phys. Lett. 114 (2019).
[256] Y. Khatami, H. Li, C. Xu, K. Banerjee, Metal-to-multilayer-graphene contact—part II: analysis of contact resistance, IEEE Trans. Electron Devices 59 (2012) 2453–2460.
[257] S. Batool, M. Idrees, S. Han, V.A.L. Roy, Y. Zhou, Electrical contacts with 2D materials: current developments and future prospects, Small 19 (2023) 2206550.
[258] I. Popov, G. Seifert, D. Tománek, Designing electrical contacts to MoS 2 monolayers: a computational study, Phys. Rev. Lett. 108 (2012) 156802.
[259] X. Tang, X. Tang, K.W.C. Lai, Scalable fabrication of infrared detectors with multispectral photoresponse based on patterned colloidal quantum dot films, ACS Photonics 3 (2016) 2396–2404.
[260] S. Zhang, et al., Spray-stencil lithography enabled large-scale fabrication of multispectral colloidal quantum-dot infrared detectors, Adv. Mater. Technol. 7 (2022) 2101132.
[261] A. Corletto, et al., Scalable fabrication of black phosphorous films for infrared photodetector arrays, Adv. Sci. 11 (2024) 2403182.
[262] X. Xu, T. Nakotte, B.N. Flanders, J. Zhou, C.A. Orme, Single-step, conformal, and efficient assembly of ligand-exchanged quantum dots for optoelectronic devices via an electric field, Nanoscale 11 (2025) 2403182.
[263] W. Yan, et al., Electrophoretic-driven in situ polymerization depositing high-quality perovskite films for photodetectors, Adv Opt Mater 10 (2022) 2200162.
[264] G. Lin, et al., Scalable fabrication of self-assembled GeSn vertical nanowires for nanophotonic applications, Nanophotonics 12 (2023) 219–228.
[265] T.K. Le, et al., Recent advances in vanadium pentoxide (V 2 O 5) towards related applications in chromogenics and beyond: fundamentals, progress, and perspectives, J. Mater. Chem. C 10 (2022) 4019–4071.
[266] Z. Yang, et al., High-accuracy dynamic target detection through low-readout channel thermopile infrared array detector enhanced by machine learning techniques, IEEE Sensors J. 24 (2024) 21300–21310.
[267] F. Soldevila, E. Salvador-Balaguer, P. Clemente, E. Tajahuerce, J. Lancis, High-resolution adaptive imaging with a single photodiode, Sci. Rep. 5 (2015) 14300.
[268] F. Zhou, A broadband plasmonic photodetector based on graphene-black phosphorus heterostructure with enhanced absorption and responsivity, IET Optoelectron. 19 (2025) e70003.
[269] J. Guo, et al., WSe2/MoS2 van der Waals heterostructures decorated with Au nanoparticles for broadband plasmonic photodetectors, ACS Appl. Nano Mater. 5 (2021) 587–596.
[270] M. Dai, et al., High-performance, polarization-sensitive, long-wave infrared photodetection via photothermoelectric effect with asymmetric van der Waals contacts, ACS Nano 16 (2022) 295–305.
[271] U. Sassi, et al., Graphene-based mid-infrared room-temperature pyroelectric bolometers with ultrahigh temperature coefficient of resistance, Nat. Commun. 8 (2017) 14311.
[272] H. Guo, W. Qi, New materials and designs for 2D-based infrared photodetectors, Nano Res 16 (2023) 3074–3103.
[273] P. Vashishtha, et al., Self-driven and thermally resilient highly responsive nano-fenced MoS2 based photodetector for near-infrared optical signal, Mater. Res. Bull. 164 (2023) 112260.
[274] M. Peng, et al., Blackbody-sensitive room-temperature infrared photodetectors based on low-dimensional tellurium grown by chemical vapor deposition, Sci. Adv. 7 (2021) eabf7358.
[275] L. Ferrante di Ruffano, et al., Optical coherence tomography for diagnosing skin cancer in adults, Cochrane Database Syst. Rev. 12 (2018) CD013189.
[276] H. Xu, et al., Flexible organic/inorganic hybrid near-infrared photoplethysmogram sensor for cardiovascular monitoring, Adv. Mater. 29 (2017) 1700975.
[277] L. van Manen, et al., The clinical usefulness of optical coherence tomography during cancer interventions, J. Cancer Res. Clin. Oncol. 144 (2018) 1967–1990.
[278] T. Zhang, et al., Six-arm stellat dendritic-PbS flexible infrared photodetector for intelligent healthcare monitoring, Adv. Mater. Technol. 7 (2022) 2200250.
[279] Y. Zhu, et al., Skin-like near-infrared II photodetector with high performance for optical communication, imaging, and proximity sensing, Chem. Mater. 35 (2023) 2114–2124.
[280] W. Jang, et al., Strong dark current suppression in flexible organic photodetectors by carbon nanotube transparent electrodes, Nano Today 37 (2021) 101081.
[281] W. Wu, et al., Ultrathin and conformable lead halide perovskite photodetector arrays for potential application in retina-like vision sensing, Adv. Mater. 33 (2021) 2006006.
[282] Y. Chen, et al., Flexible and filter-free color-imaging sensors with multicomponent perovskites deposited using enhanced vapor technology, Small 17 (2021) 2007543.
[283] J. Jiang, et al., Recent advances in 2D materials for photodetectors, Adv. Electron. Mater. 7 (2021) 2001125.
[284] N.L.P. M'Bouana, et al., Optimization of gold square-shaped nanopillars arrays for high-efficiency optronics, Opt. Commun. 512 (2022) 128073.
[285] K. Wang, et al., Evolution of short-range optical wireless communications, J. Lightwave Technol. 41 (2022) 1019–1040.
[286] N. Blaunstein, S. Engelberg, E. Krouk, M. Sergeev, Basic Elements of Optical Communication, 2020.
[287] J. Liu, et al., Fast response organic tandem photodetector for visible and near-infrared digital optical communications, Small 17 (2021) 2101316.
[288] N. Strobel, et al., Color-selective printed organic photodiodes for filterless multichannel visible light communication, Adv. Mater. 32 (2020) 1908258.

[289] T. Wang, et al., High-performance and stable plasmonic-functionalized formamidinium-based quasi-2D perovskite photodetector for potential application in optical communication, Adv. Funct. Mater. 32 (2022) 2208694.
[290] X. Deng, Z. Li, F. Cao, E. Hong, X. Fang, Woven fibrous photodetectors for scalable UV optical communication device, Adv. Funct. Mater. 33 (2023) 2213334.
[291] J. Pu, et al., Textile electronics for wearable applications, Int. J. Extrem. Manuf. 5 (2023) 42007.
[292] S. Zhou, et al., Highly sensitive SWIR photodetector using carbon nanotube thin film transistor gated by quantum dots heterojunction, Appl. Phys. Lett. 120 (2022).
[293] J. Zhang, L. Yang, L. Wang, G. Chen, X. Chen, Wavelength-dependent negative/positive photoresponses in single-walled carbon nanotube/PbS quantum dot mixed-dimensional heterostructures, Opt. Quant. Electron. 55 (2023) 144.
[294] S.H. Kim, et al., Flexible hybrid photodetector based on silver sulfide nanoparticles and multi-walled carbon nanotubes, RSC Adv. 11 (2021) 22625–22632.
[295] M. Babics, et al., Non-fullerene-based organic photodetectors for infrared communication, J. Mater. Chem. C 9 (2021) 2375–2380.
[296] Y. Xu, et al., Stabilization of black phosphorous quantum dots in PMMA nanofiber film and broadband nonlinear optics and ultrafast photonics application, Adv. Funct. Mater. 27 (2017) 1702437.
[297] M. Rein, et al., Diode fibres for fabric-based optical communications, Nature 560 (2018) 214–218.
[298] R.K. Jha, Non-dispersive infrared gas sensing technology: a review, IEEE Sensors J. 22 (2021) 6–15.
[299] S. Dello Russo, et al., Dual-tube MEMS-based spectrophone for sub-ppb mid-IR photoacoustic gas detection, Photoacoustics 40 (2024) 100644.
[300] J. Goldstein, et al., Waveguide-integrated mid-infrared photodetection using graphene on a scalable chalcogenide glass platform, Nat. Commun. 13 (2022) 3915.
[301] H. Schlicke, R. Maletz, C. Dornack, A. Fery, Plasmonic particle integration into near-infrared photodetectors and photoactivated gas sensors: toward sustainable next-generation ubiquitous sensing, Small 20 (2024) 2403502.
[302] L. Bodiou, et al., Carbon dioxide mid-infrared sensing based on Dy3+−doped chalcogenide waveguide photoluminescence, Opt. Lett. 48 (2023) 1128–1131.
[303] L. Luo, et al., PdSe2 multilayer on germanium nanocones array with light trapping effect for sensitive infrared photodetector and image sensing application, Adv. Funct. Mater. 29 (2019) 1900849.
[304] V. Guerra, J.R. Ticay-Rivas, V. Alonso-Eugenio, R. Perez-Jimenez, Characterization and performance of a thermal camera communication system, Sensors 20 (2020) 3288.
[305] H. Gong, et al., Self-driven infrared electrochromic device with tunable optical and thermal management, ACS Appl. Mater. Interfaces 13 (2021) 50319–50328.
[306] Z. Fan, T. Hwang, S. Lin, Y. Chen, Z.J. Wong, Directional thermal emission and display using pixelated non-imaging micro-optics, Nat. Commun. 15 (2024) 4544.
[307] G. Wu, et al., Visible to short wavelength infrared In2Se3-nanoflake photodetector gated by a ferroelectric polymer, Nanotechnology 27 (2016) 364002.
[308] X. Li, et al., Multi-functional platform for in-memory computing and sensing based on 2D ferroelectric semiconductor α-In2Se3, Adv. Funct. Mater. 34 (2024) 2306486.

Phuong V. Pham is a Professor in the Department of Physics at National Sun Yat-sen University (NSYSU), Taiwan. He earned his Ph.D. from SKKU Advanced Institute of Nanotechnology (SAINT), Sungkyunkwan University (SKKU), South Korea. Currently, he leads Materials Physics and Electronic Surfaces Group (https://sites.google.com/view/phuonggroup/home) within Department of Physics at NSYSU. Professor Pham has collaborated on industrial projects with major organizations, including SAMSUNG, POSCO, and government agencies such as the Korean Government, Ministry of Education and Ministry of Science and Technology of China, and the NSTC Grant Program (Taiwan). He has held various research positions, including Postdoctoral Researcher, Research Fellow, and Distinguished Research Fellow, at prestigious institutions like the School of Advanced Material Science and Engineering, SKKU, the Center for Multidimensional Carbon Materials (Director: Prof. Rodney Ruoff) at the Institute for Basic Science, South Korea, and the Hangzhou Global Scientific and Technological Innovation Center, Zhejiang University, China. Professor Pham is the recipient of several prestigious awards, including the NSF Career Award, the National Postdoctoral Award for Outstanding Young Scientists, China (2019), and the NSTC Grant Awards, Taiwan (2023, 2025). Additionally, he serves as Academic Editor for IntechOpen and Reviewer for over 60 Journals. He has authored approximately 100 peer-reviewed publications, including articles, and book chapters in top-tier journals and book publisher such as ***Chemical Reviews, Chemical Society Reviews, Advanced Materials, ACS Nano, ACS Materials Letters, Coordination Chemistry Reviews, Chemical Engineering Journal, 2D Materials, Carbon, Nanoscale Horizons, Nanoscale, Journal of Materials Chemistry C, Chinese Journal of Physics, Journal of Catalysis, Scientific Reports, Advanced Materials Interfaces, Sensors & Actuators A: Physical, Materials Chemistry and Physics, Optical Materials, and Optics Communications***, among others. His research interests span a wide range of fields, including nanotechnology, materials physics, surface physics, chemical engineering, atomic film synthesis, 2D heterostructures, nanofilm transfer, donor/acceptor systems, nanocomposites, plasma engineering for advanced electronics/optoelectronics as well as parallelly with the extending to predictive simulations associated with next-generation nanomaterials processes (kinetics, growths).

Cathrin Lims Selvakumar is an intern under the supervision of Prof. Phuong V. Pham at Material Physics and Electronic Surface Group, Department of Physics, National Sun Yat-Sen University, Taiwan. Her research interests focus on nanoparticles, quantum dots, thin films, and 2D materials for electronics and energy storage.

Anuj Kumar is working as an Assistant Professor at GLA University, Mathura, India. He received PhD degree in 2017 from Gurukula Kangri University, Haridwar, India. He moved to Beijing University of Chemical Technology, China for his Postdoctoral research. His research focus is on designing of catalytic materials for energy production and storage. He has published more than 200 articles, 5 Books, and 50 Book Chapters in reputed peer-reviewed journals (like Advanced Materials, Energy & Environmental Science, Materials Today, Applied Catalysis B: Environmental, Chemical Engineering Journal, Journal of Materials Chemistry A, Coordination Chemistry Reviews, Chemistry of Materials, Applied Energy, Small etc), in addition to 9 Patents (3 US and 6 Indian, 2 Indian patents have granted by Indian government). He has been awarded by "Young Researcher Award 2020/2021/2022" by InSc and by CEGR. He is serving as Editor (Nano LIFE), Section Editor (Organic Mini Reviews), advisory board member (Carbon Energy) Guest editor, and editorial board member for various journals. He is also working as expert consultant for research in various national and international universities.

Rajesh K. Ulaganathan specializes *in nanomaterials and devices,* particularly focusing on single crystal growth of two-dimensional (2D) materials and fabricating devices for electronics and optoelectronics applications. His research focuses on addressing challenges in electronics and optoelectronics, as well as exploring new ways to use 2D materials in emerging areas like flexible and transparent electronics. He completed his Master in Nanotechnology in **2010** at the Indian Institute of Technology, Roorkee, and pursued his doctoral dissertation at the Department of Chemistry, *National Taiwan University*, Taiwan, graduating in **2016**. Following that, he worked five years as a post-doctoral researcher at various departments and centers at *National Taiwan University*, then spent over two years as a senior post-doctoral researcher at *the Technical University of Denmark* before returning to Taiwan to continue his research at *Academia Sinica.*

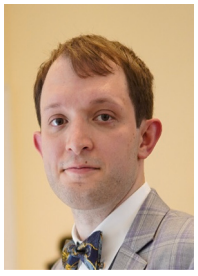

Rayko I. Stantchev is an Assistant Professor at Department of Physics, National Sun Yat-sen University (NSYSU) (2022), Taiwan and is leading Terahertz Reasearch Lab (https://rayko-research.netlify.app/). He earned a PhD in experimental physics with a THz spectrometer and spatial light modulators from the University of Exeter (2017), UK. In 2017, he spent a few years as postdoc in the THz group of E. Pickwell-MacPherson at Chinese University of Hong Kong (CUHK) (2017–2021), Hong Kong and at Department of Physics, University of Warwick (2021−2022), UK. His research interest focuses on the experimental implementation of a single-pixel THz camera for in-vivo THz imaging, non-invasive THz imaging using single-element detectors, with the addition of adaptive under sampling techniques.

Raman Sankar is an Associate Research Scientist at the *Institute of Physics, Academia Sinica, Taiwan*. He joined the faculties in 2019 after receiving his Ph.D. degree from *Anna University* (2008) and having *Postdoctoral Research* (2009–2015) and *Assistant Research Scholar* (2015–2018) training at *Academia Sinica*. His research interests are focused on quantum matter, quantum many-body physics, fundamental condensed matter physics: strongly correlated electrons, topological phases of quantum matter, quantum magnetism, superconductivity, ARPES, spin-ARPES, TR-ARPES, resonant and inelastic X-ray scattering, advanced X-ray spectroscopy, X-ray free electron lasers, ultrafast physics, crystal growth techniques (optical/IR furnace, Bridgeman), and 2D materials. He published more than **250** publications in reputed journals like ***Science***, ***Nature Nanotechnology***, ***Nature Physics***, ***Nature Communications***, ***Advanced Materials***, and so on, with an **h-index of 50** and citations above **17,500**. The *Taiwan government* awarded him the *Senior Skilled Talented* **"Plum Blossom Award-2022"** in recognition of his research achievements.